The University of Calgary

SILICON-29 NUCLEAR MAGNETIC RESONANCE STUDIES OF AQUEOUS SILICATES

by

Stephen D. Kinrade

A Thesis

Submitted to the Faculty of Graduate Studies

In Partial Fulfillment of the Requirements for the

Degree of Doctor of Philosophy

Department of Chemistry

Calgary, Alberta

April 21, 1987

ISBN Ø-315-35998-6

THE UNIVERSITY OF CALGARY

FACULTY OF GRADUATE STUDIES

The undersigned certify that they have read, and recommend to the Faculty of Graduate Studies for acceptance, a thesis entitled, "Silicon-29 Nuclear Magnetic Resonance Studies of Aqueous Silicates", submitted by Stephen D. Kinrade in partial fulfillment of the requirements for the degree of Doctor of Philosophy.

T.W. Swaddle (Supervisor)
Chemistry

T. Chivers
Chemistry

E.D. Ghent
Geology

I.E. Hutcheon
Geology

T.S. Sorensen
Chemistry

C.A. Fyfe (External Examiner)
Guelph-Waterloo Centre for
Graduate Work in Chemistry

Date 1987-04-28

Abstract

Silicon-29 nuclear magnetic resonance (NMR) spectroscopy has been used at temperatures from 0° to 200°C to investigate the identities, relative abundances and rates of interconversion of the numerous silicate oligomers that occur in aqueous alkali-metal (M = Na, K, Rb) hydroxide solutions. An empirical understanding of the structural features which are responsible for the differences between ^{29}Si resonances has led to the identification of a novel silicate anion ($Si_4O_{10}^{4-}$) consisting of four tetrahedral silicate centres that are arranged with tetrahedral geometry.

Temperature dependent broadening of ^{29}Si resonances is demonstrably due to Si-Si chemical exchange. The extreme line-broadening exhibited for easily cyclizable species reveals that intramolecular condensation occurs faster than intermolecular condensation. Doubly deprotonated centres are the principal constituents of silicate species at high pH, but are of negligible importance in polymerization compared with the singly deprotonated centres which predominate at $[M^+]:[Si^{IV}] = 1:1$. Therefore, increases in temperature and pH lead to higher proportions of monomer and small oligomers by favouring depolymerization and suppressing condensation reactions, respectively. A decrease in exchange rates at high pH reveals that the mechanism of condensation is $[H^+]$ dependent.

At sufficiently high temperatures, Si-Si chemical exchange causes gross averaging of the measured longitudinal relaxation times (T_1). The

predominant T_1 relaxation process evidently involves dipole-dipole interactions between ^{29}Si and M^+ nuclei, with minor contributions from the ^{29}Si-^1H dipole-dipole mechanism. Contributions to T_1^{-1} from the spin-rotation mechanism are apparent for the small oligomers, but in general are of minor importance.

Acknowledgements

I wish to express my gratitude to Dr. T.W. Swaddle for his guidance and support throughout the course of this research. I also give my sincere thanks to Dr. R. Yamdagni for his patient assistance in the operation of the Varian XL200 spectrometer, Mr. T.E. Mani who skillfully constructed the NMR tube, Dr. T.S. Sorensen for several helpful discussions, Dr. R.A. Kydd for kindly reviewing this manuscript, Dr. B. Sykes (University of Alberta) for use of his Nicolet 300 spectrometer, and Miss L.A. Green for her efficient preparation of this manuscript.

This research was supported by the National Sciences and Engineering Research Council of Canada (Operating Grant A-3636), the Alberta Oil Sands Technology and Research Authority through a scholarship, the University of Calgary Research Grants Committee through research and travel grants, and the Faculty of Graduate Studies and the Department of Chemistry through graduate assistantships.

To my parents

CONTENTS

SYMBOLS AND ABBREVIATIONS

Symbols

a	distance of closest intermolecular approach between nuclei
B	local magnetic field at the nucleus
B_0	static field of NMR magnet
B_1	applied rf-induced field
C	natural abundance of nuclide (%)
D	mutual translational self-diffusion coefficient
EN	electronegativity
f_x	mole fraction of nucleus x
G	transverse (x'y'-) magnetization component
h	Planck's constant ($\hbar = h/2\pi$)
i	$(1)^{1/2}$
I	(i) ionic strength
	(ii) nuclear spin quantum number
$\mathbf{I}$	1×n unit matrix
Im	imaginary part of complex number
J	nuclear spin-spin coupling constant
k	rate coefficient
k_B	Boltzmann's constant
K	equilibrium constant
K_{IP}	ion-pair formation constant
$\mathbf{K}$	exchange-rate matrix

M^+	alkali-metal cation
$M^+:Si^{IV}$	concentration ratio between $M^+(OH^-)$ and Si^{IV} in solution
M	macroscopic magnetization vector
M_0	equilibrium magnetization vector in the presence of B_0
M_z	z-component of macroscopic magnetization vector
N_x	concentration of nucleus x (per unit volume)
pK_a	negative logarithm of acid dissociation constant
P_x	relative population of spin-site x ($\sum_{x=1}^{n} P_x = 1$)
P	n×1 matrix of relative site populations
$^xQ^y_z$	tetrahedral SiO_4 centre with 4-y terminal hydroxy groups of which, on average, x are deprotonated. When applicable, z indicates the number of equivalent centres in a totally symmetric species.
$*Q^y$	activated silicate centre with y coordinated silicate groups
r	internuclear distance
Re	real part of complex number
S	(i) signal height (ii) nuclear receptivity ($=\|C\gamma^3\|$)
S	diagonalizing matrix (i.e., $\Lambda = S^{-1} \cdot R \cdot S$)
t	time
T	temperature
T_1	nuclear spin-lattice relaxation time (further subscripts refer to the relaxation mechanisms abbreviated below)
T_2	nuclear spin-spin relaxation time (further subscripts refer to T_2-contributions abbreviated below)

T_2	diagonal matrix with elements T_{2i}^{-1}
T_d	delay between successive acquisition sequences ($>5T_1$)
u	x'-component of macroscopic magnetization vector
v	y'-component of macroscopic magnetization vector
V(x)	intensity of absorption-mode spectrum at frequency x
x	independent frequency variable (Hz)
x',y'	spacial coordinate directions which rotate about the z-axis
γ_X	magnetogyric ratio of nucleus x
δ	chemical shift (ppm) (value is positive for upfrequency shift)
ΔH^*	enthalpy of activation
ΔS^*	entropy of activation
$\Delta\delta$	difference in δ (usually, with respect to Q° resonance)
$\Delta\nu_{1/2}$	half-height line width (Hz)
η	nuclear Overhauser enhancement
Λ	eigenvalue matrix
μ_0	permeability of a vacuum
ν_0	applied rf frequency
ν_X	Larmar precession frequency of nucleus x (Hz)
σ_X	shielding constant of nucleus x (further superscripts and subscripts refer to abbreviations listed below)
τ	(i) time between rf pulses (relaxation period) (ii) residence time at a spin-site
τ_0	general correlation time for molecular motion
τ_c	correlation time for molecular tumbling
ω_0,ω_X	as for ν_0 and ν_X but in rad s^{-1}
ω	diagonal matrix with elements $x - \Omega_i$

Ω_x chemical shift of nucleus x from the Larmor precession frequency in rad s^{-1} ($= \omega_x - \omega_0$)

Abbreviations

a anisotropic (superscript of σ_x)

CBA complete bandshape analysis

d diamagnetic (superscript of σ_x)

DANTE delays alternating with nutations for tailored excitation

DD dipole-dipole relaxation mechanism

DDD,DDH,DDM dipole-dipole relaxation by ^2H, ^1H and M^+ nuclei, respectively

e electronic (superscript of σ_x)

eff effective (T_2 relaxation time)

exch exchange (contribution to T_2 relaxation time)

FEP fluorinated ethylene propylene

FID free induction decay

FT Fourier transform

H hydrogen bonding (superscript of σ_x)

I.D. inside diameter

inhomo inhomogeneity (contribution to apparent T_2 relaxation time)

inter intermolecular

intra intramolecular

NMR nuclear magnetic resonance (spectroscopy)

NOE nuclear Overhauser effect

O.D. outside diameter

ppm	parts per million
r	ring current (superscript of σ_x)
rf	radio frequency
r.p.s.	revolutions per second
SA	shielding anisotropy relaxation mechanism
SC	scalar relaxation mechanism
SINCERE	selective inversion in a chemical exchange rate experiment
SIR	selective inversion-recovery
SR	spin rotation relaxation mechanism
TFE	tetrafluoroethylene
UE	unpaired electron relaxation mechanism

CHAPTER I. Introduction

1.1. Preface

Silicate compounds make up well over 90% of the earth's crust[1] and, therefore, it should not be surprising that they also are abundant within the hydrosphere (e.g., dissolved silicates constitute 9% of the salinity in average river water[2]). Consequently, knowledge of how silicon exists in natural waters is important geochemically[3,4], and this is especially true for hydrothermal fluids in which silica content is high and solution conditions vary radically[5]. An understanding of high temperature aqueous silicate chemistry is also important for the operation of many industrial hot water processes. Silica which is dissolved during the steam recovery of bitumen from tar sands, for example, reprecipitates to cause loss in formation permeability plus severe scaling and corrosion of the process machinery[6]. A similar problem exists for geothermal power generating stations[7,8].

Silicates have been identified as an important component of biological waters as well. A striking demonstration of this role is the annual production of biogenic silica by marine phytoplankton equivalent to 10^{16} g Si yr^{-1}, yet the mechanism by which silica is scavenged and protected from ocean water which is decidedly undersaturated is not clear[9]. Although little is known about how silicate ions are metabolized, evidence is accumulating to indicate that trace quantities are essential for the normal development and functioning of all life-forms[10,11].

Commercially, soluble silicates are a major chemical commodity (47th on the 1986 ACS top 50 listing[12]) with global production estimated to be 3×10^9 kg per annum (expressed as solid with molar ratio SiO_2:Na_2O = 3.4:1)[13]. Applications include detergents, catalysts, gels, adsorbants, ceramics, adhesives and coatings.

1.2. Objectives

Silicon-29 nuclear magnetic resonance (NMR) spectroscopy has been established as the most effective method of probing the constitution of aqueous silicate solutions (see Sect. 1.3.2 and 1.3.3). The primary objective of this study was to monitor by ^{29}Si NMR the equilibrium distribution of silicate oligomers, and the dynamics of interchange between them, in alkali-metal hydroxide solutions over a range of solution compositions and temperatures (0 to +200°C). Also to be evaluated were the mechanisms of ^{29}Si nuclear magnetic relaxation, and the overall viability of NMR spectroscopy as an investigative tool for hydrothermal chemistry.

1.3. Aqueous Silicate Chemistry

1.3.1. Conspectus

Equations 1.1 to 1.4 characterize the dissolution and ionization of silica in aqueous solution. The solubility[14] and ionization[15] constants given are for 298 K and ionic strengths I = 0.5 mol L^{-1} and 0.6 mol L^{-1}, respectively. The stability diagram shown in Figure 1-1 is based on these and other findings summarized in Sect. 1.3.2. Alpha-quartz is thermodynamically the most stable form of silica at normal temperatures

	log K	
SiO_2 (s, α-quartz) + $2H_2O$ = H_4SiO_4	-3.7	(1.1)
SiO_2 (s, amorphous) + $2H_2O$ = H_4SiO_4	-2.7	(1.2)
H_4SiO_4 = $H_3SiO_4^-$ + H^+	-9.437	(1.3)
$H_3SiO_4^-$ = $H_2SiO_4^{2-}$ + H^+	-12.65	(1.4)

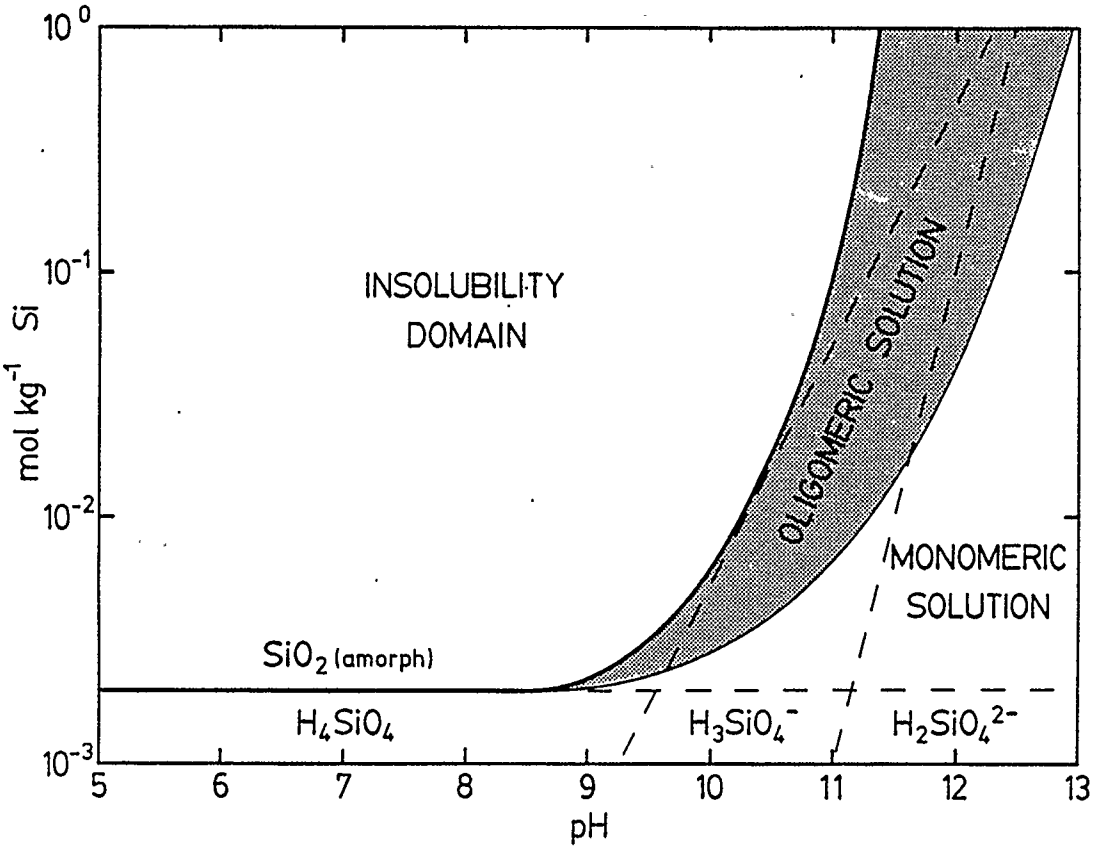

Figure 1-1. Stability diagram for soluble silicates (after Stumm and Morgan[16]). The heavy line represents the solubility curve for amorphous silica, while the dashed lines correspond to equilibrium equations 1.2 to 1.4.

and pressures, but crystallization rates of this phase are so slow that the upper limit of dissolved silica concentration is represented by the solubility curve for amorphous silica. Under alkaline conditions, ionization of silicic acid increases which results in a sharp rise in solubility and the appearance of polysilicate anions. Very high alkalinity causes further ionization and subsequent depolymerization. Thus, a substantial number of pH- and concentration-dependent equations are required to characterize the system fully. This complexity has precluded evaluation of dissociation constants for most species. Evidence suggests, however, that pK_a's increase with molecular size[15] as opposed to the behavior in polyphosphoric acid[17].

For aqueous silicate solutions in which it is assumed that the sole source of OH^- is an alkali-metal hydroxide compound MOH, alkalinity is generally characterized by the $M^+:Si^{IV}$ concentration ratio.

Several of the oligomeric silicate anions are portrayed in Figure 1-2. Each point or corner in the stick figure representations denotes a

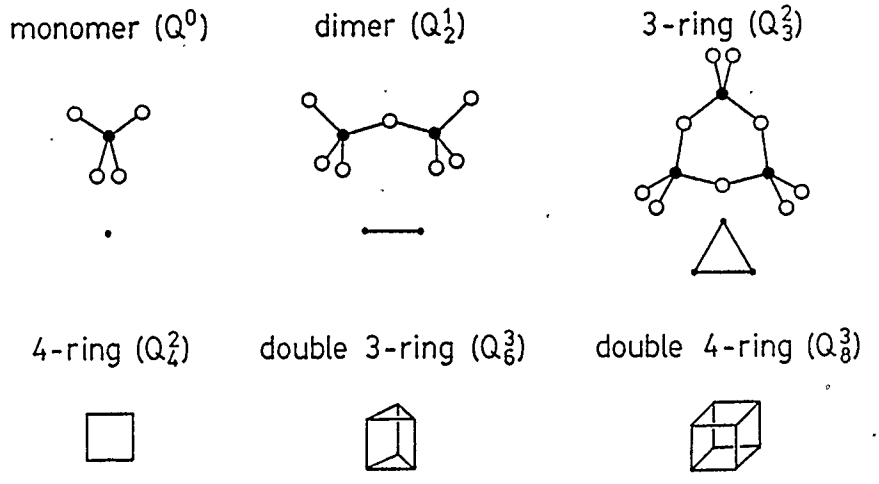

Figure 1-2. Structural representations for 6 symmetric silicate anions found in alkaline solution.

SiO_4 tetrahedron, while lines represent SiOSi bridges. Hydrogen atoms are not shown. Thus, a simple line depicts the dimer $H_4Si_2O_7^{2-}$, while the cyclic trimer $H_3Si_3O_9^{3-}$ or "3-ring" is represented by a triangle. To indicate the degree of connectivity at a Si centre, Engelhardt et al.[18] established the Q^y symbol, which signifies a SiO_4 tetrahedron with y coordinated bridging oxygens. A totally symmetric polysilicate anion with z equivalent tetrahedra can be represented as $Q^y{}_z$.

1.3.2 Early Studies

Studies prior to 1940 using, for example, viscosity[19], potentiometry[20], freezing point[21] and diffusion[22] techniques, succeeded in demonstrating that polymerization decreases with dilution or with alkalinity ($M^+:Si^{IV} > 1:1$), and that no precipitate or colloidal material is present in even highly concentrated solutions. Later, the light scattering work of Nauman and Debye[23] indicated that the average degree of connectivity increased from 1.0 to 2.5 as $Na^+:Si^{IV}$ was decreased from 4.2:1 to 1.0:1. In 1959, Lagerström[14] and Ingri[24] independently reported potentiometric titrations of solutions with $Na^+:Si^{IV} \sim 1:1$ which were interpreted as signifying the presence of H_4SiO_4, $H_3SiO_4^-$, $H_2SiO_4^{2-}$, and the tetramer $H_6Si_4O_{12}^{2-}$. Colloidal silica was observed at $Na^+:Si^{IV} < 0.8:1$. Aveston[25] interpreted ultracentrifugation results obtained at slightly higher concentrations as depicting an extended series of polysilicates. Busey and Mesmer[26] conducted precise potentiometric titrations to follow the ionization and polymerization of silicic acid up to 300°C in solutions containing 0.005 to 0.05 mol kg^{-1} Si. Low temperatures, high concentrations, and $Na^+:Si^{IV}$ ratios of 0.7:1 to 1:1 all favoured formation

of polysilicates, although individual species could not be resolved. Added NaCl had a negligible influence which was interpreted as evidence that silicate-Na^+ pairing was insignificant.

In the first Raman study of aqueous silicates, Fortnum and Edwards[27] concluded that Si in the orthosilicate anion has 4-fold coordination, rather than 6, since the spectrum was similar to that of $H_2PO_4^-$ rather than of PF_6^- or H_6TeO_6. Freund[28], in a laser-Raman investigation of solutions with $Na^+:Si^{IV}$ varying from 0.7:1 to 6:1, identified $H_3SiO_4^-$, $H_2SiO_4^{2-}$ and, at pH > 15, $HSiO_4^{3-}$. He noted that the singly charged orthosilicate anion, $H_3SiO_4^-$, only exists when $Na^+:Si^{IV} \sim 1:1$ and even under those conditions it is only a minor component, the solution being dominated by a large number of polymeric species which are indistinguishable by Raman spectroscopy. Equilibrium conditions are attained very quickly and are independent of solution history. Dutta and Shieh[29] found that the alkali metal cation M^+ had no apparent effect on the extent of polymerization. However, they noted that addition of MCl salts stimulated further condensation and, since smaller cations exerted the greatest influence, they speculated that attraction of water molecules by the cation provided the driving force. Like Raman, infrared spectroscopy is able only to distinguish between monomer (absorption at 950 cm^{-1}) and a generic polymer (1120 cm^{-1})[30,31].

Several comparatively recent studies are based on the assumption that when a low temperature solution is instantly diluted (to < 1%) and acidified to pH 2, the equilibrium distribution of polysilicate anions is temporarily "frozen-in"[32]. If the diluent contains molybdic acid, monomer will react quickly to form the yellow silicomolybdic acid.

Since polysilicates must first depolymerize, the rate of colour development can be related to the average molecular weight[33,34]. Alternatively, the structure of each silicate anion can be identified if, during the rapid acidification process, the labile silanol groups are capped with trimethylsilyl ligands to produce stable esters which can be distinguished by conventional chromatographic methods and elemental analysis. This procedure was first described by Lentz[35] who, for a 1 mol L^{-1} Si solution with $Na^+:Si^{IV}$ = 1:1, identified monomer, dimer and linear trimer in decreasing order of abundance, a significant quantity of cyclic tetramer, and about 45% colloidal silica. Upon diluting a similar solution from 1.0 to 0.001 mol L^{-1} Si, Dent Glasser and co-workers[36] observed an increase from 30 to 100% in monomer content. They later identified 3-, 4- and 6-ring species plus a double 4-ring with one open edge ($Si_8O_{21}^{9-}$), and concluded that: (i) the dominant building unit of polymeric species is the 4-ring; (ii) all SiO_4 tetrahedra in a silicate anion have, as nearly as possible, the same degree of connectivity; (iii) lability of Q groups decreases as connectivity increases; and (iv) solutions attain equilibrium rapidly regardless of the source of silicate.[37] Ray and Plaisted[38] conducted a comprehensive trimethylsilylation study from 8 to 90°C of alkali-metal and tetraalkylammonium silicate solutions in which they further identified linear tetramer, a 5-ring, and double 4-ring (predominant in tetramethylammonium solutions) and double 6-ring species. They concluded that polymerization was enhanced by increased concentration, low temperature and pH and, possibly, by heavy M^+ cations.

Subsequently, NMR studies revealed that the preliminary acidification procedure employed in the molybdic acid and trimethylsilylation investigations causes significant structural rearrangement (see Sect. 1.3.3). However, these techniques remain useful for qualitative study, especially at $M^+:Si^{IV} < 1:1$.

1.3.3. ^{29}Si NMR Studies

Silicon-29 NMR field shifts were reported for a sodium silicate solution and various other Si-containing materials in 1956[39], but the first detailed NMR investigation of aqueous silicates had to await the development and availability of modern, high-resolution spectrometers.

Of the three naturally occurring, stable isotopes of silicon, only ^{29}Si has a magnetic moment ($I = 1/2$). The magnetogyric ratio $\gamma = -5.319\times10^7$ rad T^{-1} s^{-1} indicates that ^{29}Si resonates at about 1/5 the frequency of ^1H and, since the natural isotopic abundance (C) is 4.7% (insufficient to observe spin-spin coupling), the theoretical receptivity ($S = |C\gamma^3|$) is 2.1 times that of ^{13}C. However, several factors combine to make ^{29}Si NMR experiments rather time-consuming. For instance, a larger atomic volume and comparatively different chemistry lead to lower concentrations for Si than are typical for carbon. Longitudinal relaxation times tend to be large (see Ch. IV) necessitating long recycling periods between observe pulses. Because of the negative magnetogyric ratio, decoupling of common nuclei which have a positive γ will result in a negative nuclear Overhauser enhancement (NOE).

In 1973, Marsmann[40] assigned the major ^{29}Si line positions for a commercial waterglass solution to end (Q^1), middle (Q^2) and branching (Q^3) groups by analogy with spectra of polyalkylsilicates. Simultaneously

with Gould et al.[41], he identified lines corresponding to the monomer and dimer, and speculated on assignments for the linear trimer and the cyclic tri- and tetramers[42]. A broad band in the extreme upfield region was assigned to tetrafunctional Q^4 units arising from colloid, the NMR tube and glass coil supports. Because no sharp peaks occur in this region, dissolved species presumably do not contain Q^4 centres.

In 1975, Engelhardt and co-workers proposed a variety of new NMR assignments including several ring and cage structures[16,43]. They noted that peaks shift downfield with varying degrees as the $Na^+:Si^{IV}$ ratio is increased and attributed this to changes in the equilibrium distribution between ionization states. Longitudinal (T_1) ^{29}Si relaxation times were determined to be shorter than for any other Si-containing compound and a possible explanation was proposed (see Ch. IV)[44]. In 1984, Engelhardt and Hoebbel[45] suggested that temperature dependent ^{29}Si NMR line broadening (i.e., transverse (T_2) relaxation) is due to dynamic exchange of SiO_4^{4-} groups.

R.K. Harris and co-workers, having already characterized a variety of other silicon compounds by ^{29}Si NMR[46], studied the trimethylsilylation derivatives of various silicate minerals[47] and then, in 1977, reported a detailed investigation of several sodium and potassium silicate solutions[48]. They concluded that unidentified paramagnetic contaminants exerted the principal contribution to both longitudinal and transverse ^{29}Si relaxation. Between 1980 and 1983, Harris and Knight[49-53] reported the structure of 18 polysilicate anions (see Table II-I) which they identified using a combination of techniques not previously applied to ^{29}Si NMR: (i) a very high field spectrometer

(B_o = 11.75 T); (ii) samples isotopically enriched in ^{29}Si to improve sensitivity and induce ^{29}Si-^{29}Si coupling; (iii) ^{29}Si homonuclear decoupling; and (iv) spectral analysis supported by computer simulations. In clear contrast to the findings of the trimethylsilylation studies[37,38], half of these structures contain the 3-ring unit which previously was thought to be unstable because of excessive strain[54]. An attempt using 2-D J-resolved and shift-correlation (COSY) spectroscopy to identify further silicate anions was hindered by the complexity of ^{29}Si spectra of low alkalinity solutions[55]. Recently, Knight et al.[56] verified the previously tentative assignments for the double 3- and 4-ring cages by substituting a germanium atom for Si in each of these symmetric structures, and examining the resultant linesplitting patterns. In accordance with Engelhardt and Hoebbel[45], Harris' group originally cited chemical exchange as a principal cause of temperature-dependent linebroadening[57]. They later calculated very slow exchange rates from the results of a selective saturation experiment using a solution with $K^+:Si^{IV}$ = 3.8:1 and, instead, attributed broadening to unknown paramagnetic contaminants[58]. In a second report on longitudinal relaxation[59], paramagnetic compounds were reasserted as the primary control of both longitudinal and transverse relaxation rates.

Most recently, Griffiths, Cundy and Plaisted[60] employed the Carr-Purcell-Meiboom-Gill technique[61] to quantify the contribution of exchange broadening to observed linewidths, and concurred with Harris that it is quite small.

Other relevant ^{29}Si NMR studies include a report by Cary et al.[62] that a neutral 0.0016 mol L^{-1} solution of dissolved silica contained

only monomer and ca. 6% dimer. In a combined potentiometric and ^{29}Si NMR investigation, Sjöberg et al.[15] calculated the charge on several polysilicate anions and verified the expected nuclearities. The formation of zeolites has also been studied by ^{29}Si-NMR, and results reported on precipitation mechanisms[63], synthetic controls[64], and structural precursors in solution (i.e.: a double 5-ring)[65].

1.3.4. The Silicate Si-O Bond

Two aspects of silicate bonding stand out conspicuously. First, the Si-O bond length varies widely (ca. 0.155-0.180 nm) yet, generally, is shorter than would be expected for a single bond[66]. Second, the SiOSi bond angle in silicate minerals ranges from 120 to 180° (average near 145°)[67] while simple covalent bond theory would predict a value closer to 109°. Since Pauling first invoked (d-p) π-bonding effects to satisfy his electronegativity principle for silicon[68], there has been much debate concerning the extent to which participation of silicon 3d-orbitals is responsible for these observations[66,69-71]. A recent ^{17}O NMR study of bonding in silicates by Janes and Oldfield[72], plus a previous report on correlations between ^{29}Si shielding and ligand group electronegativity[73], provide the latest experimental support for the (d-p) π-bonding hypothesis (or, alternatively, (σ^*-p) hyperconjugation[74]).

O'Keeffe and Hyde[75] suggested that <SiOSi is controlled by repulsion between Si atoms as evidenced by the remarkable uniformity in Si...Si nonbonded distance for silicate minerals (ca. 0.306 nm). They also noted that as <SiOSi decreases from 145°, the Si-O bridging bond length increases. DeJong and Brown[76] conducted semi-empirical molecular

orbital calculations for the $H_6Si_2O_7$ species and concluded that, rather than Si...Si interactions, O...O repulsions between hydroxy groups on adjacent silicons determine the structural geometry. (They found that inclusion of Si 3d-orbitals in their basis set had little effect, while Lasaga[77] noted only small improvements in optimized CNDO calculations.) Although a reduction in <SiOSi from 180 to 120° resulted in a slight redistribution of electron density towards the silicons, there was a significant shift in electron density from nonbonding to bonding and antibonding molecular orbitals centred over the bridging oxygen. The proportionately greater increase in antibonding character caused destabilization of the Si-O bridging bond. In a series of molecular orbital calculations designed to compare the stability of different size silicate rings, Chakoumakos, Hill and Gibbs[67] determined that the 3-ring is very strained and possesses a small SiOSi bond angle (130.5°C), whereas both stability and <SiOSi rise sharply for the 4-ring. Smaller increases in stability continue for the 5- and 6-membered rings.

CHAPTER II. Silicon-29 NMR Spectra and Aqueous Silicate Equilibria.

2.1. Introduction

2.1.1. Previous Studies

Potentiometric studies revealed early on that a high degree of polymerization in aqueous silicate solutions is favoured by low temperature, high Si concentration and low alkalinity[26]; Raman investigations tentatively indicated that the equilibrium distribution is independent of both solution history[28] and the alkali-metal cation (M^+) used[29]. Although useful evidence was obtained from trimethylsilylation studies[33-38], the reliable identification of individual silicate anions had to await development of high resolution ^{29}Si NMR spectroscopy. With this technique, Harris and Knight[49-53] have identified 12 structures "positively", and made tentative assignments for another 6 (listed in Table II-I). The corresponding ^{29}Si resonances occur over a wide spectral range (ca. 30 ppm) and, as the $M^+:Si^{IV}$ ratio is raised, they undergo an overall shift to higher frequencies, which has been attributed to ionization of the silicate oligomers[15,43,52]. Although resonance frequencies have also been reported to vary with sample dilution[52], there has not been a systematic investigation into how solution conditions affect ^{29}Si shielding. Such information could prove useful in the identification of new silicate anions.

Structural features which have been employed to interpret ^{29}Si shifts in spectra of silicate and aluminosilicate minerals include Si-O bond length, SiOSi bridging bond angle, bond strength, Si...Si nonbonded distance and σ-orbital hybridization[78]. Janes and Oldfield[73] recently

Table II-I. Silicate Anions and Corresponding ^{29}Si assignments.[a]

	Species	Structure	Si-Centre	Line[b,c]
I	monomer (Q^0)	•	Q^0	1(s)
II	dimer ($Q^1{}_2$)	——	Q^1	6(s)
III	linear trimer	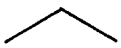	Q^1 Q^2	4(d)[d] 22(t)[d]
IV	monosubstituted cyclic trimer	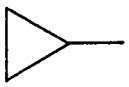	Q^1 Q^2 Q^3	3(d) 8(d) 29(q)
V	cyclic trimer ($Q^2{}_3$)		Q^2	9(s)
VI	bridged cyclic tetramer		Q^2 Q^3	12(t) 33(q)
VII	linear tetramer[e]		Q^1 Q^2	5(d)[d] 18(d)[d]
VIII	bicyclic pentamer		Q^2(X) Q^2(A) Q^3	7(t) 19(d) 23(q)
IX	tricyclic hexamer 1	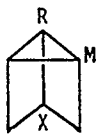	Q^2 Q^3(R) Q^3(M) Q^3(X)	15(t) 20(q) 25(t) 35(q)
X	cyclic tetramer ($Q^2{}_4$)		Q^2	16(s)

Table II-I. (Continued)

	Species	Structure	Si-Centre	Line[b,c]
XI	prismatic hexamer (Q^3_6)	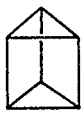	Q^3	24(s)
XII	monosubstituted cyclic tetramer[e]	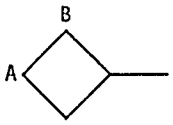	Q^1 Q^2(B) Q^2(A) Q^3	2(d) 14(t) 17(t) 34(q)
XIII	tricyclic hexamer B[e]	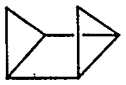	Q^2 Q^3	10 21
XIV	tricyclic hexamer C[e]	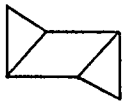	Q^2 Q^3	11 27
XV	pentacyclic heptamer[e]	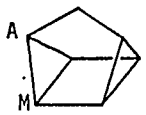	Q^2 Q^3(A) Q^3(M)	- 28 30
XVI	hexacyclic octamer[e]	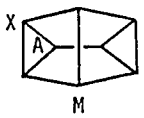	Q^3(X) Q^3(A) Q^3(M)	26 31 37
XVII	cubic octamer (Q^3_8)	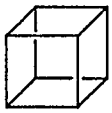	Q^3	38(s)
XVIII	doubly bridged cyclic tetramer		Q^2 Q^3	13(t) 32(d)

[a] From ref. 55 and 56. [b] Numbering corresponds to Figure 2-4. [c] ^{29}Si-enrichment leads to singlets (s), doublets (d), triplets (t) and quartets (q). [d] Signals are comparatively broad and only observed below 20°C. [e] Tentative.

claimed that, if all ligands possess the lone pair, p-hybridized orbitals necessary for (d-p)π-bonding[68], the best prediction of ^{29}Si shifts is achieved by correlation with the group electronegativity sum (ΣEN) for the four ligands bonded to silicon (Eqn. 2.1). In addition, they correlated -OSi group electronegativities calculated using Eqn. 2.1 with the SiOSi bond angles for three silica polymorphs (Eqn. 2.2). Since these relationships are based on relatively crude electronegativity data[79], the 5-figure precision implied is rather misleading. Equation 2.2 in particular should be used with caution since the concept of electronegativity[68] is not sufficiently quantitative for the small EN differences between -OSi groups to be meaningful. Furthermore, they made no allowance for the variation among reported chemical shift and <SiOSi[80] data for the minerals which were used in this correlation.

$$\delta_{Si} = -24.336\ \Sigma EN + 279.27 \qquad (2.1)$$

$$EN(OSi) = (<SiOSi/136.79) + 2.9235 \qquad (2.2)$$

2.1.2. Theory of ^{29}Si Chemical Shifts

The local magnetic field (B) experienced at a nucleus will not correspond to the external field B_o because the nucleus is screened or shielded by the electrons around it. The proportionality between B and B_o is demonstrated in Eqn. 2.3, where σ is a dimensionless tensor which

$$B = B_o\ (1-\sigma) \qquad (2.3)$$

represents the extent of shielding. Thus, the chemical shift (δ) of a nucleus is defined as the difference in shielding with respect to a given reference nucleus (Eqn. 2.4).

$$\delta = [(\nu-\nu_{ref})/\nu_{ref}]\cdot 10^6 \text{ ppm} \quad (2.4)$$

Nuclear screening is generally expressed as the sum of local (σ_{local}), intramolecular (σ_{intra}) and intermolecular (σ_{inter}) contributions[81].

$$\sigma = \sigma_{local} + \sigma_{intra} + \sigma_{inter} \quad (2.5)$$

Using Ramsey's terminology[82], the local contribution is separated into diamagnetic (σ_{local}^{d}) and paramagnetic (σ_{local}^{p}) terms (Eqn. 2.6).

$$\sigma_{local} = \sigma_{local}^{d} + \sigma_{local}^{p} \quad (2.6)$$

The diamagnetic effect induces electrons to rotate about the nucleus in opposition to B_0 such that a higher applied field (or lower frequency) is necessary to cause resonance. The magnitude of the σ_{local}^{d} term depends on the density and spherical distribution of the "core" electrons and, therefore, its contribution to shielding of heavy nuclei such as ^{29}Si is large and nearly constant compared with other screening influences[83]. Consequently, σ_{local}^{d} is usually considered to be unimportant in the analysis of ^{29}Si shift differences, although this assumption has been challenged[84]. To account for the loss in nuclear shielding caused by addition of electron density to heavy nuclei, Ramsey[82] derived a complex expression describing how "valence" electrons hinder the free rotation of core electrons and reduce the overall symmetry of the electron shell. He termed the influence "paramagnetism" because it serves to reinforce the external field. The corresponding σ_{local}^{p} term is usually cited as the principal cause of ^{29}Si shift differences[73,85].

The intra- and intermolecular terms in Eqn. 2.5 refer to shielding processes arising from electron circulation which is not localized at the nucleus of interest. Intramolecular screening (Eqn. 2.7) typically includes magnetic anisotropy (σ_{intra}^{a}) and ring current (σ_{intra}^{r}) contributions, although the latter process is not relevant to aqueous silicate solutions. A σ_{intra}^{e} term accounts for electron field distortion arising from intramolecular polar group interactions.

$$\sigma_{intra} = \sigma_{intra}^{a} + \sigma_{intra}^{r} + \sigma_{intra}^{e} \qquad (2.7)$$

The third class of nuclear shielding contributions in Eqn. 2.5 arises from intermolecular solution interactions. Solute...solvent and solute...solute intermolecular dispersion (or London) forces give rise to a rather complex van der Waals screening influence, σ_{inter}^{vdW} [86]. Additionally, polar molecules may structure the surrounding medium into a "reaction field"[87] which, depending on the dielectric strength of the solvent, will further modify the electron distribution of the solute molecule (σ_{inter}^{e})[88]. In aqueous silicate solutions, however, neither these processes nor the magnetic anisotropy contribution (σ_{inter}^{a}), which is primarily applicable to aromatic solvents, will affect nuclear shielding as much as silicate-M^{+} ionic association (σ_{inter}^{M}) and silicate...H_2O hydrogen bonding (σ_{inter}^{H}).

$$\sigma_{inter} = \sigma_{inter}^{vdW} + \sigma_{inter}^{e} + \sigma_{inter}^{a} + \sigma_{inter}^{M} + \sigma_{inter}^{H}$$
$$\sim \sigma_{inter}^{M} + \sigma_{inter}^{H} \qquad (2.8)$$

2.2. Experimental

2.2.1. Sample Preparation

Prior to use, all clean labware was soaked 12 h in a hot solution of ca. 2 mmol kg^{-1} Na_2H_2EDTA and rinsed thoroughly with doubly deionized water.

Amorphous silica was prepared by dropwise addition of redistilled silicon tetrachloride (Fisher, technical) in doubly deionized water. The resulting gel was oven dried at 110°C, crushed, and then washed repeatedly with water (to neutrality of washings). In addition, two samples of 95.1% ^{29}Si-enriched silica (A, 228 mg; and B, 210 mg) were purchased from U.S. Services Inc.. Spectrochemical analysis supplied with the second batch showed Na, Mg and Ti to be present in trace amounts (<0.01%), while another 52 elements were undetectable.

Alkali-metal hydroxide solutions were prepared inside screw-cap, polyethylene bottles by dissolving solid NaOH, KOH (both Fisher ACS Certified) or RbOH (ICN Pharmaceuticals) in freshly boiled, deionized-H_2O and/or D_2O (Bio-Rad, 99.75%). Concentrations were determined by titration with potassium hydrogen phthalate. To ensure a strong "internal" lock signal, all solutions were isotopically enriched at least 75% in ^2H (except for sample 1; see Table II-II).

Silicate solutions were prepared directly inside sealed, Teflon FEP® NMR tube liners (see Sect. 2.2.3) by dissolving a known quantity of silica, which had been dried 12 hr at 250°C, in a weighed portion of hydroxide solution at 100°C for 1 hr. The composition of each sample is given in Table II-II. Nonenriched silica dissolved completely in all

Table II-II. Aqueous Silicate Solutions and NMR Experiments Conducted.

Sample	[Si] mol kg^{-1}	$M^+:Si^{IV}$	M	^{29}Si-enriched[a]	^2H % atom	EXPERIMENT[b] CBA	SIR	T_1	NOE
1[c]	0.97	0.65	Na		36				
2	1.85	1.0	Na		75				
3	1.75	1.0	Na	A_0	76				
4	1.40	1.0	Na	A_1	76	•		•	
5	0.93	1.0	Na	A_2	76				
6	0.70	1.0	Na	A_3	75	•			
7	0.35	1.0	Na	A_4	75	•			
8	0.18	1.0	Na	A_5	75	•			
9	0.04	1.0	Na	A_6	75				
10	0.01	1.0	Na	A_7	75				
11	1.12	1.3	Na	A_8	75				
12	0.84	1.7	Na	A_9	75	•			
13	0.56	2.5	Na	A_{10}	75	•			
14	0.28	5.0	Na	A_{11}	75	•			
15	0.21	1.0	Na	A_{12}	75				
16	0.23	2.3	Na	A_{13}	75	•			
17	0.24	3.5	Na	A_{14}	75				
18	1.8	1.5	Na		100				
19	1.8	1.5	K		99		•		
20	1.8	1.5	Rb		94				
21[c]	2.3[d]	3.1	Rb		83				
22[c]	1.3[d]	5.8	Rb		83				
23[c]	2.0[d]	1.2	K		92				
24	2.80	4.5	K		82		•		

Table II-II. (Continued)

Sample	[Si] mol kg^{-1}	M^+:Si^{IV}	M	^{29}Si-enriched[a]	^{2}H % atom	EXPERIMENT[b] CBA	SIR	T_1	NOE
25	2.80	1.0	K		96		•		
26	2.79	3.8	K		85	•			
27	5.00	1.0	K		93				
28	9.25	1.0	K		87				
29	4.16	0.95	Na		100				
30	4.16	0.90	Na		100				
31	1.49	10.3	K		87		•	•	
32	0.77	20.0	K		87				
33	2.17	1.0	Na	B_0	75	•		•	•
34	2.17	4.0	Na		99			•[e]	•
35	1.55	1.0	Na	B_1	75	•		•	•
36	1.20	1.0	Na	B_2	75	•		•	
37	0.80	1.0	Na	B_3	75	•		•	•
38	2.18	1.0	Na		75			•	•
39	2.17	4.0	K		75			•	•
40	2.17	4.0	Na		74			•	
41	2.18	4.0	Rb		74			•	•
42	0.30	1.0	Na	B_4	75	•		•	•

[a] Symbols indicate whether the sample was prepared from enriched silica batch A or B, plus the order of dilution. [b] Complete bandshape analysis (CBA) and selective-inversion recovery (SIR) experiments are discussed in Ch. III. T_1 and nuclear Overhauser effect (NOE) measurements are discussed in Ch. IV. [c] Spectra acquired at low temperatures only. [d] Nominal concentration because of incomplete dissolution. [e] Also run on Nicolet 300.

solutions except those with a $M^+:Si^{IV}$ ratio significantly less than unity (i.e., sample 1 with $Na^+:Si^{IV}$ = 0.65:1 and sample 29 with $Na^+:Si^{IV}$ = 0.90:1). Silica that was enriched in ^{29}Si, however, neither dissolved completely nor as quickly. A small quantity (ca. 3 mg) of grey fines and a few white particles were centrifuged from sample 3 following its preparation from the first batch (A) of enriched silica. No further precipitation was observed in this solution nor in others derived from it. A more significant quantity of fine white powder, representing 8%wt of the second batch (B) of enriched silica, was centrifuged from sample 33 after it had been freshly prepared (concentration recalculated accordingly); further white suspension appeared in all subsequent dilutions (i.e., samples 35 to 37 and 42). Harris and co-workers[49] reported similar difficulties in preparing their solutions from enriched silica. Since extreme purity is claimed by the manufacturer, the undissolved material must be a crystalline phase of silica.

All solutions were pressurized to 1 MPa with nitrogen gas (see Sect. 2.2.3). Samples 34 to 42 were also purged with finely bubbled N_2 to minimize dissolved oxygen.

2.2.2. NMR Spectroscopy and Spectral Integration

Silicon-29 NMR spectra were obtained at 39.75 MHz on a Varian XL200 spectrometer using 10- and 16 mm-bore probeheads. Additional spectra of sample 34 were acquired at 59.61 MHz using a Nicolet 300 spectrometer with a 12 mm probehead. The ^{29}Si 90° pulse-width, nominally 44 and 49 μs for the 10 and 16 mm Varian probes and 40 μs for the Nicolet, was determined at the beginning of each operating session using hexamethyl-

disiloxane. Spectra were acquired at temperatures between ca. 0 and 150°C for all silicate solutions except samples 1 and 21 to 23 for which only low temperatures were employed.

Glass NMR tubes and coil supports gave rise to a broad ^{29}Si background signal which made spectral integration extremely difficult (see Figure 2-1). In the 16mm Varian probehead, coil supports were replaced with equivalent parts machined from Vespel SP-1® polyimide resin (E.I. du Pont de Nemours & Co.) and the coils were reattached with a Si-free, high temperature-resistant, allyl cyanoacrylate adhesive,

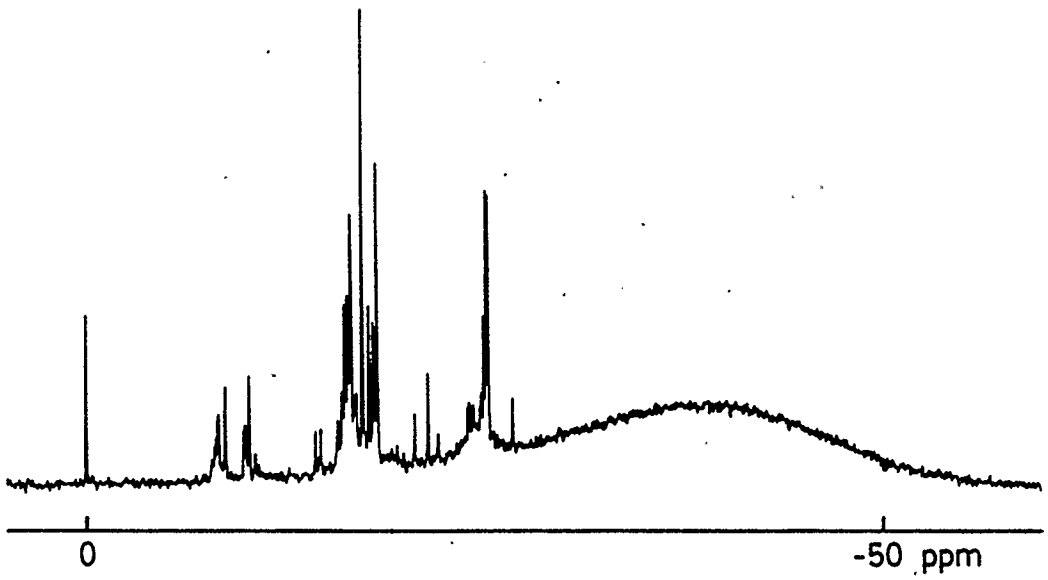

Figure 2-1. ^{29}Si spectrum at 6.2°C for sample 2 with 1.85 mol kg^{-1} Si and $Na^+:Si^{IV}$ = 1.0:1. The broad upfield band is due to glass components in the probehead.

Powerbond 920®(Permabond Corp.). The flat baseline exemplified in Figure 2-2 was finally achieved by replacing the standard glass NMR tube with a Si-free, pressurizable vessel which is described below.

A further requirement for obtaining quantitative integrations is that magnetization vectors must be restored to equilibrium prior to each observe pulse. This was ensured by use of a cycling period (= acquisition + delay intervals) greater than 3 to 5 times the longest longitudinal (T_1) relaxation time. Data from the longitudinal relaxation study discussed in Ch. IV reveal that this condition was met for samples 2 to 6 and 31 to 42.

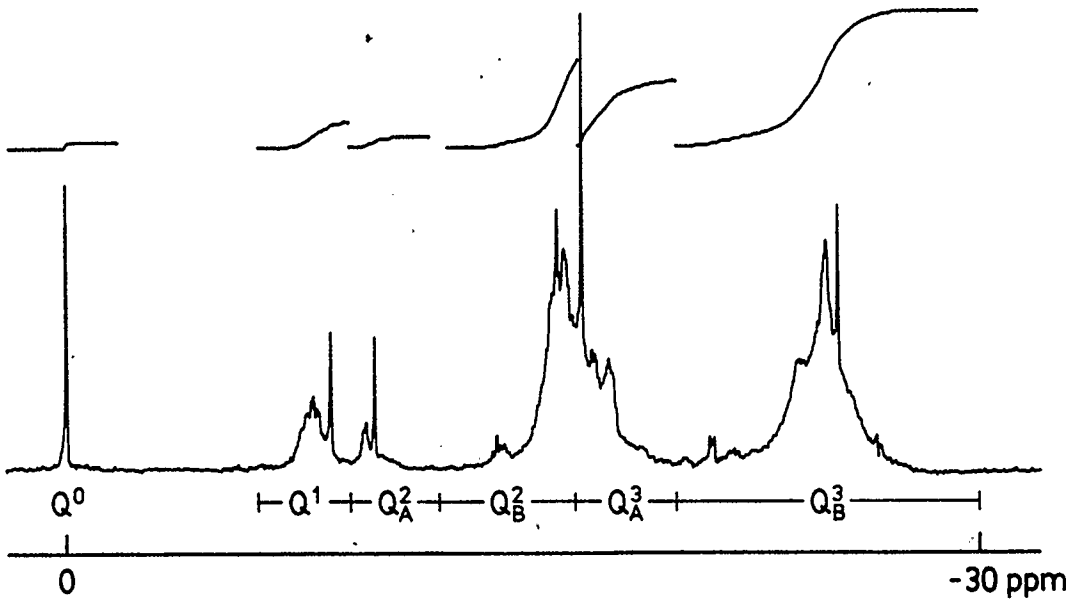

Figure 2-2. ^{29}Si-spectrum and integration at 3.3°C for sample 36 which contains 1.20 mol·kg^{-1} Si and $Na^+:Si^{IV}$ = 1.0:1 (95% ^{29}Si-enriched). Acquisition time = 3 s. Delay = 72 s. Number of acquisitions = 600. Artificial line-broadening = 1 Hz.

2.2.3. Pressurizable NMR Tube

The liquid range of aqueous solutions was extended to the 200°C limit of the XL200 spectrometer by use of a unique, pressurizable sample vessel designed by the author. The version developed for the 16 mm Varian probehead is illustrated in Figure 2-3. The pressure jacket, spinner turbine and valve-head were machined from Vespel SP-1® which is light, Si-free and remains rigid at elevated temperatures. Using reported tensile strengths[89] (since no yield-stress data were available) in Lamé's formula[90], a conservative estimate was obtained at various temperatures for the maximum containment pressure of the 16 mm O.D., 13 mm I.D. pressure jacket. Results indicate that the minimum containment pressure at 200°C is 9 MPa, i.e. 6 times greater than the vapour pressure of water, thus ensuring a wide safety margin for the entire operating range. Further strength is provided by the chemically resistant, Teflon FEP liners which were constructed by heat-molding a seal at the end of 12.8 mm O.D., 11.2 mm I.D. tubing (Cole-Palmer Instrument Co.). The pressure jacket is secured within the spinner turbine by screwing down the valvehead, which contains a brass, tubeless-bicycle-tire valve seated against a Teflon TFE gasket. When tested, the valves were found to be leak-free over the required pressure and temperature conditions. The TFE capillary-insert inhibits sample refluxing and the vortex action caused by spinning. Each assembly was pressure tested with water to 225°C prior to use in the spectrometer.

Variations on the design in Figure 2-3 which were also constructed include: (i) a 8 mm I.D. version for small sample volumes; (ii) a model incorporating a 10 mm glass NMR tube as the pressure jacket for use to

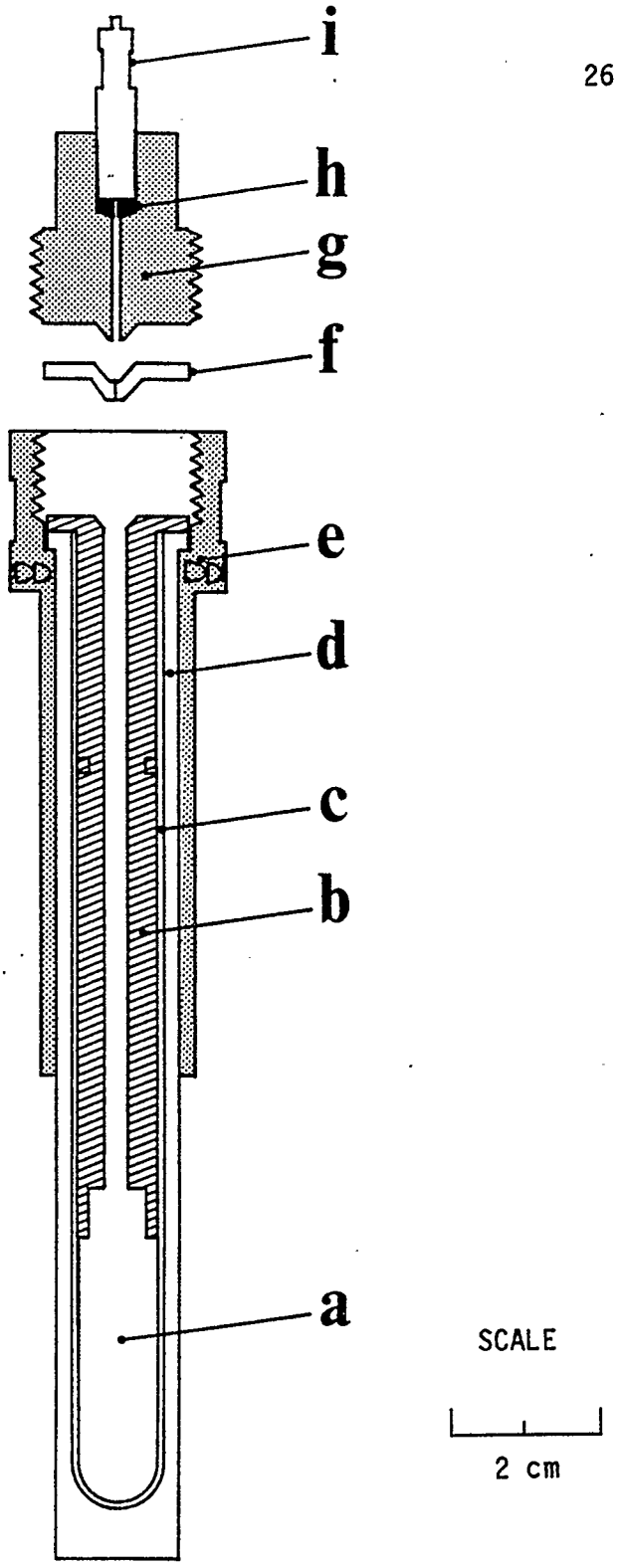

Figure 2-3. 16 mm Pressurizable NMR Tube. (a) Sample compartment. (b) Teflon TFE capillary insert with Neoprene O-rings (includes void for sample expansion). (c) Teflon FEP liner. (d) Vespel SP-1 pressure jacket. (e) Vespel spinner turbine. (f) Teflon TFE gasket. (g) Vespel valve-head. (h) Teflon TFE gasket. (i) Brass bicycle-tire valve.

150°C in the 10 mm probehead; and (iii) a second glass-sheathed assembly used for preliminary work on a Brüker WH90 spectrometer.

2.2.4. Temperature Measurement

The temperature dependence of the separation between the methylene and hydroxy ^1H resonances of ethylene glycol is well characterized[91]. By acquiring the ^1H spectrum of neat ethylene glycol (Fisher ACS Certified) via the ^1H-decoupling coil, a complete set of temperature determinations was made for each combination of spectrometer, probehead and sample tube which was employed. (Although immersed thermocouple readings correlated well with the glycol-derived measurements, they drifted with time due to thermal conductance up the thermocouple wire.) Sample spinning affected temperature ±2 K and, thus, air pressure and the spinning rate (20 r.p.s.) were kept constant throughout all experiments. Solution temperature varied by no more than 0.5 K over each run.

2.2.5. Temperature Dependence of Chemical Shifts

The monitoring of chemical shifts as a function of temperature can be very difficult since all NMR resonances are inherently temperature dependent. Even if a relatively temperature-insensitive compound could be found, it almost certainly would react in the alkaline silicate solution if employed as an internal reference. If, instead, the compound were sealed in a coaxial capillary tube and used as an external reference, differences from the bulk solution in magnetic susceptibility and temperature would inevitably result in measurement errors.

The referencing technique used in this study exploits the excellent field stability of the XL200 superconducting magnet (field divergence ≤

0.01 ppm/12 hr) which enables the "absolute" temperature dependence of a ^2H signal ($\nu_{^2H}$) to be monitored while the spectrometer is unlocked. When the ^{29}Si transmitter frequency (ν_{rf}) is locked to a characterized ^2H signal, the frequency shift arising from temperature change T_A to T_B is given by Eqn. 2.9, in which $R = \nu_{rf} - \nu_{signal}$. This method was used to determine the temperature dependence of ^{29}Si resonances for samples 39 to 41.

$$\Delta\nu_{^{29}Si} = [(R_B - R_A) - (\nu_{^2H,B} - \nu_{^2H,A})]/\nu_{rf} \qquad (2.9)$$

2.3. Silicon-29 Chemical Shifts

2.3.1. Results

In Figure 2-4, low temperature ^{29}Si NMR spectra are compared for two sodium silicate solutions, one 95% enriched in ^{29}Si (sample 3) and the other nonenriched (sample 2), each of which contain ca. 1.8 mol kg^{-1} Si with $Na^+:Si^{IV} = 1.0:1$. Aside from enhancing signal intensities, isotopic enrichment induces linesplitting which enables signals in Figure 2-4 to be correlated with the assignments of Harris and Knight[52,53] listed in Table II-I. Silicon-29 nuclei resonate at progressively lower frequencies as silicate connectivity increases and, therefore, spectra are divisible into regions Q^0, Q^1, Q^2 and Q^3 (Figure 2-2). Resonances within the Q^2 and Q^3 regions can be further segregated into distinct subregions, A and B. The 22 lines most confidently assigned by Harris and Knight are listed in Table II-III along with structural characteristics of the corresponding Q-centres.

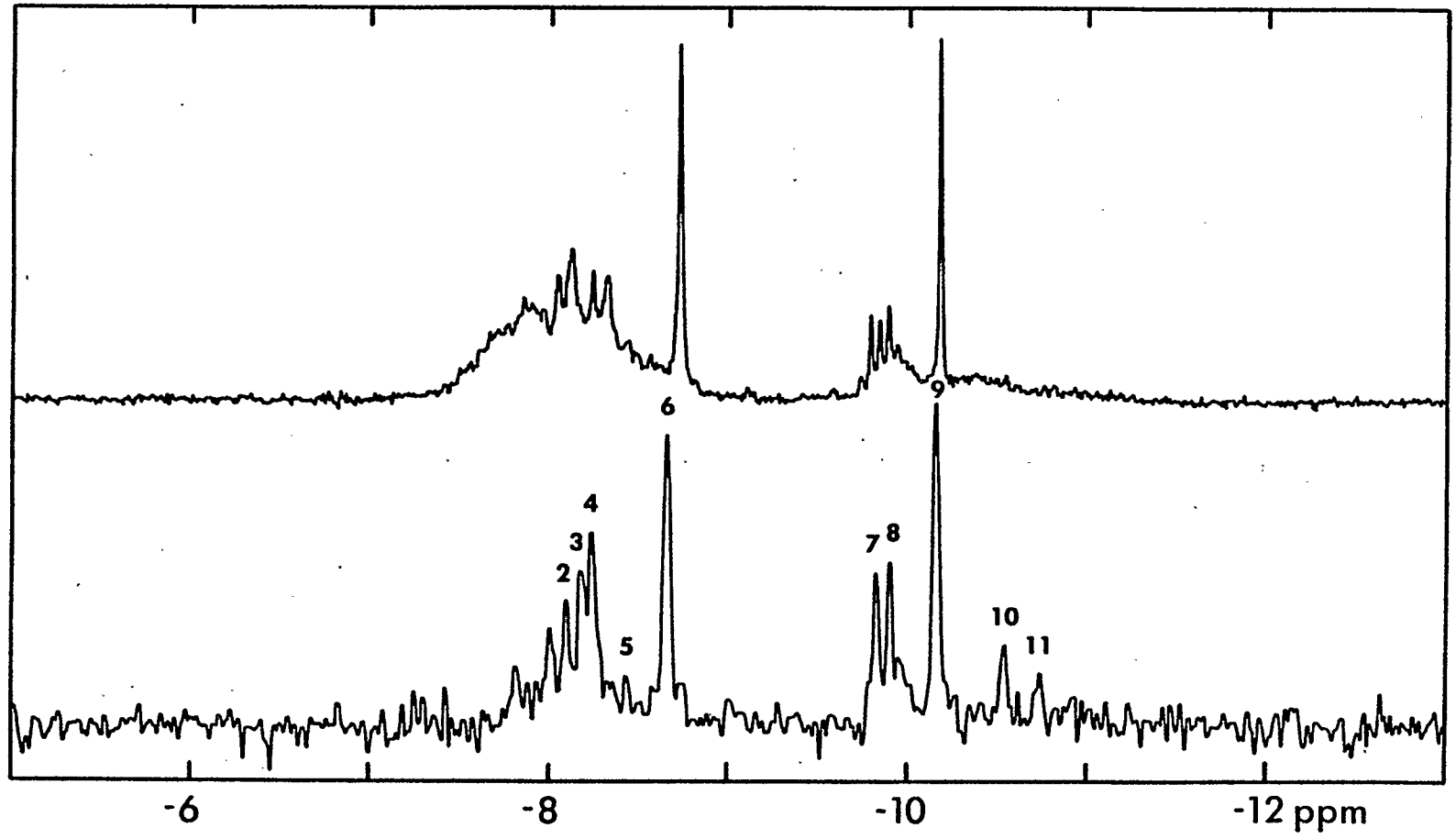

Figure 2-4a. ^{29}Si NMR spectra at -3.8°C for samples containing ca. 1.8 mol kg^{-1} Si with Na^+:Si = 1:1. Lower spectrum is of non-enriched sample 2 (21000 transients, 3 s recycle time), and upper spectrum is of 95% ^{29}Si-enriched sample 3 (3000 transients, 7.7 s recycle time). Each contains 0.1 Hz artificial linebroadening. Peaks are numbers in accordance with the assignments of Harris and Knight[52,53] which are listed in Table II-I.

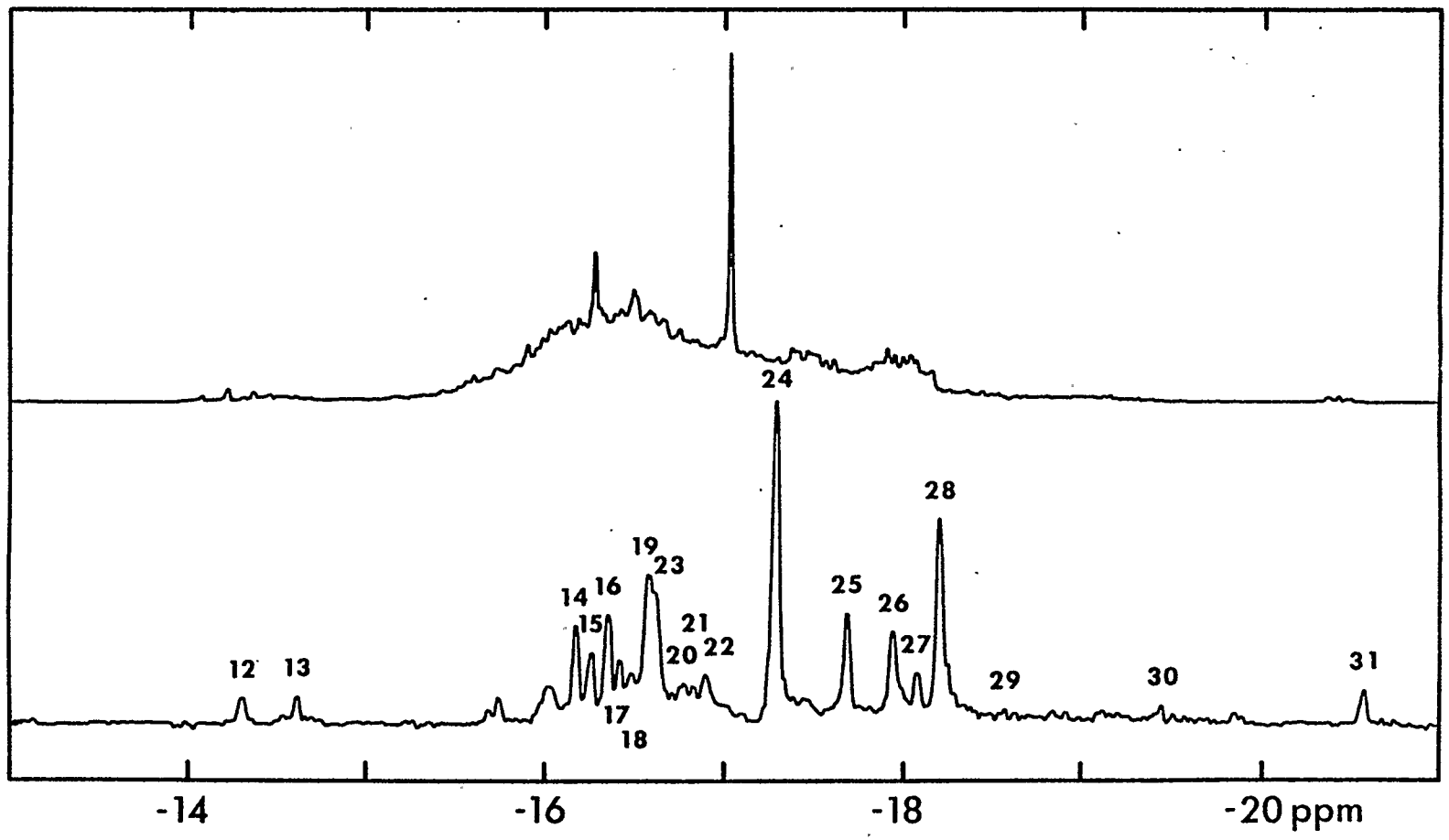

Figure 2-4b. As Figure 2-4a.

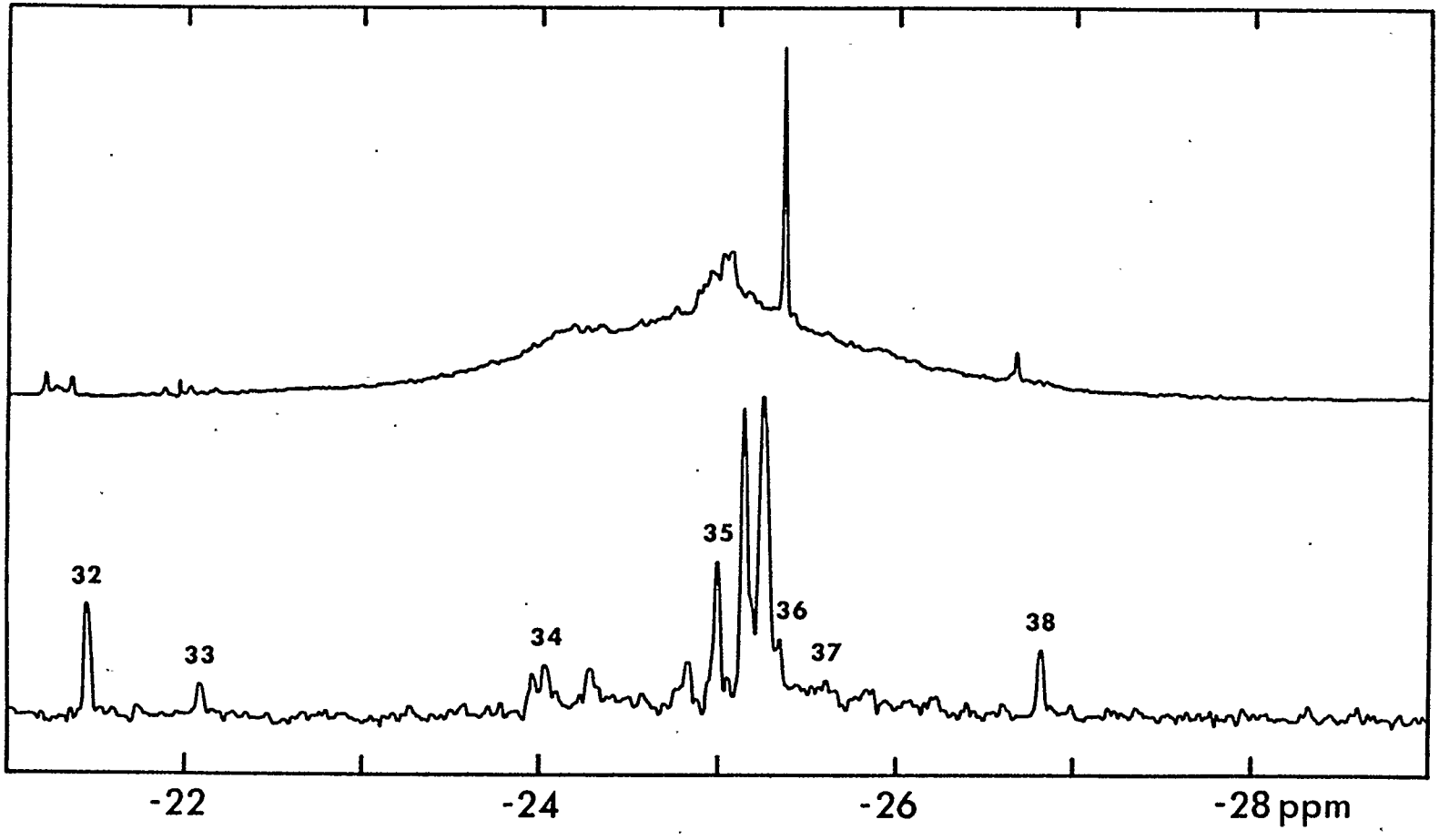

Figure 2-4c. As Figure 2-4a.

Table II-III. Relative ^{29}Si Line Positions and Some Controlling Factors.

Line	Species	Connectivity	Rings containing the Si nucleus		Adjoining SiO_4 tetrahedra			Effect on $\|\Delta S\|$[a,b] of increased	
			3-ring	4-ring	Q^1	Q^2	Q^3	Temp.	Conc.[c]
1	I (Q^0)	Q^0							
3	IV						1	0	-
4	III	Q^1				1		-	-
6	II ($Q^1{}_2$)				1			-	-
7	VIII		1				2	+	+
8	IV		1			1	1	+	+
9	V ($Q^2{}_3$)		1			2		+	+
12	VI			2			2	+	+
13	XVIII	Q^2		2			2	+	+
15	IX			1			2	-	
16	X ($Q^2{}_4$)			1		2		-	-
19	VIII			1		1	1		
22	III				2			0	-
20	IX		1	2			3	+	
23	VIII		1	1		2	1	+	
24	XI ($Q^3{}_6$)		1	2			3	+	+
25	IX		1	2		1	2	+	
29	IV		1		1	2		+	
32	XVIII	Q^3		3		1	2	+	+
33	VI			3		3		+	+
35	IX			2		2	1	+	
36	($Q^3{}_z$)[d]						3	+	-
38	XVII ($Q^3{}_8$)			3			3	+	-

[a] $|\Delta\delta|$ is the absolute ppm separation from the monomer resonance. [b] For solutions with $Na^+:Si^{IV}$ = 1:1. [c] At concentrations >1.0 mol kg^{-1} Si. [d] Identified in this report as the tetrahedral tetramer ($Q^3{}_4$).

In accordance with previous studies[15,43,52], it would appear that all ^{29}Si resonances move upfrequency ("downfield") as alkalinity is increased. For instance, a rise in the $Na^+:Si^{IV}$ ratio from 1:1 to 4:1 in solutions which were otherwise identical (samples 38 and 40; see Table II-IV) caused the monomer peak to shift upfrequency about 0.4 ppm relative to the transmitter signal. Figure 2-5 demonstrates that all the other resonances moved towards the monomer peak, and that the order of relative upfrequency shifts was: $Q^0 < Q^2{}_3 < Q^2{}_4 < Q^1{}_2$.

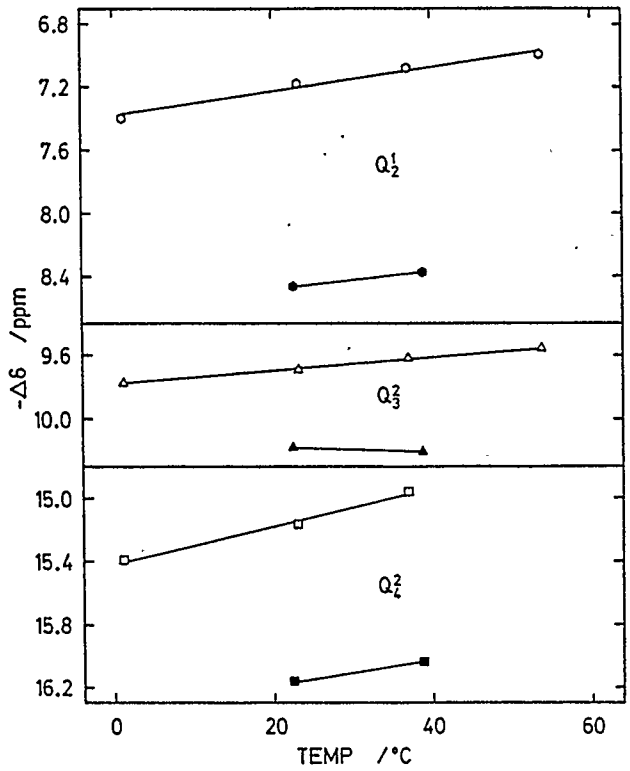

Figure 2.5. Temperature dependence of ^{29}Si line positions relative to the respective Q^0 signals for sample 38 with $Na^+:Si^{IV}$ = 1:1 (closed symbols) and sample 40 with $Na^+:Si^{IV}$ = 4:1 (open symbols); each 2.17 mol kg^{-1} in Si.

Table II-IV. Temperature Dependence of ^{29}Si Signals in Solutions which contain 2.2 mol kg^{-1} Si.

Temp /°C	$(\nu_{rf} - \nu_{Q0})^a$ /Hz	$\lvert\Delta\delta\rvert$/ppm[b] $Q^1{}_2$	$Q^2{}_3$	$Q^2{}_4$
a. Sample 33 (Na^+:Si^{IV} = 1.0:1)				
3.3	-1677.6	8.633	10.182	16.166
15.2	-1683.8	8.568	10.189	16.118
22.4	-1687.9	8.515	10.181	16.073
30.6	-1692.6	8.472	10.187	16.044
38.8	-1696.7	8.425	10.189	16.026
55.0	-1704.2			15.983
68.0	-1710.6			
b. Sample 34 (Na^+:Si^{IV} = 4.0:1)				
3.3	-1701.4	7.219	9.779	15.262
23.1	-1711.3	7.105	9.672	15.025
37.2	-1718.0	6.995	9.586	
53.2	-1724.2	6.900	9.510	
65.4	-1730.0	6.842	9.464	
83.2	-1736.5	6.757	9.420	
100.8	-1742.4	6.692	(9.346)	
113.8	-1748.7	6.676		
131.5	-1750.0	6.710		
c. Sample 34 Using Nicolet 300				
-3.0	91.9	7.271	9.823	
8.6	83.8	7.197	9.765	15.197
22.9	78.2	7.123	9.699	15.047
39.0	70.0	7.038	9.617	
48.3	64.9	6.992	9.574	
d. Sample 38 (Na^+:Si^{IV} = 1.0:1)				
22.4	-1694.3	8.478	10.190	16.166
38.8	-1701.9	8.390	10.202	16.042
61.5	-1709.6			

Table II-IV. (Continued)

Temp /°C	$(\nu_{rf} - \nu_{Q0})^a$ /Hz	$\lvert\Delta\delta\rvert$/ppm[b] $Q^1{}_2$	$Q^2{}_3$	$Q^2{}_4$
e. Sample 39 (K^+:Si^{IV} = 4.0:1)				
3.3	-498.6	7.156	9.700	15.080
14.5	-500.7	7.136	9.700	15.057
23.1	-502.2	7.127	9.707	15.042
37.2	-505.8	7.102	9.711	
53.2	-508.8	7.083	9.708	
100.8	-519.2	7.059	9.723	
f. Sample 40 (Na^+:Si^{IV} = 4.0:1)				
1.0	-1700.5	7.299	9.768	15.388
23.1	-1711.2	7.192	9.693	15.171
37.2	-1715.7	7.077	9.621	14.958
53.2	-1721.9	6.992	9.554	
74.3	-1731.2	6.875	9.463	
100.8	-1739.5	6.769	9.396	
g. Sample 41 (Rb^+:Si^{IV} = 4.0:1)				
1.0	-481.1	7.230	9.685	15.206
14.5	-483.7	7.208	9.700	15.169
23.1	-483.2	7.164	9.687	15.139
37.2	-489.0	7.178	9.722	15.112
53.2	-493.4	7.157	9.738	15.088
74.3	-489.1	7.142	9.753	
100.8	-501.9	7.092	9.745	

[a] Frequency difference between transmitter and Q^0 ^{29}Si signals. The value depends on spectral width and transmitter offset, and has a typical uncertainty of ±0.3 Hz. [b] Uncertainty typically ±0.003 ppm.

As temperature was raised, the ^2H signals recorded for samples 39 to 41 each moved downfrequency approximately 11 to 12 Hz/100 K (see Table II-V and Figure 2-6). These results were employed in Eqn. 2.9 to determine the temperature dependence of the ^{29}Si resonances. As exemplified in Figure 2-7, all ^{29}Si signals moved upfrequency with rising temperature. The relative order of line displacement was $Q^0 < Q^2_3 < Q^1_2 < Q^2_4$ (see also Figure 2-8).

Table II-V. Temperature Dependence of ^2H Lock Signal[a,b].

Temp /°C	50% ^2H_2O	Sample 39	Sample 40	Sample 41
3.2	-6.3	0	.	.
11.2	-9.2	-1.1	.	.
21.2	-12.9	-2.4	.	.
26.2	.	-3.2	-2.7	-5.6
41.2	-19.0	-4.9	-4.8	-7.6
62.1	-24.7	-7.1	-7.1	-10.3
81.3	-29.3	-9.3	-9.5	-12.6
96.5	-32.6	-10.6	-11.2	-13.9

[a] In Hz with uncertainty ±0.3 Hz. [b] All signals referenced to the ^2H signal position for sample 39 at 3.2°C.

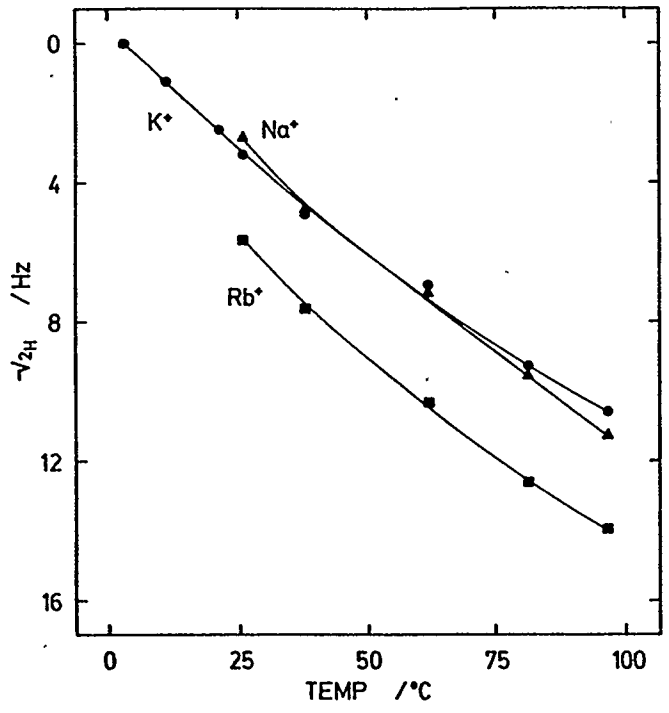

Figure 2-6. Temperature dependence of ^2H signals for samples 39 (M = K), 40 (M = Na) and 41 (M = Rb). All signals are referred to the signal position for sample 39 at 3.2°C.

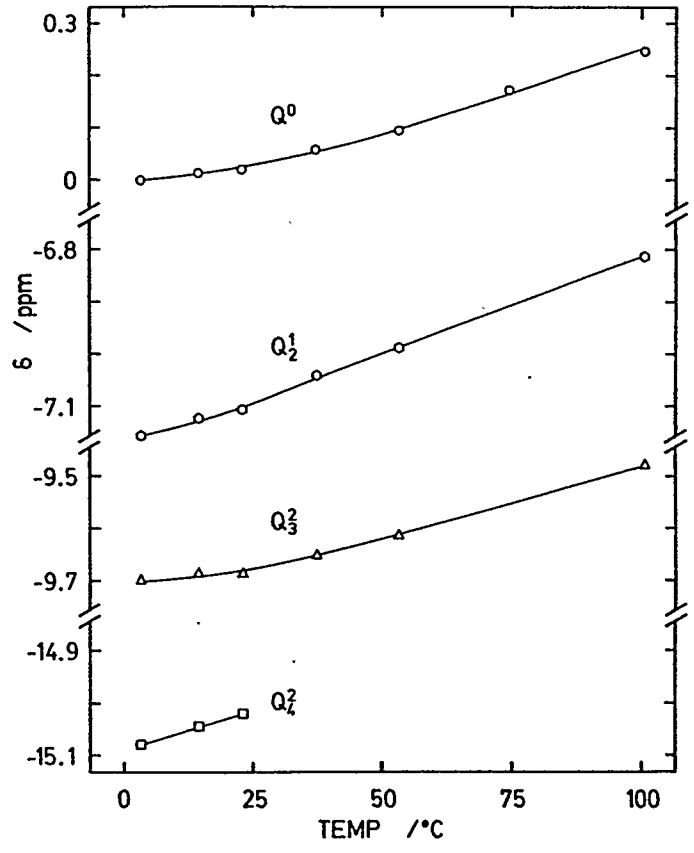

Figure 2-7. Temperature dependence of all ^{29}Si resonances for sample 39 with 2.17 mol kg^{-1} Si and $K^+:Si^{IV}$ = 4.0:1. Signals are referred to the Q^0 position at 3.3°C.

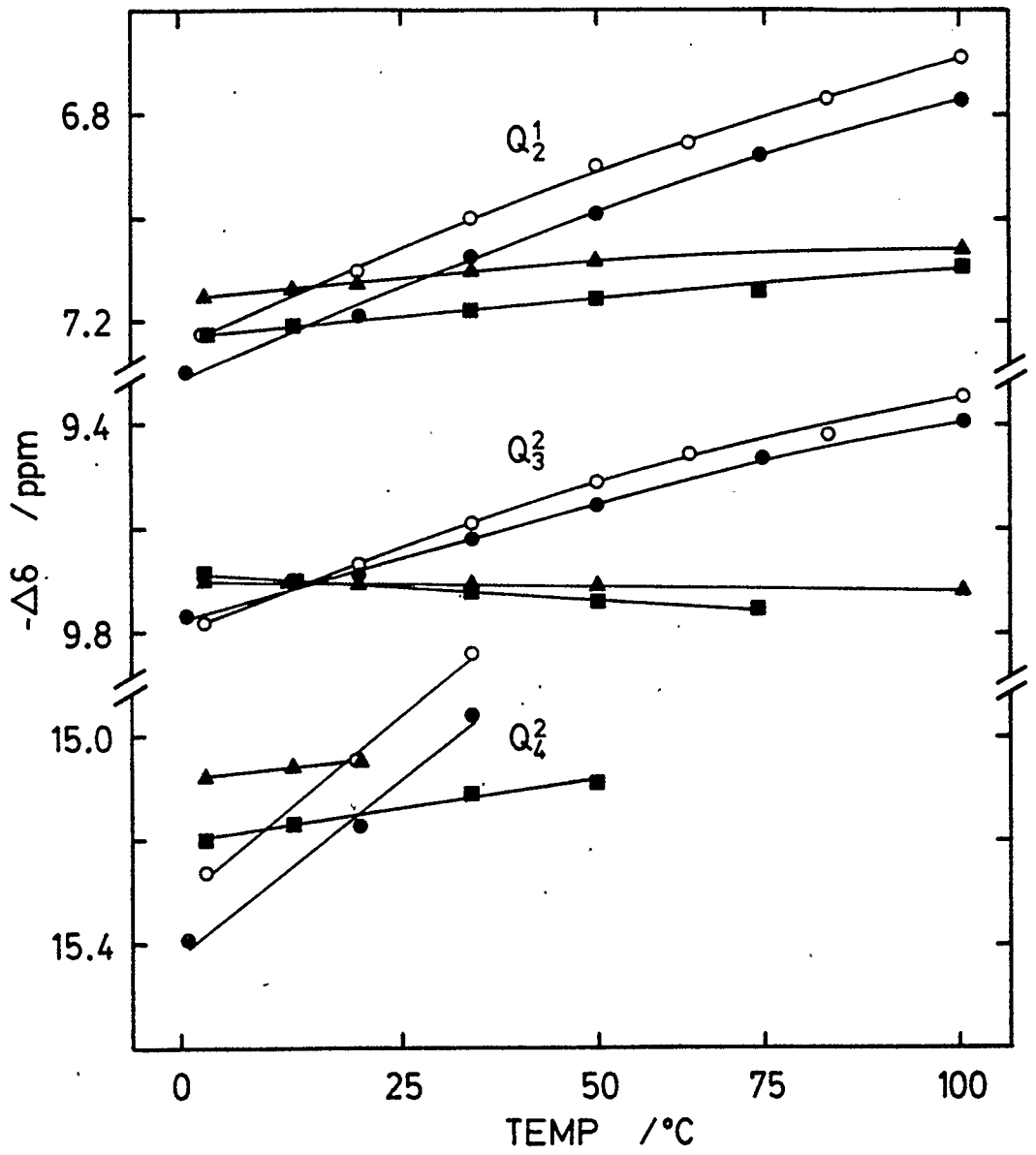

Figure 2-8. Temperature dependence of ^{29}Si line positions relative to the Q^0 signal for samples 34 (○) and 40 (●) with M = Na, sample 39 (▲) with M = K, and sample 41 (■) with M = Rb. All solutions contain 2.2 mol kg^{-1} Si and $M^+:Si^{IV}$ = 4.0:1. Sample 34 is 99% ^2H-enriched while all others are 75% ^2H-enriched.

In Table II-VI, line positions relative to the Q^0 resonance (= $\Delta\delta$) are listed for 15 of the signals observed in spectra of solutions with $Na^+:Si^{IV}$ = 1.0:1. Figure 2-9 illustrates that as temperature is raised, lines situated in the Q^1 and Q^2_B regions advance towards the monomer signal, while Q^2_A and all Q^3 resonances move away (summarized in Table II-III).

The silicon-29 chemical shift was also influenced by sample concentration, as illustrated in Figure 2-10. In very dilute solutions with $Na^+:Si^{IV}$ = 1.0:1, a small rise in Si concentration causes $\Delta\delta$ to decrease for all lines except the Q^3_6 resonance. Above 0.6 mol kg^{-1} Si, $\Delta\delta$ continues to decrease for Q^1, Q^2_B, and Q^3_B resonances, while it increases for lines in the Q^2_A and Q^3_B regions (see Table II-III). There was no common reference signal in these samples with which to determine the concentration dependence of the monomer peak. However, Harris and Knight[52] reported that the monomer signal moves upfrequency as the Si concentration is increased at constant $Na^+:Si^{IV}$ ratio.

The very precise chemical shift measurements which were conducted for samples 39 to 41 (Table II-IV) revealed a dependence on the alkali-metal cation. Figure 2-11 shows that the Q^0 resonance resonates at progressively lower frequencies for M^+ = Na^+, K^+ and Rb^+, and Figure 2-8 indicates that the other resonances are shifted even further downfrequency. The relative order of line displacement is: $Q^0 \leqslant Q^2_3 < Q^1_2 \leqslant Q^2_4$. The same cation dependence is apparent in Figure 2-12 for the numerous resonances observed at low alkalinity (samples 18 to 20).

Table II-VI. Temperature Dependence of $|\Delta\delta|^{a,b}$ for Solutions with $Na^+:Si^{IV}$ = 1.0:1.

Temp /°C	Line 3	4	6	7	8	9	12	13	16	22	24	32	33	36	38
a. Sample 3 (1.75 mol kg^{-1} Si)															
-5.6	8.174	8.252	8.753	9.848	9.850	10.186	14.229		16.294		17.037	21.277	21.954	25.344	
-3.8	8.173	8.240	8.749	9.849	9.850	10.185	14.231	14.475	16.291	16.596	17.048	21.287	21.956	25.374	26.666
1.2	8.171	8.234	8.721	9.847	9.856	10.187	14.238	14.489	16.275	16.560	17.085	21.317	(21.957)	25.437	26.691
6.2	8.168	8.228	8.698	9.858	9.863	10.193	14.244	15.505	16.259	16.598	17.123	21.347	21.976	25.496	26.719
11.2		(8.213)	8.674	9.865	9.868	10.193	14.255	14.521	16.244	16.598	17.164	21.377	21.983	25.554	26.741
16.2			8.646	9.865	9.873	10.193	14.257	14.536	16.223	16.598	17.198	21.404	21.989	25.606	25.764
21.2			8.624	9.877	9.879	10.191	14.264	14.547	16.205	(16.576)	17.230	21.429		25.654	26.782
26.6			8.587	9.872	9.877	10.190	14.273	14.569	16.187		17.264	21.457	22.001	25.701	26.809
31.2			8.565	9.879	9.883	10.192	14.284	14.576	16.167		17.291	21.484	22.010	25.742	26.827
46.2			8.523				(14.293)	14.591	(16.151)		17.368	21.529	22.019	(25.841)	(26.865)
51.2								(14.596)	(16.128)		17.414	21.566	22.038	(25.930)	
71.2											17.585				
b. Sample 4 (1.40 mol kg^{-1} Si)															
-3.8	8.182	8.268	8.778	9.853	9.841	10.175	14.229	14.469	16.316	16.616	17.008	21.269	21.946	25.393	26.683
1.2	8.180	8.258	8.753	9.845	9.849	10.179	14.238	14.486	16.300	16.623	17.048	21.303	21.959	25.458	26.704
11.2	8.178	8.238	8.698	9.854	9.863	10.182	14.250	14.515	16.266	16.617	17.125	21.365	21.975	25.575	26.756
21.2		8.202	8.649	9.868	9.874	10.186	14.226	14.555	16.237	16.621	17.199	21.427	21.995	25.680	
31.2			8.593	9.877	9.882	10.186	14.273	14.581	16.207	(16.554)	17.268	21.481	22.019	25.772	
51.2			(8.475)	(9.903)		(10.187)	14.294	(14.594)	16.130		17.377	21.564	22.037		
71.2											17.487				
c. Sample 5 (0.93 mol kg^{-1} Si)															
-3.8	8.184	8.285	8.809	9.828	9.835	10.163	14.229	14.475	16.355		16.959			25.435	26.708
11.2			8.734			10.178			16.311		17.089			25.627	
31.2			8.637			10.184			16.262		17.238			25.826	
51.2			8.529			10.182			16.212		17.372				
71.2			(8.427)						(16.162)						

Table II-VI. (Continued)

Temp /°C	Line 3	4	6	7	8	9	12	13	16	22	24	32	33	36	38
d. Sample 6 (0.70 mol kg^{-1} Si)															
-3.8	8.208	8.307	8.837	9.825	9.827	10.156	14.240	14.479	16.395		16.952	21.256	21.940	25.480	26.741
1.2	8.210	8.294	8.808	9.831	9.840	10.160	14.254	14.506	16.380		16.971	21.299	21.955	25.553	26.773
11.2		(8.280)	8.763			10.175	14.284	14.549	16.362		17.070	21.378	21.994	25.686	26.843
21.2		(8.236)	8.707			10.182	14.301	14.590	16.335		17.153	21.452	22.024	25.793	26.890
31.2			8.646			10.179	14.320	14.624	16.308		17.232	21.518	22.056	25.892	(26.935)
51.2			8.535			10.166	14.367	14.710	16.268		17.374	21.646	22.137	26.059	
61.2			8.470			10.151	(14.428)	(14.778)	(16.283)		17.426			26.129	
e. Sample 7 (0.35 mol kg^{-1} Si)															
-3.8	8.223	8.315	8.852	9.829	9.832	10.151	14.259	(14.350)	16.430	(16.643)	16.916	21.278	21.953	25.555	26.785
1.2	8.224	8.316	8.826	9.843	9.851	10.160	14.278	14.531	16.424	(16.654)	16.967	21.322	21.976	25.627	26.825
11.2	8.231	8.294	8.777	9.858	9.871	10.171	14.303	14.575	16.407	(16.671)	17.058	21.400	22.014	25.752	26.887
21.2		8.278	8.727	9.876	9.892	10.179	14.328	14.615	16.391		17.145	21.481	22.050	25.862	26.944
31.2			9.669	(9.879)	(9.909)	10.179	14.347	14.645	16.367		17.221	21.554	22.082	25.952	
46.2			8.595			10.187			16.351		17.340	(21.636)		26.092	
61.2			8.508						(16.339)		17.442				
f. Sample 8 (0.18 mol kg^{-1} Si)															
1.2	8.269	8.338	8.859	9.859	9.864	10.163	14.321	(14.407)	16.517	(16.819)	16.945	21.362	22.016	25.744	26.909
11.2	(8.262)	8.325	8.809	(9.889)	9.895	10.179	14.365		16.517		17.062	(21.389)	22.071	25.885	26.987
21.2		8.292	8.760	9.898	9.919	10.186	14.401		16.510		17.159		(22.117)	26.006	27.057
31.2		(8.276)	8.711		9.954	10.193			16.501		17.249			26.106	27.093
46.2			8.637			10.193			16.502		17.358			26.246	
61.2			8.581			10.201			16.481		(17.437)				
g. Sample 9 (0.04 mol kg^{-1} Si)															
1.2			8.937			10.216					16.834				
21.2			8.860			10.253					(16.842)				
31.2			(8.822)												

a $\Delta\delta$ is the ppm shift relative to the Q^0 signal. b Uncertainty is typically ± 0.003 ppm.

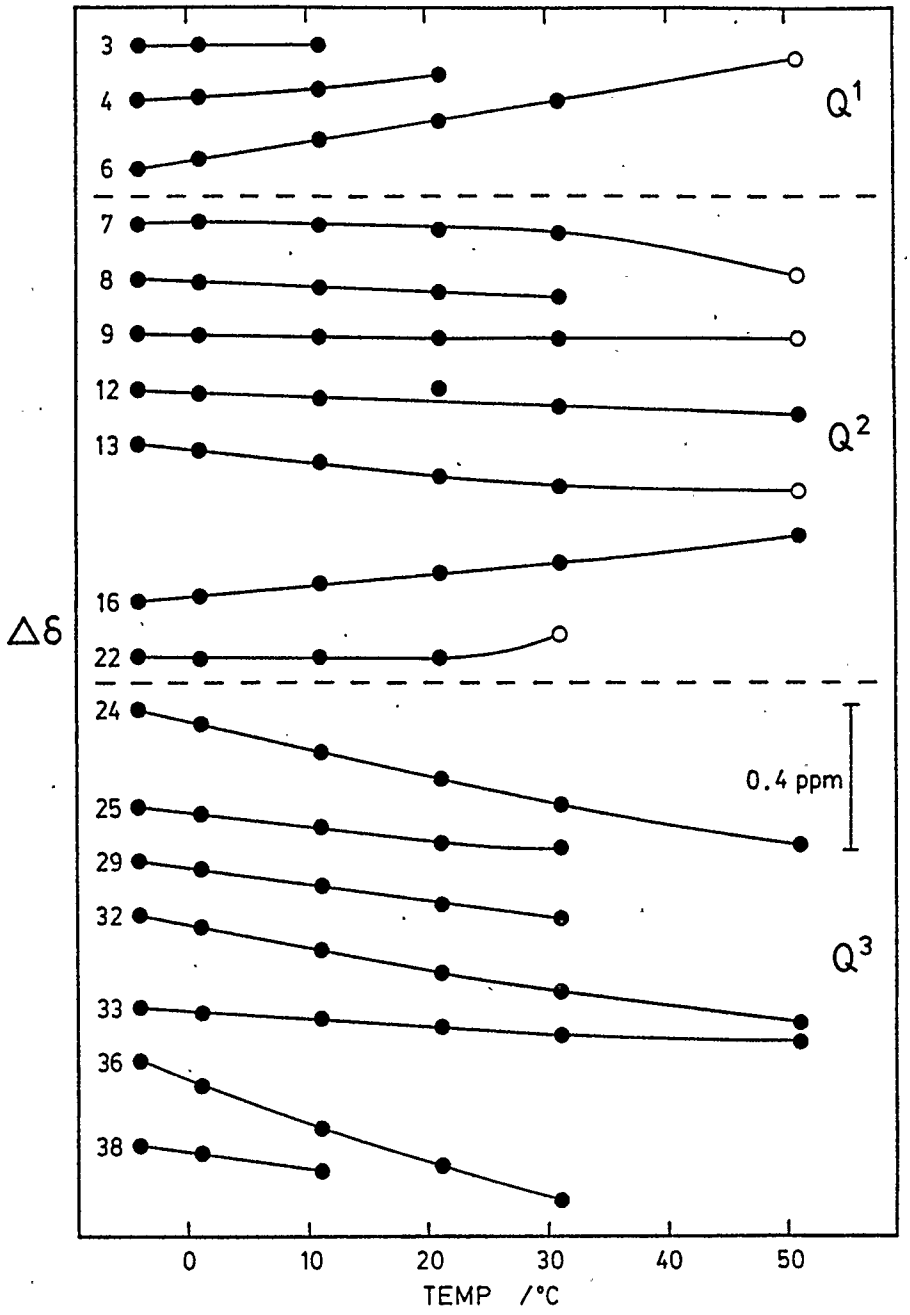

Figure 2-9. Temperature dependence of ^{29}Si line positions (labelled in accordance with Table II-I) relative to the Q^0 signal for sample 4 which contains 1.40 mol kg^{-1} Si with $Na^+:Si^{IV}$ = 1.0:1. The $\Delta\delta$ scale for temperature dependence is shown. The relative signal positions are not represented to scale. Open symbols signify less certain assignments.

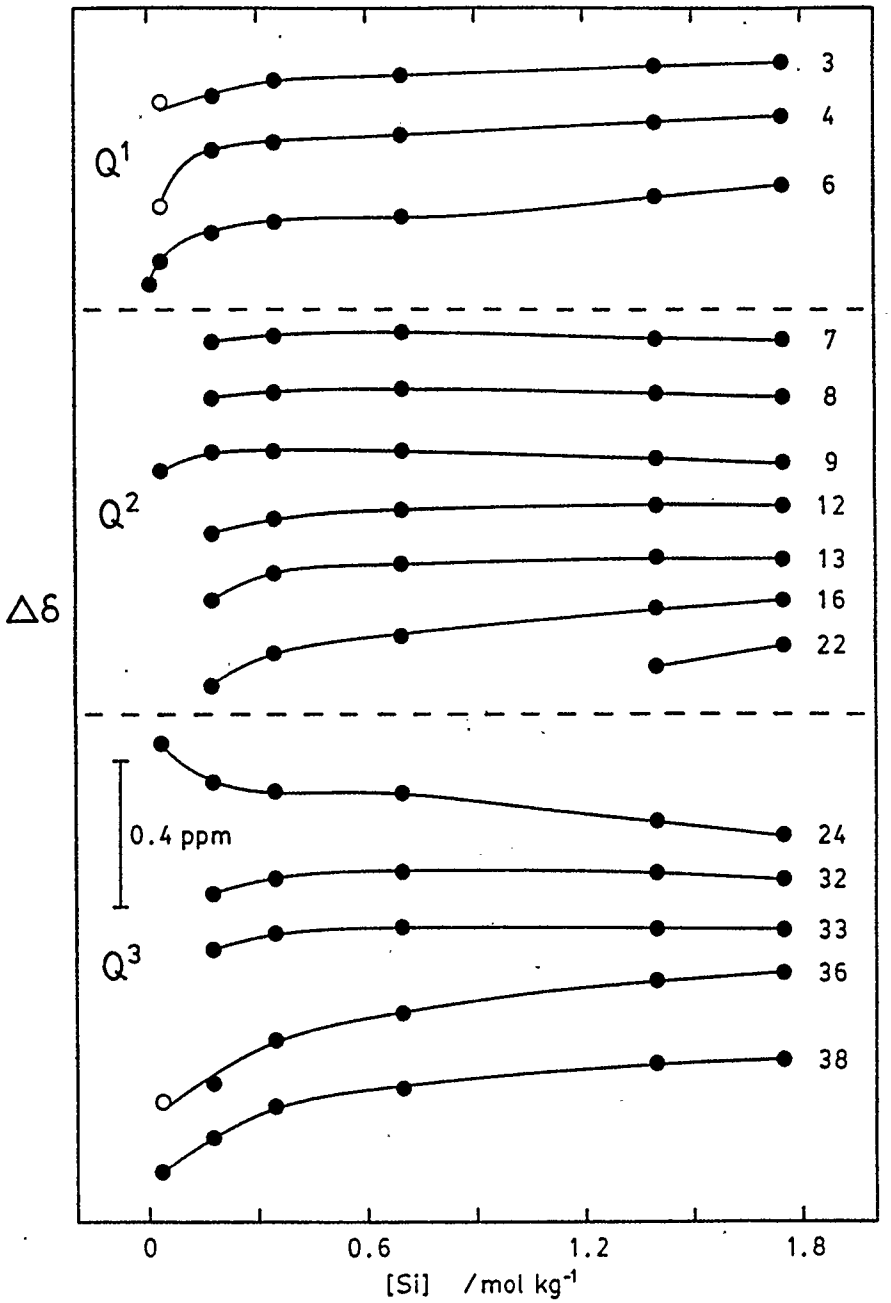

Figure 2-10. Si concentration dependence of ^{29}Si line positions (labelled in accordance with Table II-I) relative to the Q^0 signal at 11.2°C for samples 3 to 10, each with $Na^+:Si^{IV}$= 1.0:1. The $\Delta\delta$ scale is shown. The relative signal positions are not represented to scale. Open symbols signify less certain assignments.

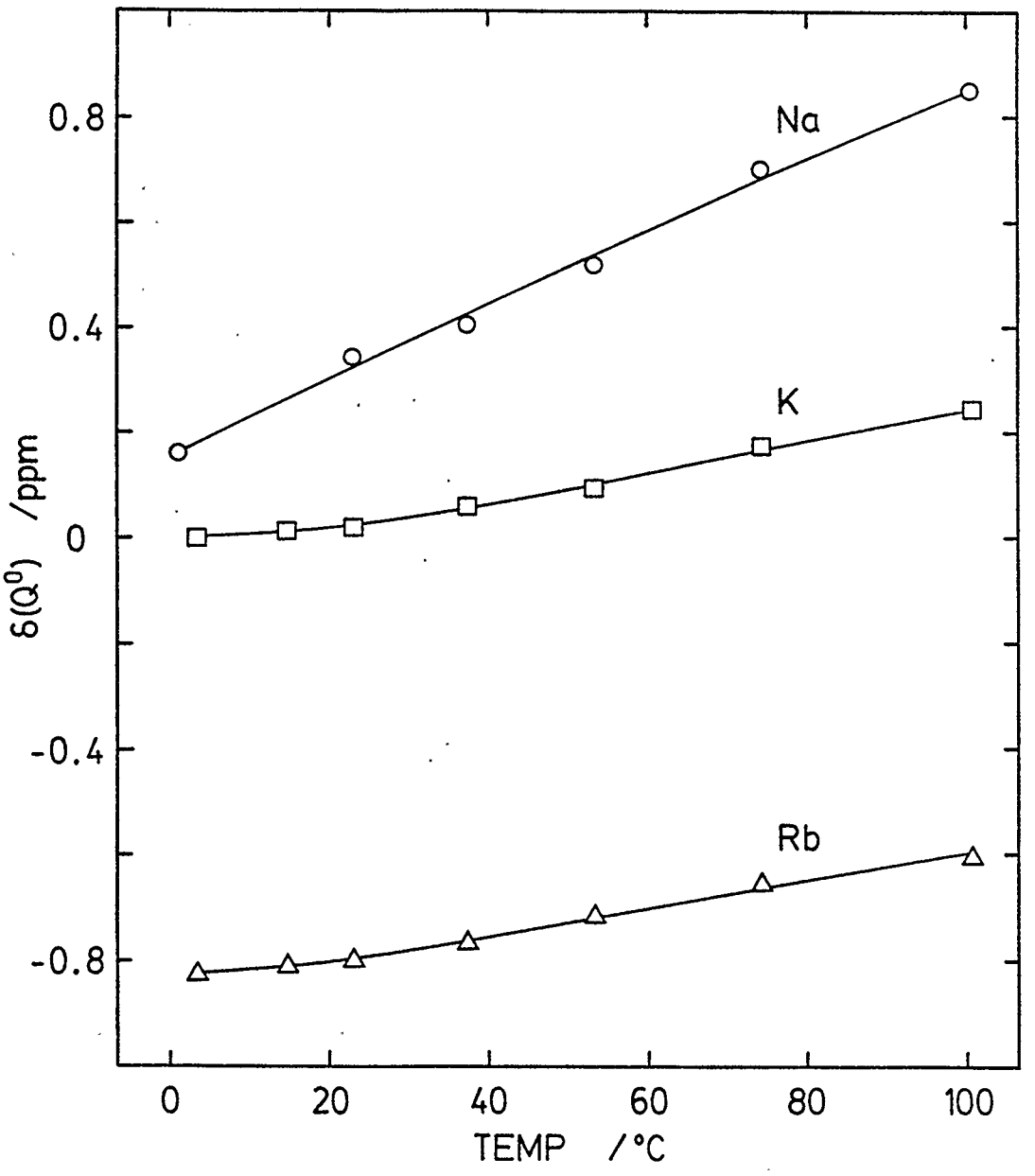

Figure 2-11. Absolute temperature dependence of Q^0 signal for samples 39 (M = K), 40 (M = Na) and 41 (M = Rb); all 2.2 mol kg^{-1} in Si with $M^+:Si^{IV}$ = 4.0:1. Signals are referred to the Q^0 position for sample 39 at 3.3°C.

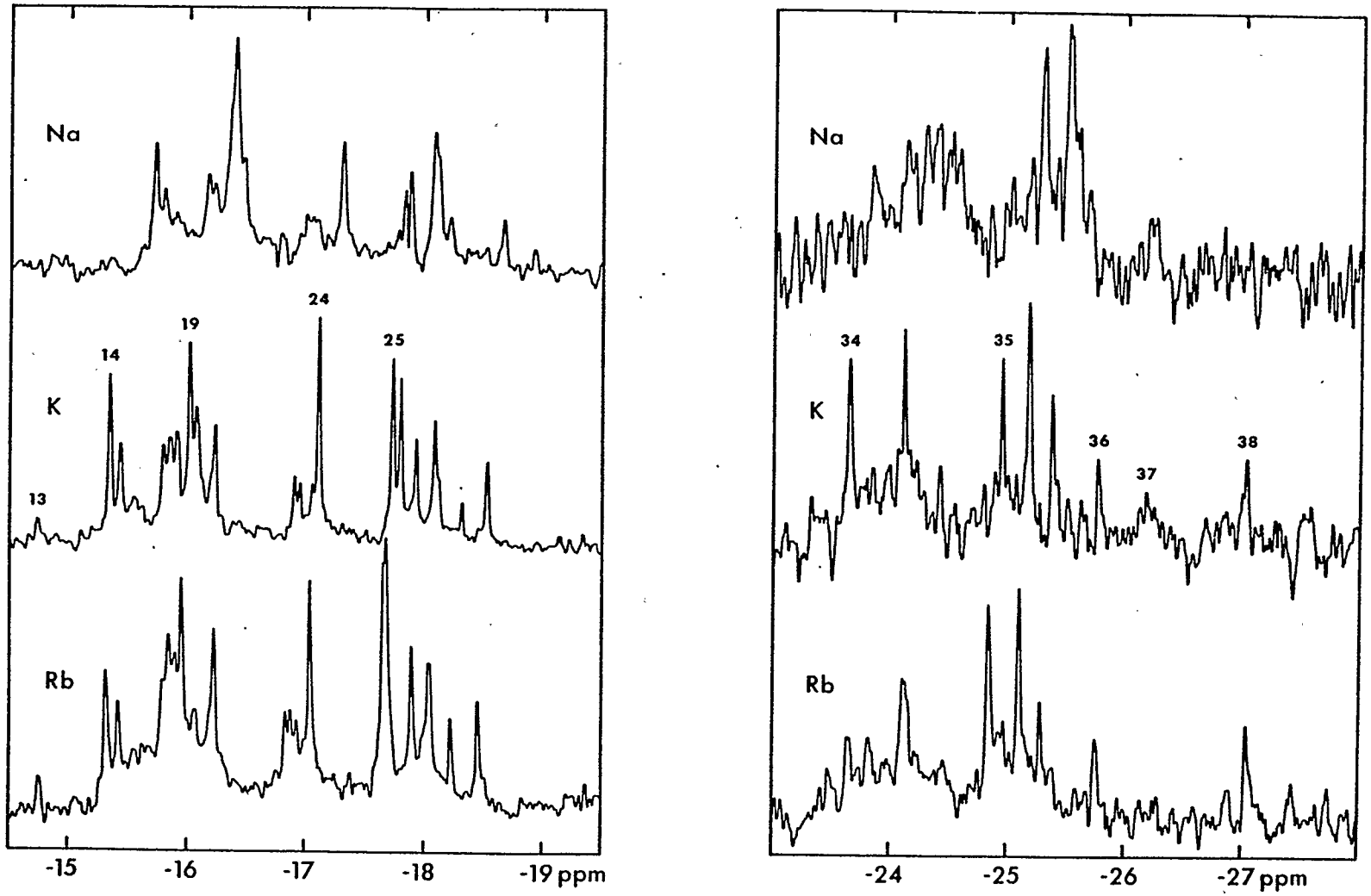

Figure 2-12. ^{29}Si NMR spectra of samples 18 (M = Na), 19 (M = K) and 20 (M = Rb), all of which contain 1.8 mol kg^{-1} Si with $M^{+}Si^{IV}$ = 1.5:1. Spectra include 0.6 Hz artifical linebroadening.

Table II-VII. Correlation of ^{29}Si Shielding with structure and solution conditions.

Factor increased	Overall response observed[a]	Nuclei most affected	Expected Contribution[a,b] σ_{local}^{p}	σ_{intra}^{e}	σ_{inter}^{M}	σ_{inter}^{H}
local connectivity	+	high local connectivity	+	+		
Occurrence in ring units	-	in 3-ring	-	-		
Adjacent Connectivity	-	low adjacent connectivity	-	-		
$M^+:Si^{IV}$	-	in least strained species	-[c]	(-)	-	(-)
Concentration[d]	-				-	
Atomic wt of M^+	-			(-)	-	
% ^2H enrich.	-					-
% ^{29}Si enrich.	-	in small species	-	-		
Temperature	-	in least rigid species (?)	+?	-	(-)	(+)

[a] Increased, +, or decreased, -, shielding. [b] Brackets signify minor contribution. [c] Due to deprotonation of coordinated hydroxy groups. [d] $M^+:Si^{IV}$ ratio constant.

Interestingly, Figures 2-8 and 2-11 reveal that the temperature dependence of shifts is significantly greater for $M^+ = Na^+$, than for $M^+ = K^+$ or Rb^+.

Other factors which influenced chemical shift include the isotopic concentrations of ^2H and ^{29}Si. Raising the deuterium content from 74 to 99% (samples 34 and 40; see Table II-IV) caused all lines to move upfrequency. Figure 2-8 shows that the relative displacement was $Q^0 < Q^2{}_3 < Q^1{}_2 < Q^2{}_4$. An increase in ^{29}Si content from 4.7 to 95.1% (samples 38 and 33; see Table II-IV) shifted the monomer signal (with respect to ν_{rf}) 0.16 ppm upfrequency at 22°C and 0.13 ppm at 38°C. Figure 2-4 indicates that ^{29}Si-enrichment produced a net upfrequency shift of varying magnitude for most resonances, with lines corresponding to the large cage structures being least affected.

All of the preceding observations are summarized in Table II-VII.

An additional, although unexpected, influence on ^{29}Si ppm chemical shifts was the external magnetic field B_o (see Table II-IV). Figure 2-13 indicates that signals recorded for sample 34 at 7.10 T (on the Nicolet 300) were less temperature dependent than those obtained at 4.70 T (on the Varian XL200), and that the change of temperature dependence varied slightly between resonances.

2.3.2. Discussion

The most important factor influencing ^{29}Si shifts is the local degree of silicate connectivity (Q^y), which is responsible for the fundamental ca. 8.5 ppm separation between major signal groupings. One might expect that, since Si has a lower electronegativity than H [68], increased connectivity at the resonating nucleus should lead to an in-

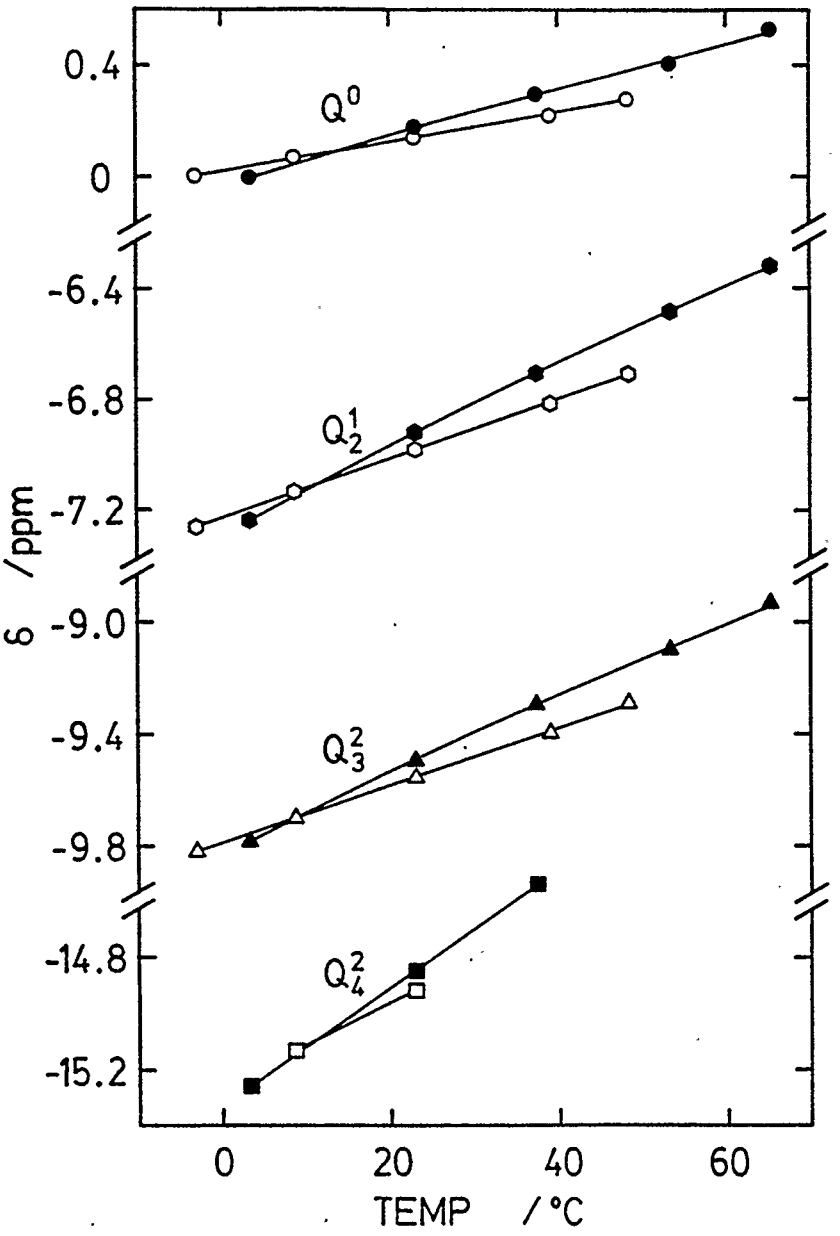

Figure 2-13. Absolute temperature dependence of ^{29}Si line positions for sample 34 with 2.17 mol kg^{-1} Si and $Na^+:Si^{IV}$ = 4.0:1. Signals are referred to the Q^0 position at 3.3°C for B_0 = 4.70 T (closed symbols), and to the Q^0 position at -3°C for B_0 = 7.10 T (open symbols).

ductive increase in σ_{local}^{p} deshielding. However, increased connectivity actually results in a downfrequency shift and, therefore, in enhanced shielding. This would suggest that the extraordinarily strong Si-O bond (arising from (d-p)π-character ?) results in higher group electronegativities for -OSi than for -OH (Eqn. 2.1 yields 4.0 and 3.6 respectively; see Table II-VIII). Although Eqn. 2.2 was derived for solid silicates and probably overextends the concept of electronegativity in any case, SiOSi bond angles obtained from it may be indicative of the true values for aqueous silicate anions. Indeed, angles calculated for the unsplit ^{29}Si resonances seem to support the structural assignments of Harris and Knight[52,53] (Table II-VIII).

Table II-VIII. Predicted Group Electronegativities and Bridging Bond Angles.

Line	δ/ppm[a]	ΣEN[b]	(-R) EN	SiOSi Angle[c]
1 (Q^0)	-71.3	14.41	(-OH) 3.60[d]	-
6 (Q^1_2)	-80.12	14.77	($-Q^1$) 3.97	143
9 (Q^2_3)	-81.44	14.82	($-Q^2$) 3.81	121
16 (Q^2_4)	-87.78	15.08	($-Q^2$) 3.94	139
24 (Q^3_6)	-88.25	15.10	($-Q^3$) 3.72	109
36 (Q^3_Z)	-97.01	15.46	($-Q^3$) 3.95	140
38 (Q^3_8)	-98.16	15.51	($-Q^3$) 3.97	143

[a] Chemical shifts for sample 14 at -5°C with respect to the reported[55] tetramethylsilane signal position. [b] Sum of group electronegativities calculated from Eqn. 2.1. [c] Bridging bond angle calculated from Eqn. 2.2. [d] Assumed to be constant for all subsequent species.

The next most prominent shielding influence revealed in Table II-III is the presence of the resonating nucleus in a cyclic building unit which causes an upfrequency shift from the fundamental 8.5 ppm spacing pattern. For example, Q^2 nuclei situated in a 4-ring resonate slightly upfrequency from the Q^2 signal of the acyclic trimer, while those occurring simultaneously in two 4-rings resonate even further upfrequency in the Q^2_B subregion. Lines which are shifted far into the Q^2_A subregion all correspond to nuclei found in 3-rings. A similar trend is apparent in Table II-III for the Q^3 resonances. Theoretical calculations have shown that the 3-ring is highly strained compared with the 4-ring, which in turn, is more strained than acyclic species[67]. The smaller SiOSi bridging angles and the longer Si-O bonds arising from molecular strain[67] will be associated with less efficient overlap between σ_{SiO}- bonding orbitals (and/or between π-bonding orbitals) and will lead to enhanced $\sigma_{local}{}^{p}$ deshielding. In addition, strain intensifies the repulsive interactions between the high electron densities of hydroxy groups on adjacent silicons[76] and, therefore, may reduce the effective electronegativity of these ligands (and the π-character of Si-OH bonds ?) resulting in $\sigma_{intra}{}^{e}$ deshielding.

In Table II-III, the relative distribution of lines 3 to 6, 7 to 9, and 15 to 22 indicates that shielding is further reduced by high connectivity at <u>adjoining</u> SiO_4 tetrahedra. Molecular models demonstrate that "high-Q" substituents are bulky and increase molecular strain, which, as in the preceding case, will result in $\sigma_{local}{}^{p}$ and possibly $\sigma_{intra}{}^{e}$ deshielding influences.

At high alkalinity, the deprotonation of hydroxy groups will increase the paramagnetic deshielding (σ_{local}^{p}) at coordinated silicon nuclei. As suggested previously[15,42,53], ionization is therefore an important factor contributing to the dependence of chemical shift on the $M^+:Si^{IV}$ ratio. Unfortunately line shifts cannot be used alone to determine the relative ease of ionization because it is impossible to isolate deprotonation from all the other shielding influences affected by the $M^+:Si^{IV}$ ratio (e.g., silicate-M^+ ion-pairing).

Line shifts arising from ^{29}Si-enrichment are probably caused by changes induced in the vibrational and rotational molecular states and, therefore, in σ_{local}^{p} and σ_{intra}. The effect is understandably smallest for "high-Q" centres of large oligomers because these are motionally restricted.

Anisotropic contributions to shielding σ_{intra}^{a} and σ_{inter}^{a} can probably be disregarded for these relatively compact, rapidly tumbling anions, especially since no evidence was found of shielding-anisotropy contributions to longitudinal relaxation (Ch. IV).

Changes in solution composition affected ^{29}Si shielding to an extent sometimes approaching that of minor structural differences (up to 1 ppm). Raising the $M^+:Si^{IV}$ ratio, concentration, atomic weight of M^+, or the level of ^{2}H-enrichment all led to similar upfrequency shifts (see Table II-VII). For the 4 simplest symmetrical species, the relative order of line displacement ($Q^0 \leq Q^2_3 \leq Q^1_2 \sim Q^2_4$) coincides with that of predicted group electronegativities (Table II-VIII) which correlate in turn with the SiOSi bond angle. This apparent dependence on "molecular strain" is further exemplified in Figure 2-10 by the correlation between

the concentration dependence of $\Delta\delta$ for each resonance and the relative displacement from the fundamental 8.5 ppm spacing pattern.

The difference between the various line displacements which were induced by increased $M^+:Si^{IV}$ ratio or by increased M^+ concentration (at a fixed $M^+:Si^{IV}$ ratio) indicates that the $\sigma_{inter}{}^{M}$ shielding contribution varies significantly between nuclei. Similarly, since deuterium enrichment resulted in variable line shifts, silicate...H_2O hydrogen-bonding and, therefore, $\sigma_{inter}{}^{H}$ also must vary between silicate centres. At least some of the total shielding difference between ^{29}Si nuclei can thus be attributed to an inequality in the tendency towards intermolecular encounters. On this basis one would expect that the chemical shift dependence on the nature of the M^+ cation is due to an increase from Na^+ to K^+ to Rb^+ in the silicate-M^+ ion-pair formation constant K_{IP}. However, crude Fuoss-type calculations[92] indicate that K_{IP} is nearly the same (6-7 L mol^{-1}) for the Na^+-, K^+-, and Rb^+-$H_3SiO_4^-$ pairs and, therefore, any increase in ion-pairing is probably very small.

Detailed consideration of the effect of temperature on chemical shift may be unwarranted since the Varian XL200 and the Nicolet 300 spectrometers inexplicably gave significantly different temperature dependencies (see below). Temperature is in any event the most difficult influence on chemical shift to interpret because it will affect <u>all</u> contributions to nuclear shielding. Of these, the influence on σ_{local} is most important yet it is also the most difficult to anticipate because of its complex nature. The relative order of upfrequency line shifts (Figures 2-7 to 2-9) is not easily related to any one structural parameter. Signals corresponding to oligomers with low rigidity seem to

be preeminently affected, however, while the Q^0 signal is shifted least of all. This would suggest that temperature dependent deshielding is enhanced by unhindered flexibility of the SiOSi moiety, which may, in part, be due to greater interaction between hydroxy groups (σ_{intra}^{e}). In accordance with the Fuoss equation[92], M^+ and silicate ions spend more time in close proximity as temperature is raised, and, therefore, increased σ_{inter}^{M} may account for much of the deshielding observed. Additionally, ^{29}Si spin-site exchange (discussed in Ch. III) will cause all lines to be drawn slightly towards the weighted centre of the spectrum as temperature is raised.

The change observed in the temperature dependence of ppm chemical shifts at different magnetic field strengths (Figure 2-13) would appear to be a real effect since: (i) temperature was carefully determined for both spectrometers; (ii) shift differences far exceed digitization uncertainty; and (iii) the variation in temperature dependence is not the same for all resonances. However, an actual dependence of ppm chemical shift on magnetic field would defy the fundamental concepts of nuclear shielding (Eqns. 2.3 and 2.4) and, therefore, differences observed are likely to be an instrumental artifact. Incongruent thermal expansion of the two rf coils could not account for the apparent field dependence because only the intensity of the free induction decay would be affected. If the magnetic susceptibility of the components in each probehead is not equal, however, thermal expansion would influence the field inside each probehead differently. The temperature dependence of the monomer line position (measured from 0 to 50°C) differed between the two spectrometers by 0.004 ppm K^{-1}. Because the monomer resonance was

referred to the temperature corrected ^{2}H signal, this represents a change in relative field strength of approximately 0.02 ppm K^{-1} (= 16 Hz K^{-1}/9 MHz for the XL200) which is rather large to have arisen from magnetic susceptibility differences. At present, no satisfactory explanation of these findings can be offered, especially one that can account for the variation in temperature dependence being different for different resonances.

The numerous lineshift measurements which have been compiled for the known silicate structures can be used to aid in the identification of new species. For instance, resonances assigned [52,53] to the 6 tentative structures shown in Table II-I conform quite well to the shielding patterns established in Tables II-III and II-VII. Presumably, the relative line positions corresponding to species XIII and XIV arise from repulsion between the Q^2 groups in the cisoid configuration (σ_{local}^{p} and σ_{intra}^{e} deshielding). Assignments proposed for species XV and XVI are consistent with molecular orbital calculations[67] which indicate that the 5-ring is slightly less strained than the 4-ring.

Line 36 is an unsplit resonance situated in the Q^3_B subregion at $\Delta\delta \sim -25.6$ ppm and, thus, represents a completely symmetric silicate anion consisting of z magnetically equivalent Q^3 centres (Q^3_z). Although Harris' group once attributed this signal to the Q^3_8 anion[50,53], it is unassigned at present. Of all the resonances monitored, line 36 was displaced least upfrequency as temperature was raised and most upfrequency with increased concentration (Figures 2-9 and 2-10). In accordance with the shift patterns established above (see Tables II-II and II-VII), this signifies that line 36 represents an exceptionally un-

strained, rigid molecule. Ball and stick models indicate that Q^3_z structures with $z > 10$ are quite flexible and, because of steric interactions (primarily O...O repulsion), they are probably very strained as well. Symmetric species with $z = 6$ and 8 are already known, and those with $z = 1$, 2, 3, 7 and 9 are not physically possible. The strained double 5-ring (Q^3_{10}) anion has been tentatively identified ($\Delta\delta$ = -26.5 ppm), but only in a solution containing tetrapropylammonium cations and dimethyl sulphoxide[65].

This leaves Q^3_4 (Structure XIX), i.e. $Si_4O_{10}^{4-}$, which models show to be very rigid. Although the structure consists entirely of 3-rings, the tetrahedral configuration maintains the unstrained OSiO angle of the orthosilicate anion and achieves maximum separation between hydroxy groups. There can be little doubt, therefore, that line 36 corresponds to a silicate structure with adamantane-like geometry. This structure is otherwise unknown in any silicate phase, although the $H_4Si_4S_6$ analogue has been synthesized and found to be very stable[93].

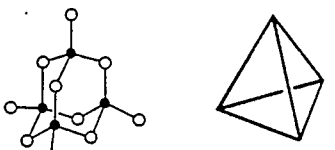

Structure XIX

2.4. Silicate Equilibria

2.4.1. Results

Figure 2-14 demonstrates that the proportion of resonances which corresponds to high-connectivity Q-centres decreases sharply as the $M^+:Si^{IV}$ ratio is raised above 1:1. Hence, increased alkalinity causes silicate anions to depolymerize.

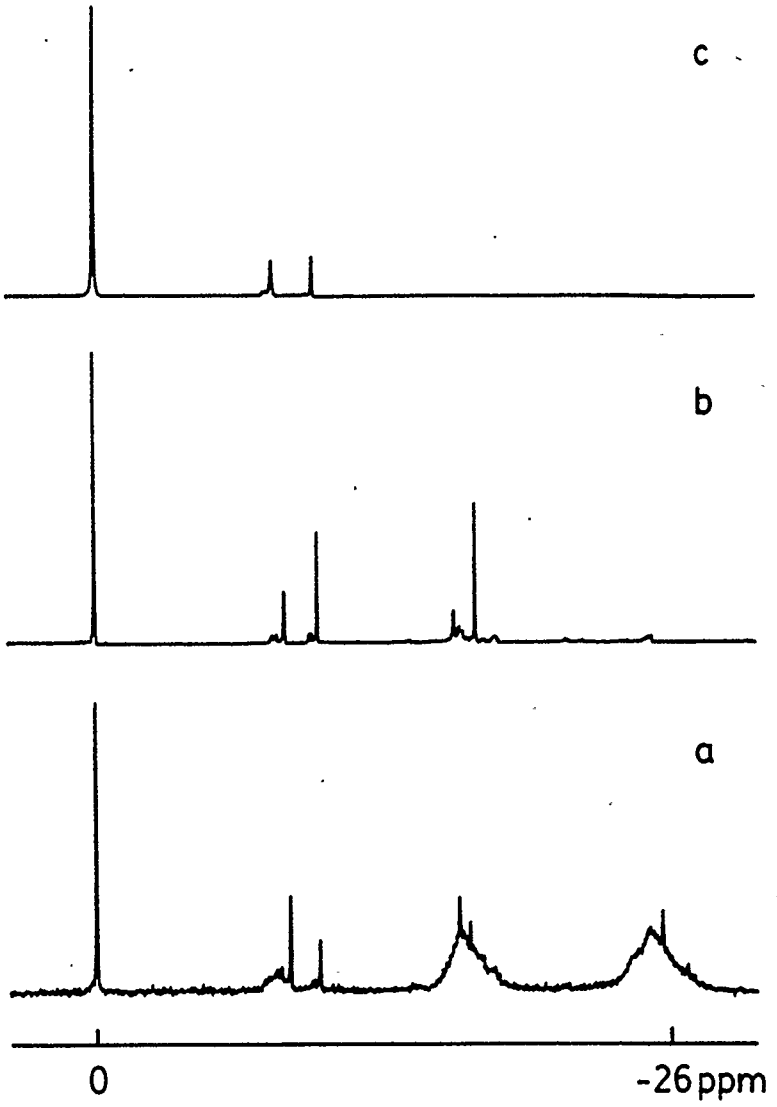

Figure 2-14. ^{29}Si NMR spectra at 7.4°C of (a) sample 42 with 0.30 mol kg^{-1} Si and $Na^+:Si^{IV}$ = 1.0:1, (b) sample 16 with 0.23 mol kg^{-1} Si and $Na^+:Si^{IV}$ = 2.3:1, and (c) sample 14 with 0.28 mol kg^{-1} Si and $Na^+:Si^{IV}$ = 5:1. Spectra contain 0.1 Hz artificial linebroadening.

Unfortunately, the integration of individual resonances is rarely possible because of signal overlap, temperature dependent linebroadening (see Ch. III) and ^{29}Si spin-spin coupling in enriched solutions. Nevertheless, the equilibrium distribution of silicate anions can be monitored in terms of the 6 spectral regions defined in Figure 2-2 (Q^0, Q^1, $Q^2{}_A$ $Q^2{}_B$, $Q^3{}_A$ and $Q^3{}_B$). Accordingly, Table II-IX contains a list of integrations obtained for 106 representative spectra (of 16 samples).

Data presented in Figure 2-15 indicate that condensation equilibria shift in favour of the monomer and low molecular weight species as temp-

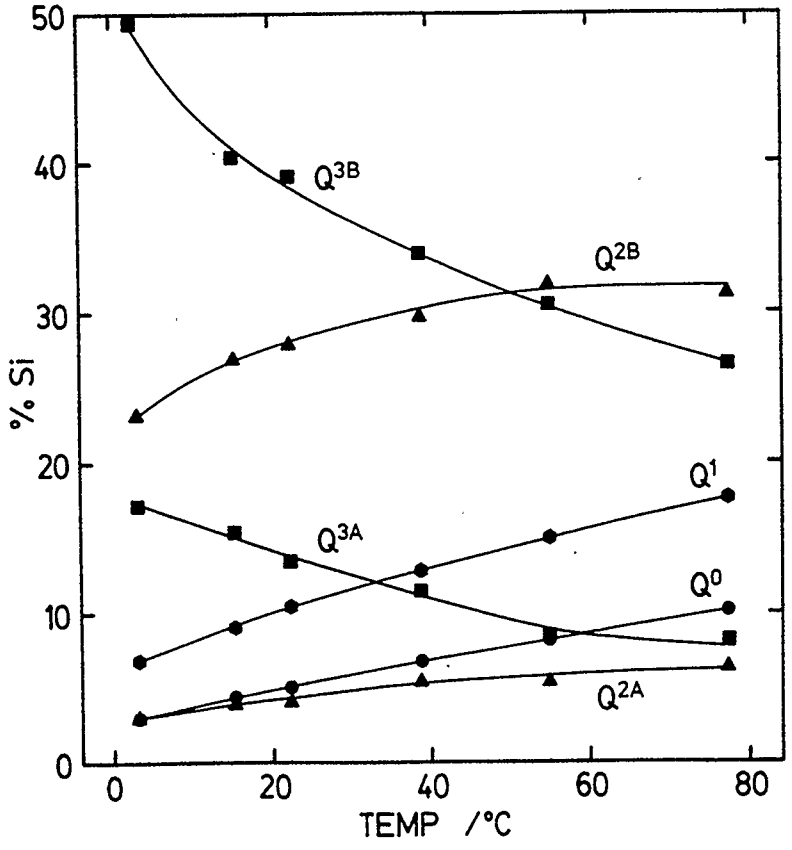

Figure 2-15. Temperature dependence of spectral integration for sample 37 which contains 0.80 mol kg^{-1} Si with $Na^+:Si^{IV}$ = 1.0:1.

Table II-IX. Spectral Integration (% Si)[a] for Solutions with $M^+:Si^{IV}$ = 1:1 and 4:1.

Temp/°C	Q^0	Q^1	Q^2_A	Q^2_B	Q^3_A	Q^3_B
a. Sample 3 (1.75 mol kg^{-1} Si; $Na^+:Si^{IV}$ = 1.0:1)						
-5.6	1.4	4.5	1.8	24.0	22.2	46.2
-3.8	1.6	6.7	2.7	23.8	19.7	45.5
1.2	1.8	7.7	2.8	25.8	17.2	44.8
6.2	2.0	8.4	2.9	28.3	15.3	43.0
11.2	2.4	9.1	3.6	26.6	18.5	39.8
16.2	2.8	10.3	3.9	28.6	15.3	39.2
21.2	2.9	10.6	4.2	27.4	18.0	36.9
26.6	3.0	11.4	4.3	28.4	15.8	37.1
31.2	3.1	12.0	4.2	28.4	15.3	37.0
41.2	3.5	12.8	4.5	30.0	13.3	35.8
51.2	3.8	13.4	4.8	30.2	13.5	34.3
71.2	4.6	14.7	4.7	33.4	11.5	31.1
b. Sample 4 (1.40 mol kg^{-1} Si; $Na^+:Si^{IV}$ = 1.0:1)						
-3.8	2.6	7.0	2.8	24.2	17.6	45.8
1.2	2.8	7.3	2.9	24.9	18.4	43.6
11.2	2.8	8.7	3.0	28.5	15.5	41.5
21.2	3.2	9.5	4.5	26.4	17.7	38.6
41.2	4.9	12.2	5.1	28.9	14.8	34.1
61.2	5.6	15.1	5.2	30.6	9.5	34.0
91.2	6.9	15.7	4.9	32.3	11.8	28.3
c. Sample 6 (0.70 mol kg^{-1} Si; $Na^+:Si^{IV}$ = 1.0:1)						
-3.8	3.9	8.1	3.4	24.8	17.2	42.6
1.2	4.4	8.9	3.1	25.0	16.6	42.0
11.2	5.7	10.2	4.0	25.8	15.9	38.3
21.2	7.1	12.3	4.4	27.5	13.1	35.7
31.2	7.7	13.3	5.1	29.1	11.1	33.6
51.2	9.5	16.2	4.7	30.3	8.6	30.7
61.2	11.1	17.8	6.0	30.0	8.4	26.8
81.2	12.9	19.3	4.9	28.1	7.9	26.9

Table II-IX. (Continued)

Temp/°C	Q^0	Q^1	$Q^2{}_A$	$Q^2{}_B$	$Q^3{}_A$	$Q^3{}_B$
d. Sample 7 (0.35 mol kg^{-1} Si; $Na^+:Si^{IV}$ = 1.0:1)						
-3.8	5.9	8.5	3.4	25.2	14.7	42.4
1.2	6.7	9.6	3.5	25.9	14.5	39.8
11.2	8.5	11.4	4.9	24.6	15.8	34.8
21.2	9.7	13.0	4.7	26.7	11.8	34.1
31.2	10.5	14.8	4.6	28.7	8.1	33.4
46.2	12.1	17.1	4.9	28.8	6.8	30.3
61.2	14.8	18.4	4.5	28.5	6.1	27.8
81.2	17.7	20.0	5.5	27.0	6.5	23.4
e. Sample 8 (0.18 mol kg^{-1} Si; $Na^+:Si^{IV}$ = 1.0:1)						
1.2	11.2	10.9	4.2	23.5	15.0	35.2
11.2	13.9	14.3	4.6	24.7	10.3	32.2
21.2	17.2	16.2	4.8	25.0	8.4	28.4
31.2	17.6	17.4	(10.0)	(17.0)	8.2	29.8
46.2	21.7	19.4	4.6	24.5	6.5	23.3
61.2	25.1	20.0	6.2	21.0	8.4	19.5
81.2	29.2	22.2	4.7	20.1	5.3	18.6
f. Sample 9 (0.04 mol kg^{-1} Si; $Na^+:Si^{IV}$ = 1.0:1)						
1.2	41	16	——— 19 ———		——— 23 ———	
g. Sample 26 (2.79 mol kg^{-1} Si; $K^+:Si^{IV}$ = 3.8:1)						
65.4	52.5	30.8	13.8	3.6	0.7	
83.2	53.7	30.6	10.7	4.6	0.8	
113.8	57.9	29.8	9.0	2.5	0.5	
131.5	59.0	30.9	6.5	3.1	0.6	
140.0	58.0	31.9	7.0	2.7	0.5	
144.2	61.2	30.1	4.6	2.8	0.6	
h. Sample 33 (2.17 mol kg^{-1} Si; $Na^+:Si^{IV}$ = 1.0:1)						
3.3	1.7	6.3	4.4	30.4	19.8	37.5
15.2	2.4	8.5	5.2	31.2	17.9	34.8
22.4	2.6	9.3	5.6	33.8	16.1	32.6
30.6	3.1	10.3	6.0	32.4	16.6	31.7
38.8	3.9	13.1	7.4	35.3	14.3	26.0
55.0	4.5	13.2	7.1	34.8	13.2	27.3
68.0	5.3	16.4	8.6	36.2	10.8	21.8

Table II-IX. (Continued)

Temp/°C	Q^0	Q^1	$Q^2{}_A$	$Q^2{}_B$	$Q^3{}_A$	$Q^3{}_B$
i. Sample 34 (2.17 mol kg^{-1} Si; $Na^+:Si^{IV}$ = 4.0:1)						
3.3	58.9	20.9	18.1	1.2	0.9	
23.1	60.4	23.0	13.9	2.1	0.6	
37.2	60.3	22.8	13.2	3.1	0.6	
53.2	59.9	27.2	9.0	3.0	0.9	
65.4	56.3	28.7	9.2	5.1	0.6	
83.2	55.6	28.9	10.9	4.0	0.7	
100.8	56.6	31.1	7.7	4.2	0.5	
j. Sample 35 (1.55 mol kg^{-1} Si; $Na^+:Si^{IV}$ = 1.0:1)						
3.3	2.1	7.0	4.2	27.8	20.6	38.4
15.2	2.5	8.2	4.4	30.3	16.9	37.8
22.4	2.8	9.5	4.9	32.1	15.8	34.9
38.8	4.5	12.8	6.7	32.5	15.5	28.0
55.0	5.4	14.8	7.0	32.2	14.0	26.6
68.0	5.4	15.3	6.7	34.0	10.8	27.9
86.7	6.3	17.9	7.0	32.9	11.3	24.7
102.5	7.6	20.3	8.6	30.8	11.7	21.0
k. Sample 36 (1.20 mol kg^{-1} Si; $Na^+:Si^{IV}$ = 1.0:1)						
3.3	2.3	7.6	3.6	26.6	18.6	41.3
22.4	3.9	9.7	5.1	30.0	15.7	35.6
38.8	5.5	12.6	5.2	31.1	13.2	32.4
68.0	7.0	15.9	6.2	32.5	10.2	28.2
102.5	9.0	18.5	6.8	32.0	8.6	25.1
l. Sample 37 (0.80 mol kg^{-1} Si; $Na^+:Si^{IV}$ = 1.0:1)						
3.3	2.9	7.0	2.9	23.2	17.2	49.8
15.2	4.3	9.1	3.9	26.9	15.4	40.4
22.4	4.9	10.5	4.1	27.9	13.5	39.1
38.8	6.7	12.8	5.4	29.7	11.5	33.9
55.0	8.1	15.0	5.4	32.5	8.5	30.4
77.4	10.1	17.6	6.4	31.2	8.2	26.5

Table II-IX. (Continued)

Temp/°C	Q^0	Q^1	$Q^2{}_A$	$Q^2{}_B$	$Q^3{}_A$	$Q^3{}_B$
m. Sample 39 (2.17 mol kg^{-1} Si; $Na^+:Si^{IV}$ = 4.0:1)						
3.3	48.9	23.4	22.9	2.4	2.4	
14.5	48.7	23.6	22.5	2.8	2.4	
23.1	49.6	25.2	18.9	3.4	2.9	
37.2	52.0	25.0	16.6	5.3	1.1	
53.2	55.8	24.5	14.0	4.3	1.4	
74.3	51.6	30.1	12.3	4.4	1.6	
100.8	55.7	28.7	11.2	2.7	1.7	
n. Sample 40 (2.17 mol kg^{-1} Si; $Na^+:Si^{IV}$ = 4.0:1)						
1.0	60.2	21.1	15.9	1.5	1.3	
23.1	58.8	23.7	14.2	2.5	0.9	
37.2	60.8	25.4	10.8	2.2	0.9	
53.2	59.0	28.0	8.6	3.6	0.8	
74.3	56.3	30.4	8.0	4.3	1.0	
100.8	55.9	31.3	6.7	5.6	0.6	
o. Sample 41 (2.17 mol kg^{-1} Si; $Na^+:Si^{IV}$ = 4.0:1)						
1.0	43.9	23.8	26.5	3.7	2.1	
23.1	48.0	24.6	22.3	3.3	1.8	
37.2	47.3	26.8	19.4	4.6	1.9	
53.2	48.5	27.2	17.0	4.9	2.4	
74.3	51.8	28.3	15.4	3.4	1.1	
100.8	51.2	29.7	12.9	5.3	1.0	
p. Sample 42 (0.30 mol kg^{-1} Si; $Na^+:Si^{IV}$ = 1.0:1)						
3.3	6.1	8.1	2.8	20.8	14.7	47.5
22.4	10.8	11.6	3.4	21.3	13.3	40.0
38.8	13.1	15.0	4.2	25.7	9.4	32.6
55.0	12.4	14.3	3.0	21.5	11.9	37
68.0	15.1	16.5	3.2	20.9	13.0	31.4

[a] Typical uncertainties range from ±5% (of integration value) at low temperature to ±10% at highest temperatures.

erature is raised. Despite significant structural differences represented by the wide frequency separation, the temperature dependence of the Q^2_A and Q^2_B integrations is quite similar, as it is for the Q^3_A and Q^3_B centres.

Figure 2-16 reveals that depolymerization is also favoured by sample dilution. At 0.01 mol kg^{-1} Si (sample 10; Figure 2-17), only the monomer and a trace of dimer can be detected despite a $M^+:Si^{IV}$ ratio of 1:1.

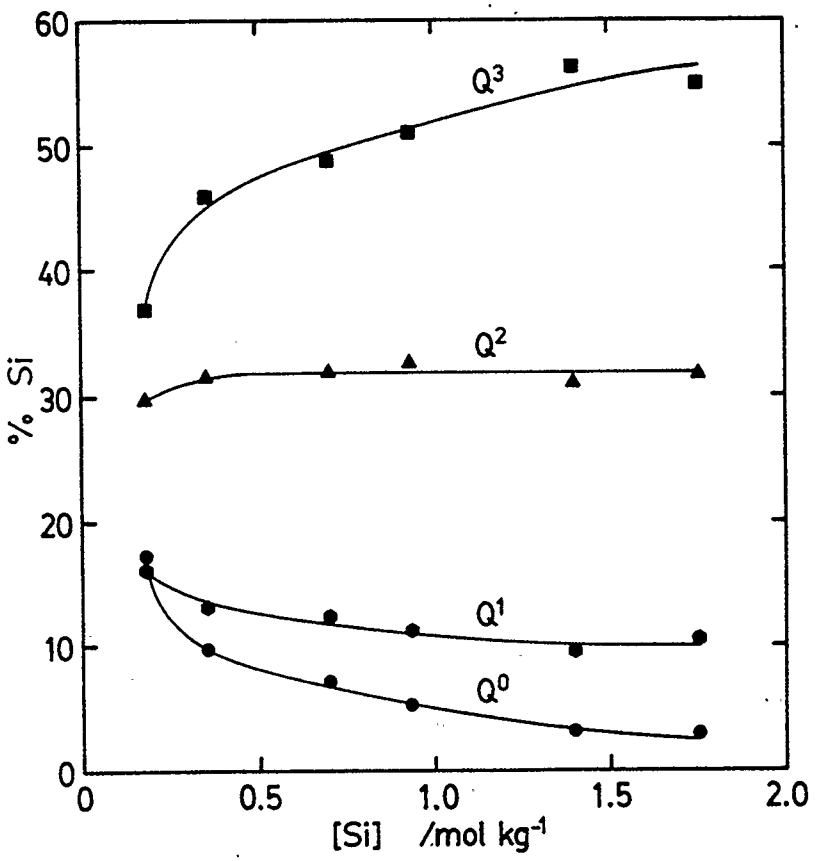

Figure 2-16. Si concentration dependence of spectral integration at 21.2°C for samples 3 to 8 for which $Na^+:Si^{IV}$ = 1.0:1.

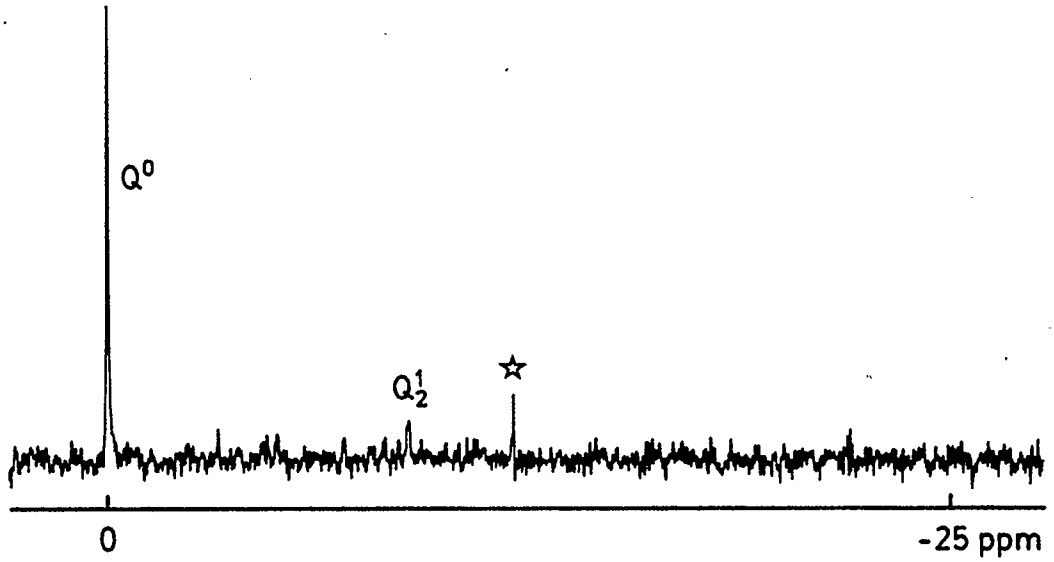

Figure 2-17. ^{29}Si NMR spectrum at 22.4°C of sample 10 which contains 0.01 mol kg^{-1} Si with $Na^+:Si^{IV}$ = 1.0:1. Recycle time = 70 s. Number of acquisitions = 1000. Artificial linebroadening = 0.5 Hz. Transmitter signal respresented by *.

Spectra in Figures 2-18 and 2-19 would suggest that the alkali-metal cation has no major influence on the distribution of silicate anions at any alkalinity. However, Figure 2-20 indicates that small changes did occur for solutions with 2.2 mol kg^{-1} Si and $M^+:Si^{IV}$ = 4.0:1. Substitution of Na with K, and then Rb, caused oligomer concentrations to be enhanced at the expense of the monomer. Concentration differences were relatively small at 100°C but increased at lower temperatures. At 5°C, the proportional changes in abundance when Na was replaced with Rb were roughly -26% for Q^0, +13% for Q^1, +50% for Q^2_A and +140% for Q^2_B. Although spectra of low alkalinity solutions are too

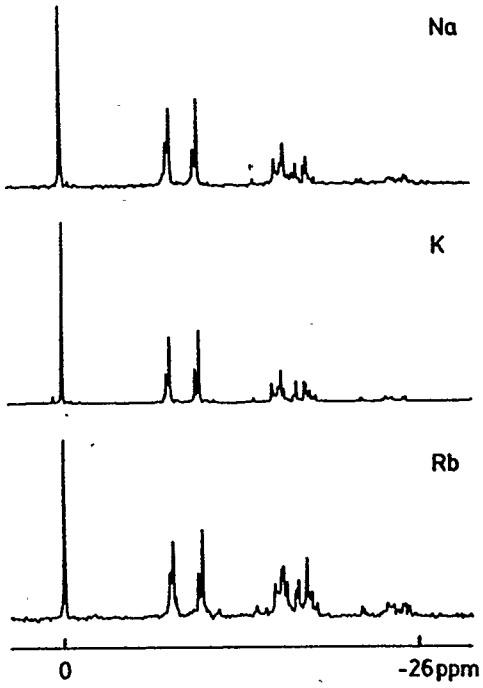

Figure 2-18. ^{29}Si NMR spectra at 30.6°C of samples 18 (M = Na), 19 (M = K) and 20 (M = Rb), all containing 1.8 mol kg^{-1} Si with $M^{+}:Si^{IV}$ = 1.5:1. Relatively low intensity of the Q^2 and Q^3 peaks for sample 19 is due to insufficient recycling time. Artificial linebroadening = 1.0 s.

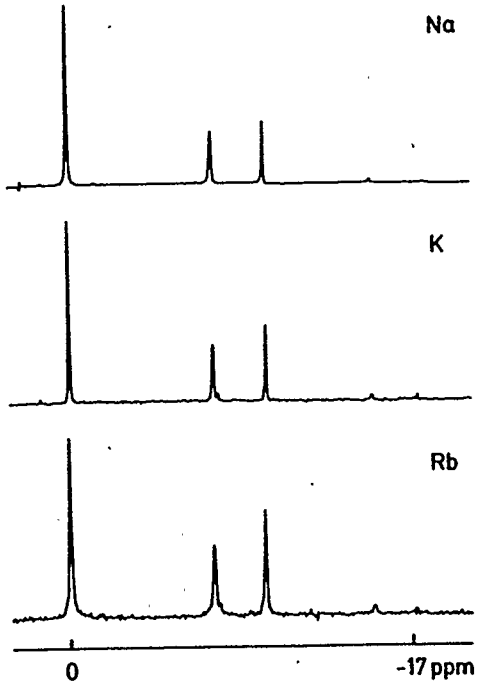

Figure 2-19. ^{29}Si NMR spectra at 23.1°C of samples 34 (M = Na), 39 (M = K) and 41 (M = Rb), all containing 2.2 mol kg^{-1} Si with $M^{+}:Si^{IV}$ = 4.0:1. Artificial line-broadening = 0.5 s.

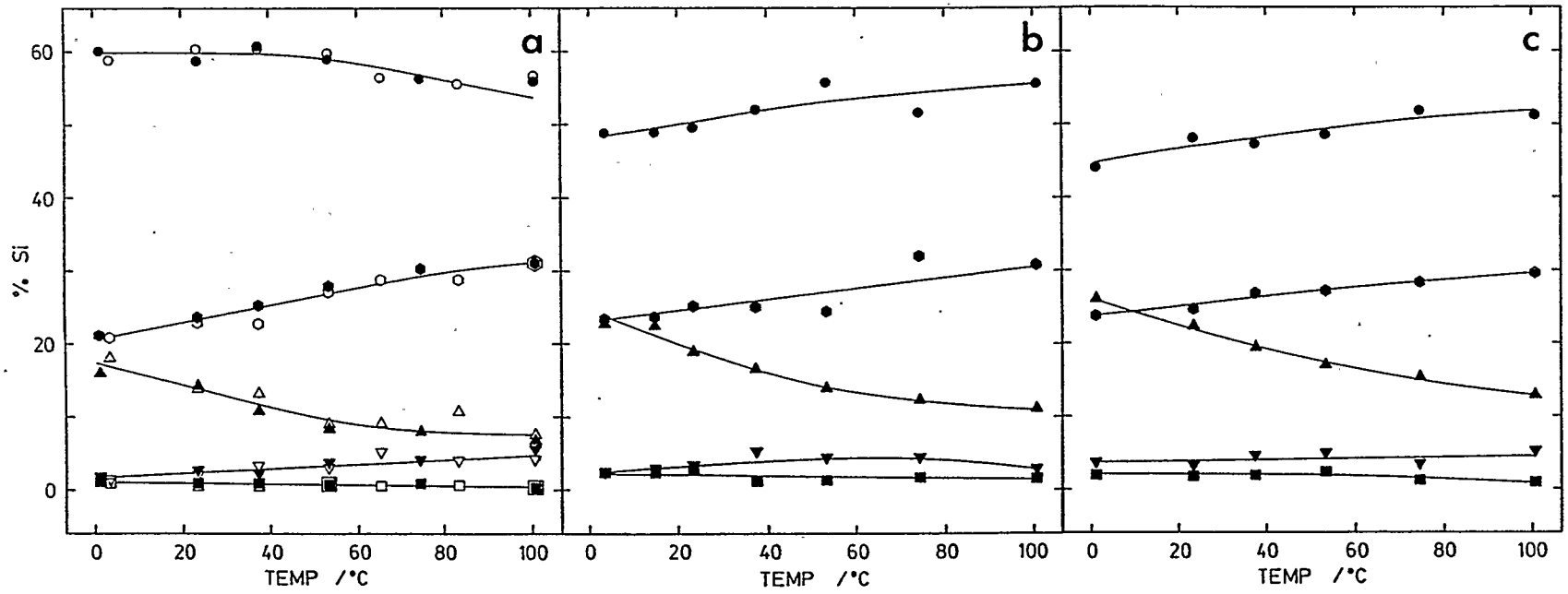

Figure 2-20. Temperature dependence of spectral integrations for (a) samples 34 (open symbols) and 40 with M = Na, (b) sample 39 with M = K, and (c) sample 41 with M = Rb. All samples contain 2.2 mol kg^{-1} Si with $M^{+}:Si^{IV}$= 4.0:1.

complex for cation effects to be easily resolved, at $M^+:Si^{IV}$ = 1.5:1 (Figure 2-12) lines corresponding to certain species (e.g.: lines 13, 25 (Q^3_6) and 38 (Q^3_8)) appear to grow in relative intensity when Na^+ is replaced with K^+ and then with Rb^+.

In Figure 2-20a, integrations are virtually identical for the two solutions which vary only in the level of ^2H-enrichment (samples 34 and 40). Thus, deuterium content has no apparent influence on silicate polymerization.

2.4.2. Discussion

The complexity of aqueous silicate ^{29}Si NMR spectra prohibits the determination of equilibrium data for individual molecular species. Nevertheless, by monitoring changes in Q-centre connectivity, we have demonstrated that condensation is favoured by low temperature, low alkalinity and high solution concentration.

The dependence of condensation equilibria on the alkali-metal cation has not been observed previously by NMR. Using Raman spectroscopy, Dutta and Shieh[29] found no difference between solutions prepared with M = Li, Na, K and Cs. However, earlier trimethylsilylation studies by Ray and Plaisted[38] support the present findings.

The nature of the alkali-metal's influence on polymerization is by no means certain. Dutta and Shieh[29] suggested that the attraction of water molecules by smaller cations provides a "driving force" for polymerization; however, this hypothesis is refuted by the present observation that polymerization is actually favoured by large M^+ cations. It would appear instead that heavy cations associate more readily with

the large oligomers, and thereby afford them additional stability. Although formation constants for the silicate-M^+ ion-pairs are not available at present, chemical shift observations in Sect. 2.3.2 have indicated that K_{IP}'s indeed increase from $M^+ = Na^+$ to K^+ to Rb^+, albeit slightly, with the increase being smallest for the monomer-M^+ pair. As further support of the above hypothesis, we note that K_{IP} measurements reported for the vanadate system[94] decrease sharply from $M^+ = Na^+$ to K^+ for HVO_4^{2-}-M^+ while values for $V_{10}O_{28}^{6-}$-M^+ are comparatively large and increase from $M^+ = Na^+$ to K^+ to Rb^+.

2.5. Conclusion

We have identified the principal factors which give rise to shielding differences between ^{29}Si nuclei in aqueous, alkali-metal silicate solution. Not surprisingly, local and intramolecular shielding contributions influenced by changes in silicate connectivity and "molecular strain" have the most significant effect on relative line positions. However, detailed interpretation of chemical shifts based on electronegativity arguments, or on a $(d\text{-}p)\pi$ mechanism, should be made with caution. Variations in solution composition affect shielding primarily via a change in the degree of intermolecular association, most notably with alkali-metal cations. Since the resulting line displacements range up to 1 ppm and differ between resonances, σ_{inter} must make a significant contribution to total shielding differences. The large compilation of chemical shift data provides a model for predicting ^{29}Si line positions

and has aided in the identification of the tetrahedral $Si_4O_{10}^{4-}(Q^3_4)$ anion.

This has been the first truly quantitative study of aqueous silicate equilibria by ^{29}Si NMR. The results, which demonstrate that polymerization is favoured by low temperature, low alkalinity and high Si concentration, provide the basis for the mechanistic rate study discussed in Ch. III. The small influence of the alkali-metal cation on silicate anion distribution may be indicative of the control which cations are thought to have over the size and shape of silicate units in silicate and aluminosilicate minerals[5,10].

CHAPTER III. Transverse ^{29}Si Relaxation and the Dynamics of Silicate Polymerization.

3.1. Introduction

3.1.1. Previous Studies

During the course of this investigation, controversy has arisen in the literature concerning the origin of line-broadening in ^{29}Si NMR spectra of aqueous silicate solutions as temperature is increased (see Figure 3-1). Engelhardt and Hoebbel[45] speculated that broadening is caused by chemical exchange of SiO_4 tetrahedra between different silicate anions. Although Harris' group arrived at similar conclusions originally[57], they later reported[58] spin saturation-transfer experiments yielding exchange rates about two orders of magnitude lower than those

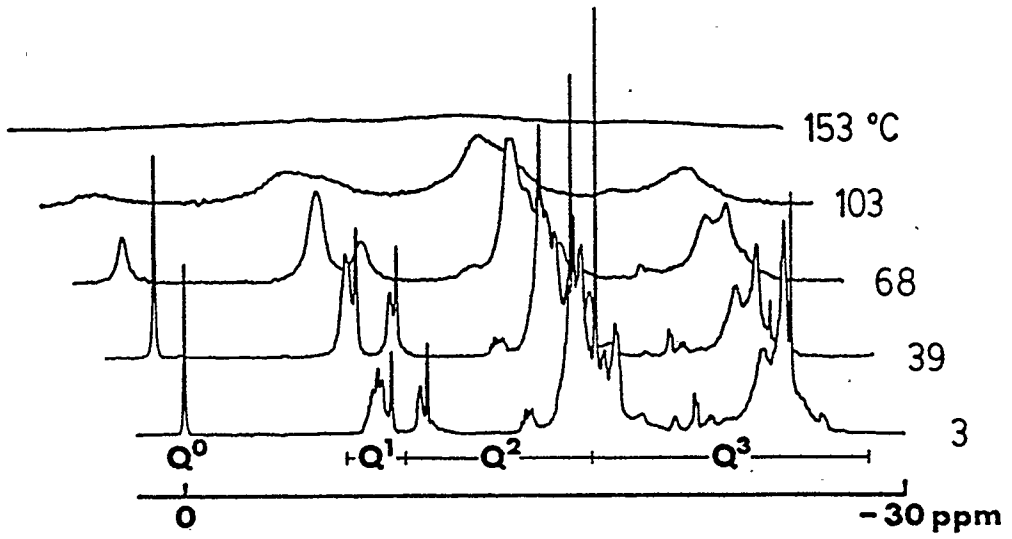

Figure 3-1. ^{29}Si spectra for sample 35 which contains 1.55 mol kg^{-1} Si with $Na^+:Si^{IV}$ = 1.0:1 (95% ^{29}Si-enriched).

estimated from linewidths. Because irreversible line-broadening had occurred when silicate solutions were heated in unlined glass tubes, but not when liners were used[57], they concluded that unidentified paramagnetic contaminants introduced during sample preparation and/or by leaching from the NMR tubes are the most likely cause of both transverse and longitudinal ^{29}Si relaxation[58]. Both of these research groups have reported that the temperature dependence of line-broadening varies between individual resonances[45,57].

Griffiths, Cundy and Plaisted[60] recently employed the Carr-Purcell-Meiboom-Gill pulse technique[61] to quantify the contribution of Si-Si exchange to observed linewidths. Unfortunately, several procedural shortcomings combine to invalidate most of their findings. These include use of unlined NMR tubes which resulted in aberrant relaxation measurements, neglect of instrumental contributions to line-broadening, and insufficient data on which to base conclusions.

3.1.2. Transverse Relaxation and Bandshape Analysis

Methods of calculating the bandshapes of complex spectra have been developed by extending both the classical and quantum mechanical theories of nuclear spin exchange. A quantum mechanical treatment, such as the density matrix method[95], is normally employed with strongly coupled systems since these can not be attended to by classical theory. However, if all multiplet lines are treated as individual sites, classical modelling often will suffice, provided that all possible spin-state combinations are accounted for[96]. Fortunately, different spin-states need not be considered in the case of intermolecular exchange, since a

nuclear spin transferring from one molecule to another may be in any of its possible spin-states with equal probability.

The Bloch equations[97] describe the classical motion of the macroscopic magnetization vector M as it relaxes to its equilibrium position (M_o) parallel to B_o, following perturbation by the applied field B_1. The motion of M is analysed most conveniently in terms of a rotating coordinate system in which the z-axis is parallel to B_o, and the x'- and y'- axes (as distinguished from the stationary xy coordinates) rotate about z with angular frequency ($\omega_o = 2\pi\nu$) equal to the frequency of the applied rf field. Given that u, v and M_z represent projections of M along the x'-, y'- and z-directions, and that $\Omega_a = \omega_a - \omega_o$ is the chemical shift of nucleus a, the Bloch equations take the form shown in Eqn. 3.1.

$$\frac{du}{dt} = v\Omega_a - uT_2^{-1} \tag{3.1a}$$

$$\frac{dv}{dt} = -u\Omega_a - vT_2^{-1} + \gamma B_1 M_z \tag{3.1b}$$

$$\frac{dM_z}{dt} = -(M_z - M_o)T_1^{-1} - v\gamma B_1 \tag{3.1c}$$

The relaxation times, T_1 and T_2, are inversely related to the first-order rate constants describing the processes by which the components of M return to their respective thermal equilibrium values. The <u>longitudinal</u> or <u>spin-lattice</u> relaxation time, T_1, is the time constant for M_z to reach M_o, which corresponds to the restoration of the Boltzmann spin distribution. This relaxation process and its importance with regard to the aqueous silicate system is the subject of Ch. IV. <u>Transverse</u> or <u>spin-spin</u> relaxation time, T_2, defines the decay rate of the net x'y'-

magnetization vector. This decay results from the loss of phase coherence between individual precessing magnetic moments due to their interaction with local fluctuating fields[98].

Transverse magnetization is defined in Eqn. 3.2, and its time dependence (Eqn. 3.3) is obtained by combining expressions 3.1a and

$$G = u + iv \tag{3.2}$$

$$\frac{dG}{dt} = -G\alpha_a + iC \tag{3.3}$$

$$\alpha_a = i\Omega_a + T_2^{-1}$$

$$C = \gamma_a B_1 M_z \quad [99]$$

3.1b. The steady-state solutions for magnetization components u and v represent the dispersion and absorption mode spectrums, respectively. Hence, the imaginary part of G corresponds to a Lorentzian absorption line having natural half-height line width $\Delta\nu_{1/2}$ (Eqn. 3.4).

$$\Delta\nu_{1/2} = (\pi T_2)^{-1} \tag{3.4}$$

Invariably, an additional pseudo-T_2-relaxation contribution ($T_{2inhomo}$) arises from inhomogeneities in B_0 which cause the Larmor frequencies in different parts of the sample to differ. At best, therefore, linewidths yield only the effective T_2 value (Eqn. 3.5).

$$T_{2eff}^{-1} = T_2^{-1} + T_{2inhomo}^{-1} \tag{3.5}$$

Chemical exchange will contribute to transverse relaxation (Eqn. 3.6), provided that T_{2exch}^{-1} is on the order of $\gamma^{-1}B_1^{-1}$ and is not significantly larger than T_{2eff}^{-1}.

$$T_{2total}^{-1} = T_{2eff}^{-1} + T_{2exch}^{-1} \tag{3.6}$$

Thus, lineshapes can be analysed to determine rates of reversible exchange processes with activation energies between 20 and 100 kJ mol^{-1} [100]. Because spin-site concentrations are fixed, exchange rates are always describable by a pseudo-first-order rate constant, regardless of the true order of the reaction mechanism.

Equation 3.7 describes the reversible transfer of magnetization between sites A and B, which have respective populations P_A and P_B. By combining the corresponding rate expressions with Eqn. 3.3, one obtains

$$A \underset{k_-}{\overset{k_+}{\rightleftharpoons}} B \tag{3.7a}$$

$$P_A + P_B = 1 \tag{3.7b}$$

$$k = \frac{k_+}{P_A} = \frac{k_-}{P_B} \tag{3.7c}$$

the extended Bloch equations (3.8),

$$\frac{dG_A}{dt} = -G_A\alpha_A + iC_A - k_+G_A + k_-G_B$$

$$= -G_A(\alpha_A+kP_B) + G_BkP_A + iC_A \tag{3.8a}$$

$$\frac{dG_B}{dt} = -G_B\alpha_B + iC_B - k_-G_B + k_+G_A$$

$$= -G_B(\alpha_B+kP_A) + G_AkP_B + iC_B \tag{3.8b}$$

which describe the time dependence of the transverse magnetization at each site. The imaginary part of the steady-state solution of Eqn. 3.8[101,102] will yield a complete absorption spectrum. This is represented in Figure 3-2 for several values of k. In the slow exchange limit (Figure 3-2a) the peaks retain the "preexchange" linewidth (Eqn. 3.9).

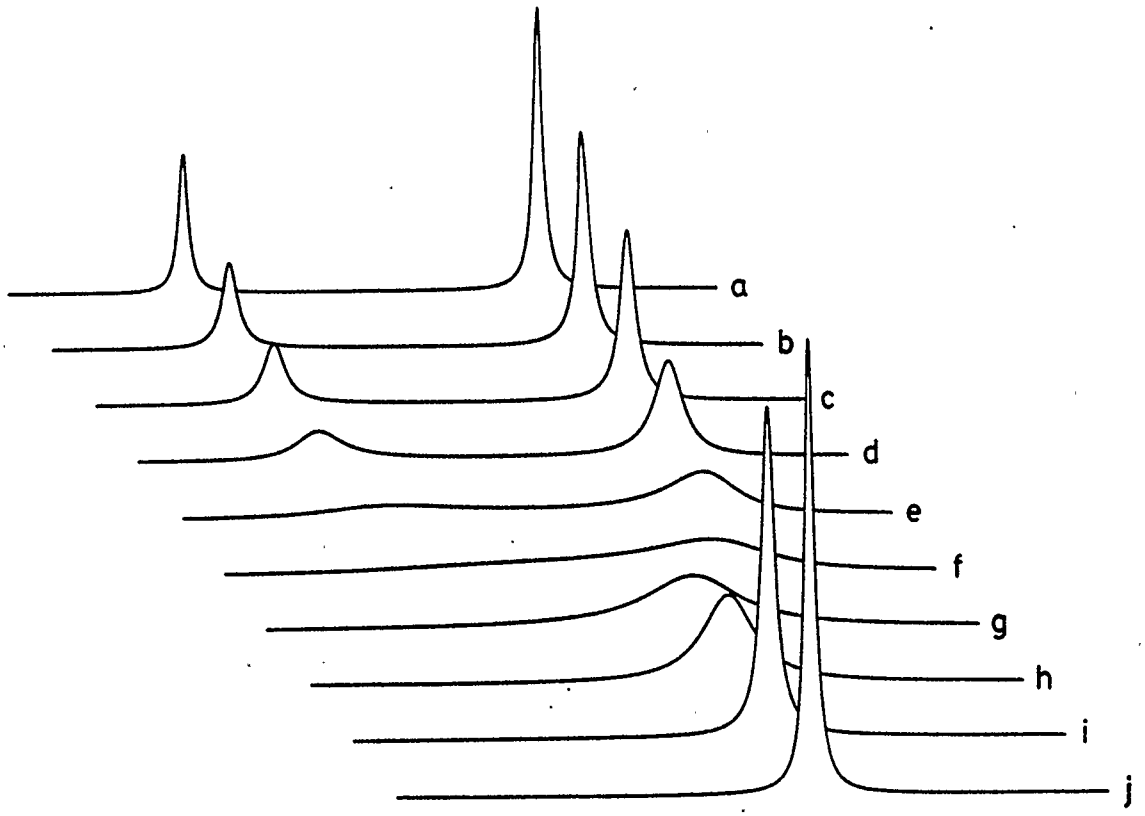

Figure 3-2. Calculated bandshapes for a two-site exchange system with $P_A = 0.33$, $P_B = 0.66$, $\Delta\nu = 50$ Hz, $T_2 = 0.2$ s^{-1}, and rate constant k (see Eqn. 3.7c) = 0.1(a), 2(b), 10(c), 30(d), 50(e), 100(f), 200(g), 500(h), 10^3(i), and 10^5 s^{-1}(j).

$$\Delta\nu_{1/2} = (\pi\, T_{2eff})^{-1} \tag{3.9}$$

As the rate of exchange increases (Figure 3-2 b to f), each line will begin to broaden as described in Eqn. 3.10.

$$\Delta\nu_{1/2,A} = [\pi(k_+ + T_{2eff,A})]^{-1} \tag{3.10a}$$

$$\Delta\nu_{1/2,B} = [\pi(k_- + T_{2eff,B})]^{-1} \tag{3.10b}$$

When the lines have just coalesced into a single broad line (Figure 3-2g), the frequency of exchange is on the order of the initial peak separation $\pi\Delta\nu_{AB}$. Eventually (Figure 3.2j), the spectrum collapses into a single peak with position described by Eqn. 3.11,

$$\nu = P_A\nu_A + P_B\nu_B \tag{3.11}$$

and linewidth equal to the weighted average of the individual pre-exchange linewidths.

Thus, approximate rate estimates can be made by analysing the temperature dependence of linewidth, peak separation or line intensities. However, accurate determinations (especially for exchange systems with more than 2 sites) can only be achieved by complete bandshape analysis (CBA), which is an iterative process of fitting experimental spectra to bandshapes generated from the exchange-modified Bloch equations[102].

In 1958, Sack[103] derived an extended Bloch equation (3.12) to

$$G(x) = -i\omega_o M_o I[T_2 + K + i\omega]^{-1}\cdot P$$

handle any number n of sites, for which x is the independent frequency variable, I is a 1×n unit vector, T_2 is a diagonal matrix with element T_{2i}^{-1} corresponding to the i^{th} site, ω is a diagonal matrix with elements $x-\Omega_i$, P is an n×1 matrix containing the relative site populations P_i, and K is the exchange rate matrix with $K_{ij} = -k_{ji}$, $j \neq i$ and $K_{ii} = -\sum_{j(\neq i)=1}^{n} (K_{ij}P_j/P_i)$. The absorption spectrum would then be defined by Eqn. 3.13, where Im and Re signify the imaginary and real components of complex expressions.

$$V(x) = Im[G(x)] = Re[-\omega_o M_o (T_2 + K + i\omega)^{-1}\cdot P]$$

Solution of Eqn. 3.13 requires inversion of the complex matrix sum $(T_2 + K + i\omega)$ for each value of the frequency variable x. A more efficient procedure, based on the method of Gordon and McGinnes[104,105], requires a single diagonalization of the frequency independent part R which is defined by Eqn. 3.14, where Ω is a diagonal matrix with

$$(T_2 + K + i\omega) = R + ixI \tag{3.14a}$$

$$R = (T_2 + K + i\Omega) \tag{3.14b}$$

elements Ω_i. If S is the matrix which diagonalizes R to give the eigenvalue matrix Λ such that $\Lambda = S^{-1} \cdot R \cdot S$, then Eqn. 3.13 is reduced to a series of simple matrix operations (Eqn. 3.15).

$$V(x) = Re[-\omega_o M_o I \cdot S \cdot (\Lambda + ixI)^{-1} \cdot S^{-1} \cdot P] \tag{3.15}$$

3.1.3. The Selective Saturation Experiment

Exchange rates on a time scale comparable with longitudinal relaxation can be determined using a technique first described by Forsén and Hoffmann[106]. It involves monitoring the time dependence of the z-magnetization (M_z) at one spin site, following perturbation of another site with which it is exchanging. The perturbation can be either a steady saturating field[106] or a selective excitation signal[107]. Modified Bloch equations (3.16) which describe the time dependence of longitudinal

$$\frac{d M_{zA}}{dt} = -(M_{zA} - M_{oA})T_{1A}^{-1} - v_A\gamma_A B_1 - k_+ M_{zA} + k_- M_{zB}$$

$$= M_{oA}T_{1A}^{-1} - M_{zA}(T_{1A}^{-1} + kP_B^{-1}) + M_{zB}kP_A^{-1} - v_A\gamma_A B_1 \tag{3.16a}$$

$$\frac{d M_{zB}}{dt} = -(M_{zB} - M_{oB})T_{1B}^{-1} - v_B\gamma_B B_1 - k_+ M_{zB} + k_- M_{zA}$$

$$= M_{oB}T_{1B}^{-1} - M_{zB}(T_{1B}^{-1} + kP_A^{-1}) + M_{zA}kP_B^{-1} - v_B\gamma_B B_1 \tag{3.16b}$$

magnetization for the two-site equilibrium (3.7) are created by combining the corresponding rate expressions with Eqn. 3.1c. If site A is selectively saturated and exchange occurs between sites A and B before M_{zA} has been restored to M_{oA}, there will be a temporary reduction in the intensity of the B signal. This is a qualitative means of detecting exchange rates which are on the order of T_1^{-1}.

In the selective inversion recovery (SIR) experiment[61], one resonance is selectively inverted 180° by a DANTE pulse sequence[107]. After a delay interval t, a non-selective observe pulse is applied to monitor the z-magnetization of all peaks as a function of recovery time. If the corresponding T_1 values are known (T_1's can be determined from the same experiment for the two site case), k can be solved by curve-fitting the decay-recovery data to Eqn. 3.16.

3.2. Experimental

As documented in Ch.II, spectra were acquired at temperatures between ca. 0 and 150°C for all samples, except 1 and 21 to 23. Spectra were integrated and half-height line widths ($\Delta\nu_{1/2}$) of the easily resolved, uncoupled signals were measured.

Complete bandshape analyses were conducted using Fortran program GNMR[108] (based on Eqn. 3.15 and listed in Appendix A) for spectra acquired of the 14 samples which are indicated in Table II-II. For each solution, a low temperature (<20°C), non-broadened spectrum was simulated by manually iterating the positions, linewidths and areas of up to 70 computer-generated Lorentzian peaks. Many reaction models were tested to find appropriate sets of rate equations (i.e., kinetic matrix) K

which might replicate the observed temperature dependent line-broadening.

Selective inversion-recovery (SIR) experiments were conducted for 5 samples (see Table II-II) by employing the pulse sequence program SINCERE (in Appendix B).

In an effort to obtain spectra under pre-equilibrum conditions, three solutions were rapidly prepared at 0°C (samples 21 to 23; nominal compositions are listed in Table II-II) and then, beginning 15 min from the start of sample preparation, spectra were recorded at 0°C.

3.3. Results and Discussion

3.3.1. Solutions with $M^+:Si^{IV}$ = 1:1

Linewidths which were measured for 30 spectra of solutions with $Na^+:Si^{IV}$ = 1:1 are listed in Table III-I. Despite additional inhomogeneity broadening expected from use of the lined, pressurizable NMR tube, linewidths were narrower than those reported for comparable solutions which were contained in unlined, glass tubes[48,57,60].

Comparison of the data in Table III-I indicates that linewidths were not significantly affected by either ^{29}Si enrichment (cf. samples 33 and 38) or sample dilution (Figure 3-3). The close similarity between spectra in Figure 2-18 would suggest that the alkali-metal cation (M^+ = Na^+, K^+ and Rb^+) also has little influence on $\Delta\nu_{1/2}$. Since consistent linewidths were obtained from solutions made with silica and MOH from different sources, any contribution to transverse relaxation from paramagnetic impurities is therefore negligible.

Table III-I. Temperature Dependence of ^{29}Si Linewidths[a] for $Na^+:Si^{IV} = 1.1$.

Temp/°C	Q^0	$Q^1{}_2$	$Q^2{}_3$	$Q^3{}_6$
a. Sample 33 (2.17 mol kg^{-1} Si)				
3.3	1.1	1.8	1.3	1.4
15.2	1.5	1.9	(1.6)	1.6
22.4	1.8	2.5	(2.3)	1.6
30.6	2.3			1.9
38.8	2.7			1.4
55.0	8.8			
68.0	12.3			
b. Sample 35 (1.55 mol kg^{-1} Si)				
3.3	1.5	2.0	1.6	1.4
22.4	1.4	2.0	1.5	1.4
38.8	2.5	3.7	2.8	1.1
55.0	6.7			2.3
c. Sample 36 (1.20 mol kg^{-1} Si)				
3.3	1.0	1.8	1.1	
22.4	1.3	1.6	1.3	1.4
38.8	3.1			
68.0	(18.2)			
d. Sample 37 (0.80 mol kg^{-1} Si)				
3.3	1.1	1.5	1.2	
15.2	1.0	1.3	1.1	
22.4	1.2	1.7	1.4	
38.8	2.6	3.3	2.9	
55.0	6.9			
72.4	13.6			
e. Sample 38 (2.18 mol kg^{-1} Si; nonenriched)				
22.4	1.9			
38.8	3.5			
61.5	12.8			
f. Sample 42 (0.30 mol kg^{-1} Si)				
3.3	1.3	1.6	1.6	
22.4	1.3	1.8	1.8	
38.8	2.9	(4.5)		
55.0	7.4			
68.0	16.5			
86.7	32.5			

[a] Measurements have a typical uncertainty of ±0.3 Hz.

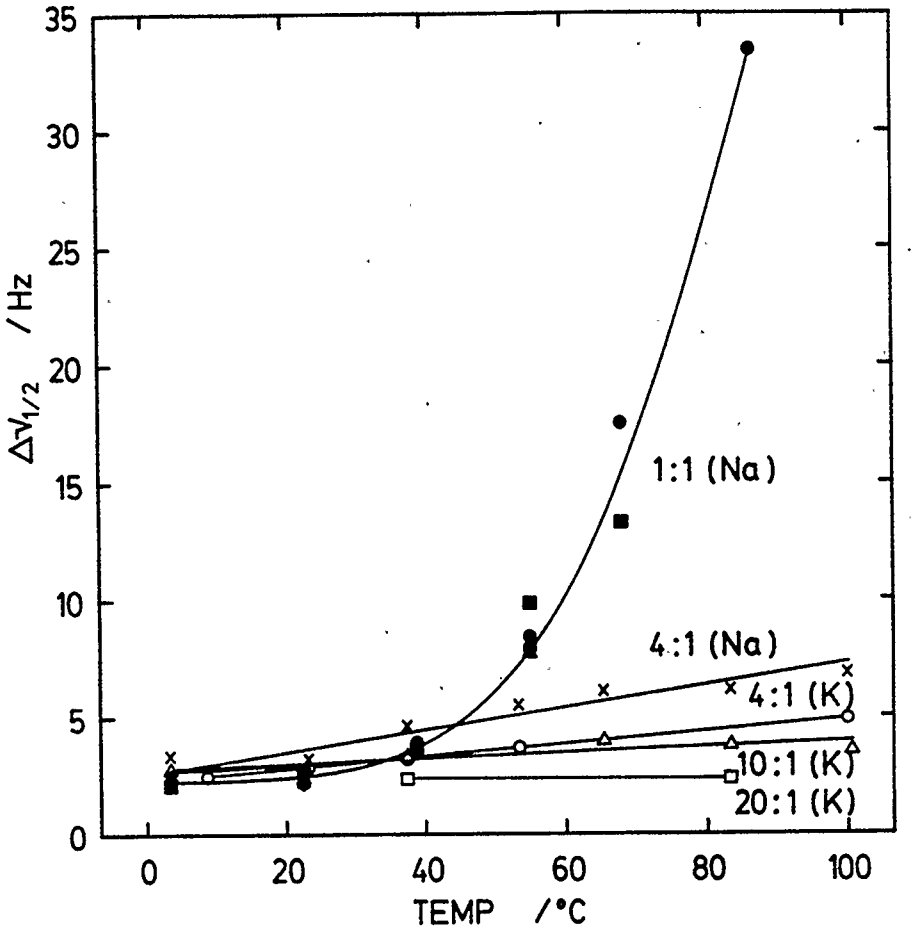

Figure 3-3. Temperature dependence of the monomer linewidth in samples: 33 (●), 35 (⬢), 36 (▲), and 37 (■), all with $Na^+:Si^{IV}$ = 1:1 but differing in Si concentration; 34 with $Na^+:Si^{IV}$ = 4:1 (×); 39 with $K^+:Si^{IV}$ = 4:1 (○); 31 with $K^+:Si^{IV}$ = 10:1 (△); and 32 with $K^+:Si^{IV}$ = 20:1 (□). All linewidths include 1 Hz artificial broadening.

For solutions with $M^+:Si^{IV}$ = 1:1, temperature dependent line-broadening is relatively insignificant below 20°C, but increases sharply at higher temperatures (Figure 3-3). Hence, spectra recorded at temperatures < 20°C were employed as the pre-exchange basis set in bandshape

modelling studies which were performed to determine whether Si-Si exchange can account for the observed broadening.

Many reaction models were tested in order to find exchange matrices (**K**) which, when employed in conjunction with program GNMR, could replicate the observed temperature dependent broadening. Ultimately, we established that any exchange matrix in which all diagonal elements are equal will furnish acceptable simulations, provided that **K** is balanced in accordance with the conditions given for Eqn. 3.12. In apparent contrast to previous findings[45,57], this result signifies that all principal resonances broaden uniformly with temperature. The accuracy of bandshape simulations, attested to in Figure 3-4, seems to support the hypothesis that temperature dependent T_2-relaxation is induced primarily by chemical exchange. If that hypothesis is correct, uniform line-broadening indicates that the residence time at all principal spin-sites must be equal. Inverted spin-site lifetimes derived from the CBA procedure for 8 samples with $Na^+:Si^{IV}$= 1.0:1 are listed in Table III-II. In accordance with Figure 3-3, lifetimes appear to be independent of sample concentration.

There are a few minor resonances which do broaden more than the majority; these represent species such as the linear trimer and tetramer which can undergo rapid cyclization. Because the cyclic and cage structures remain in equilibrium with smaller units, the slower ring-breaking processes must occur at least as rapidly as intermolecular condensation. Since these peaks are relatively weak and observable only below ca. 20°C, however, they do not contribute materially to the line-broadening analysis.

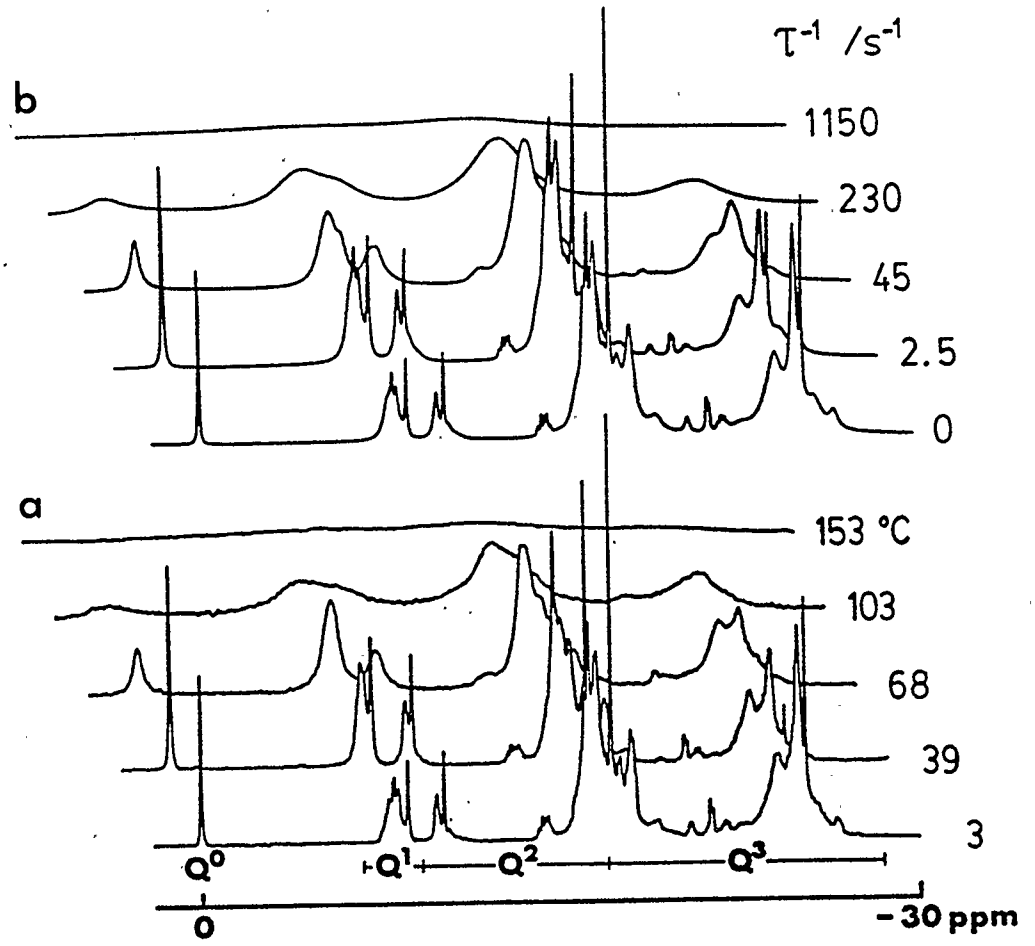

Figure 3-4. Comparison of experimental (a) and simulated (b) spectra for sample 35 which contains 1.55 mol kg^{-1} Si with $Na^+:Si^{IV}$ = 1.0:1 (95% ^{29}Si-enriched). The spectrum at 3°C was used as the basis set for simulations (i.e., assuming that inverse spin-site lifetime $\tau^{-1} = 0\ s^{-1}$ at 3°C). Program GNMR can not account for the small, independent variation in line positions which is caused by phenomena other than spin-site exchange (discussed in Ch. II).

Table III-II. Inverse Spin-Site Lifetimes For Samples with $Na^+:Si^{IV} = 1.0:1$[a].

Sample 4 1.40 mol kg^{-1} Si		Sample 6 0.70 mol kg^{-1} Si		Sample 7 0.35 mol kg^{-1} Si		Sample 8 0.18 mol kg^{-1} Si	
T/°C	τ^{-1}/s^{-1}	T/°C	τ^{-1}/s^{-1}	T/°C	τ^{-1}/s^{-1}	T/°C	τ^{-1}/s^{-1}
41.5	7 (2)	31.5	2.5(1)	31.5	5(1.5)	46.5	8 (1)
61.5	25 (5)	51.5	12 (2)	46.5	10 (2)	61.5	23 (1)
91.5	130 (20)	61.5	36 (2)	61.5	30 (5)	81.5	55 (5)
121.5	650(100)	81.5	96 (6)	81.5	110 (10)	101.5	180 (10)
151.5	1700(200)	101.5	330 (50)	101.5	250 (50)	141.5	500(200)
		121.5	700 (50)	121.5	700(100)		
				141.5	1100(100)		
$\Delta H^* = 53(2)$ kJ mol^{-1}		$\Delta H^* = 53(3)$ kJ mol^{-1}		$\Delta H^* = 49(2)$ kJ mol^{-1}		$\Delta H^* = 50(3)$ kJ mol^{-1}	
$\Delta S^* = -61(5)$ J mol^{-1} K^{-1}		$\Delta S^* = -57(8)$ J mol^{-1} K^{-1}		$\Delta S^* = -70(6)$ J mol^{-1} K^{-1}		$\Delta S^* = -69(8)$ J mol^{-1} K^{-1}	

Sample 33 2.70 mol kg^{-1} Si		Sample 35 1.55 mol kg^{-1} Si		Sample 37 0.80 mol kg^{-1} Si		Sample 42 0.30 mol kg^{-1} Si	
T/°C	τ^{-1}/s^{-1}	T/°C	τ^{-1}/s^{-1}	T/°C	τ^{-1}/s^{-1}	T/°C	τ^{-1}/s^{-1}
38.8	4 (1)	38.8	2.5(1)	38.8	4 (2)	38.8	6 (2)
55.0	22 (2)	55.0	16 (2)	55.0	18(1.5)	55.0	18.5(1)
68.0	35 (5)	68.0	45 (4)	77.4	80 (4)	68.0	45 (3)
102.5	250 (30)	86.7	76 (4)	86.7	109 (4)	86.7	90 (4)
137.3	900 (50)	102.5	230 (30)	102.5	220 (20)	102.5	450 (60)
152.7	2200(400)	137.3	720 (50)	137.3	650 (60)		
		152.7	1150(100)	152.7	950 (50)		
$\Delta H^* = 50(2)$ kJ mol^{-1}		$\Delta H^* = 48(3)$ kJ mol^{-1}		$\Delta H^* = 41(2)$ kJ mol^{-1}		$\Delta H^* = 51(7)$ kJ mol^{-1}	
$\Delta S^* = -69(6)$ J mol^{-1} K^{-1}		$\Delta S^* = -77(7)$ J mol^{-1} K^{-1}		$\Delta S^* = -94(6)$ J mol^{-1} K^{-1}		$\Delta S^* = -70(20)$ J mol^{-1} K^{-1}	

a. Activation parameters ΔH^* and ΔS^* were determined by a least-squares fit of weighted rate data[109] to the Eyring equation[110] (3.18).

3.3.2. Solutions with $M^+:Si^{IV}$ > 1:1

Table III-III contains linewidths which were measured for 36 spectra of solutions with $M^+:Si^{IV}$ > 4:1. Again, these are narrower than any previously recorded for comparable solutions[48,57,60].

Figure 3-3 reveals that the $M^+:Si^{IV}$ ratio had comparatively little influence on linewidths below ambient temperature, (see also Table III-I); the width of the Q^0 signal was about 1 to 2 Hz for all solutions in this temperature range. At higher temperatures, linewidths remained constant for very alkaline solutions ($M^+:Si^{IV}$ = 20:1), but increased as the $M^+:Si^{IV}$ ratio was reduced. The uniformity of $\Delta\nu_{1/2}$ at low temperature and/or high alkalinity is further indication that paramagnetic impurities can not be the cause of temperature dependent line-broadening. At increased $M^+:Si^{IV}$ ratios, line-broadening is no longer uniform for all signals as it was for $M^+:Si^{IV}$ = 1:1 (Figures 3-5 and 3-6).

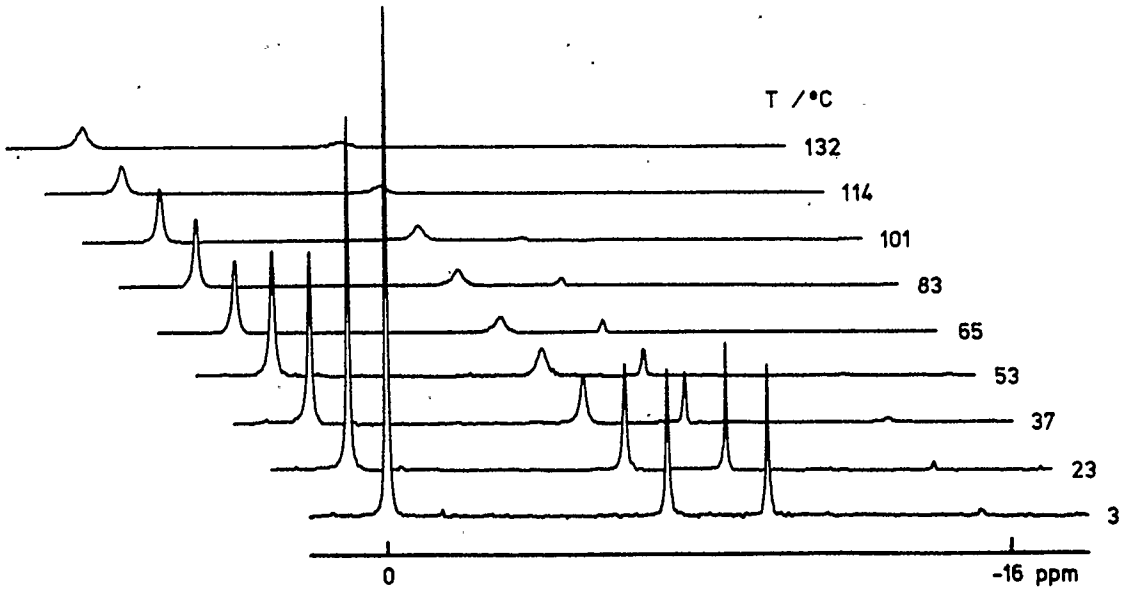

Figure 3-5. ^{29}Si spectra for sample 34 with 2.17 mol kg^{-1} Si and $Na^+:Si^{IV}$ = 4.0:1. Spectra contain 0.5 Hz artificial line-broadening.

Table III-III. Temperature Dependence of ^{29}Si Linewidths[a] for High Alkalinity Samples.

Temp/°C	Q^0	$Q^1{}_2$	$Q^2{}_3$	$Q^2{}_4$
a. Sample 31 (1.49 mol kg^{-1} Si; $K^+:Si^{IV}$ = 10.3:1				
3.3	1.7	1.9	1.4	
23.1	1.7	2.3	0.9	
37.2	2.3	4.8	0.9	
65.4	3.0	9.0	1.4	
83.2	2.8	7.8	1.2	
100.8	2.5		2.0	
113.8	2.6	(5.6)		
131.5	2.4	(6.9)		
b. Sample 32 (0.77 mol kg^{-1} Si; $K^+:Si^{IV}$ = 20.0:1)				
37.2	1.5	4.3	0.6	
83.2	1.4	6.4		
c. Sample 34 (2.17 mol kg^{-1} Si; $Na^+:Si^{IV}$ = 4.0:1)				
3.3	2.4	2.9	2.1	
23.1	2.3	3.4	1.3	2.3
37.2	3.6	5.6	2.2	
53.2	4.5	11.1	3.2	
65.4	5.1	11.7	4.2	
83.2	5.1		5.6	
100.8	5.8			
113.8	8.7			
131.5	11.6			
d. Sample 39 (2.17 mol kg^{-1} Si; $K^+:Si^{IV}$ = 4.0:1)				
3.3	1.3	1.5	0.9	2.4
14.5	1.5	2.4	1.1	2.9
23.1	1.8	3.0	1.2	4.9
37.2	2.2	4.4	1.6	
53.2	2.7	5.7	1.7	
100.8	3.9	8.5	8.2	
e. Sample 40 (2.17 mol kg^{-1} Si; $Na^+:Si^{IV}$ = 4.0:1)				
1.0	2.3	2.6	2.2	
23.1	2.3	3.4	1.3	
37.2	4.6	7.2	3.2	
53.2	5.4	10.1	4.7	
f. Sample 41 (2.17 mol kg^{-1} Si; $Rb^+:Si^{IV}$ = 4.0:1)				
1.0	1.3	1.6	0.9	2.9
14.5	1.6	3.1	0.8	3.2
23.1	3.7	5.0	2.9	
37.2	3.3	5.5	1.7	5.3
53.2	4.0	6.4	2.4	
74.3	5.3	9.5	3.4	
100.8	8.0	38.5	14.1	

[a] Measurements have a typical uncertainty of ±0.3 Hz.

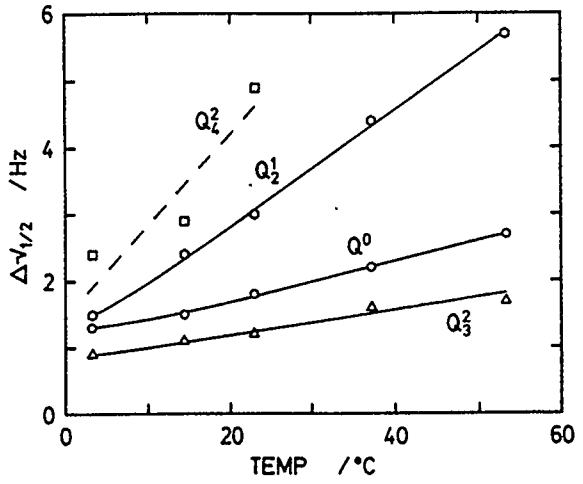

Figure 3-6. Temperature dependence of linewidths for sample 39 which contains 2.17 mol kg^{-1} Si with $K^+:Si^{IV}$ = 4.0:1.

A comparatively minor change in linewidths and their temperature dependence was observed with solutions differing only in the M^+ cation (Figure 3-7). Although it is conceivable that such changes could arise from dissimilarities in viscosity or other solution characteristics, the apparent order of T_2 values ($T_{2K} > T_{2Rb} \gtrsim T_{2Na}$) correlates with that observed for T_1 relaxation (cf. Figure 4-8) which is caused primarily by M-^{29}Si dipole-dipole interactions (Ch. IV).

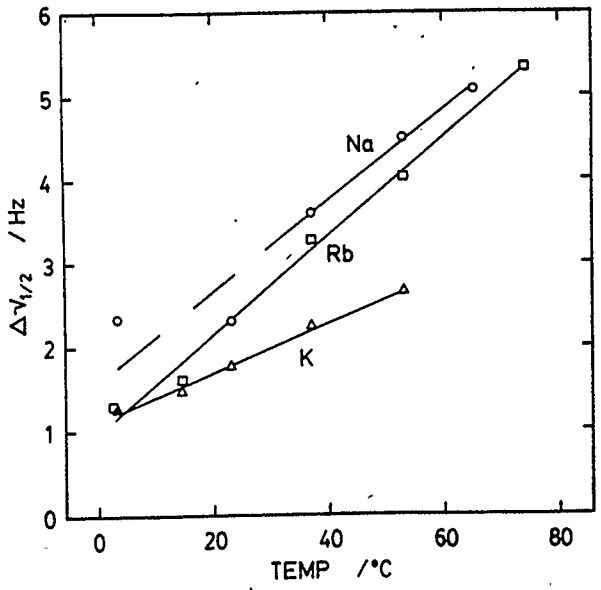

Figure 3-7. Temperature dependence of the monomer linewidth in samples 34 (M=Na), 39 (M=K) and 41 (M=Rb); each with $M^+:Si^{IV}$ = 4.0:1.

Comparison of Figures 2-14 and 3-3 reveals that, as the $M^+:Si^{IV}$ ratio is raised, the extent of polymerization is closely related to the overall degree of line-broadening. At the extreme alkalinity of sample 32 ($K^+:Si^{IV}$ = 20.0:1), almost all dissolved silicon is monomeric and the Q^0 line-width is constant up to at least 87°C. Hence, there can be little doubt that when temperature dependent line-broadening does occur, the primary cause is Si-Si chemical exchange. Since broadening is not the same for all signals, however, bandshape simulations of samples with $M^+:Si^{IV} >> 1:1$ (samples 12 to 14, and 16) consistently fail when exchange matrices which had been used successfully for $M^+:Si^{IV}$ = 1:1 are employed (see Figure 3-8).

Selective inversion recovery (SIR) experiments which were conducted with 2.80 mol kg^{-1} potassium silicate solutions succeeded in detecting spin exchange rates on the order of T_1^{-1} at temperatures between 80 and 100°C for $K^+:Si^{IV}$ = 4.5:1 (sample 36; see Figures 3-9 and 3-10), and at 30°C for $K^+:Si^{IV}$ = 1.0:1 (sample 25; see Figure 3-11). For small oligomers, T_1 values should not vary by more than a factor of 2 or 3 between the two solutions at their respective temperatures (refer to Ch.IV, noting Figure 4-8). Thus, the SIR experiments reveal that exchange rates increase roughly 100-fold as the $K^+:Si^{IV}$ ratio is decreased from 4.5:1 to 1.0:1.

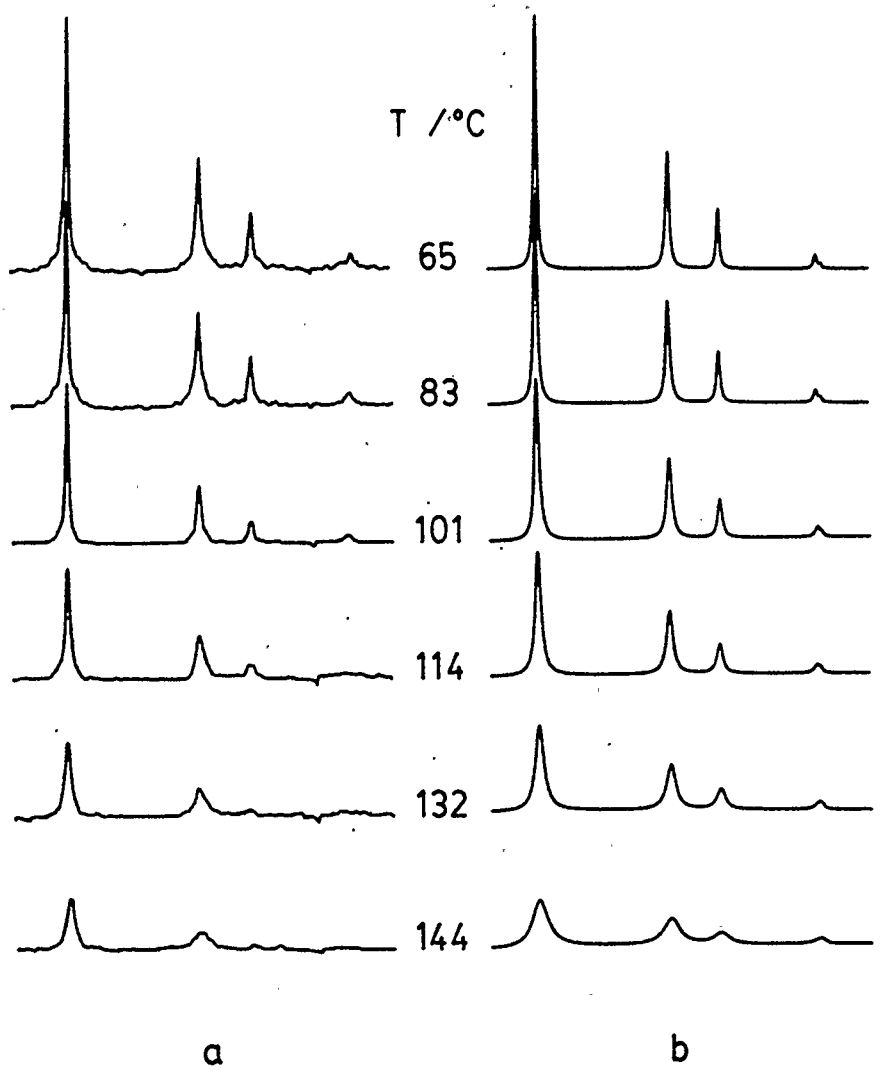

Figure 3-8. Comparison of experimental spectra (a) and unsuccessful simulations (b) for sample 26 which contains 2.79 mol kg^{-1} Si with $K^+:Si^{IV}$ = 3.80:1. Spectral width = 20 ppm. Simulations were derived from the same exchange matrix used for $M^+:Si^{IV}$ = 1:1. They fail because line-broadening is not uniform in the experimental spectra.

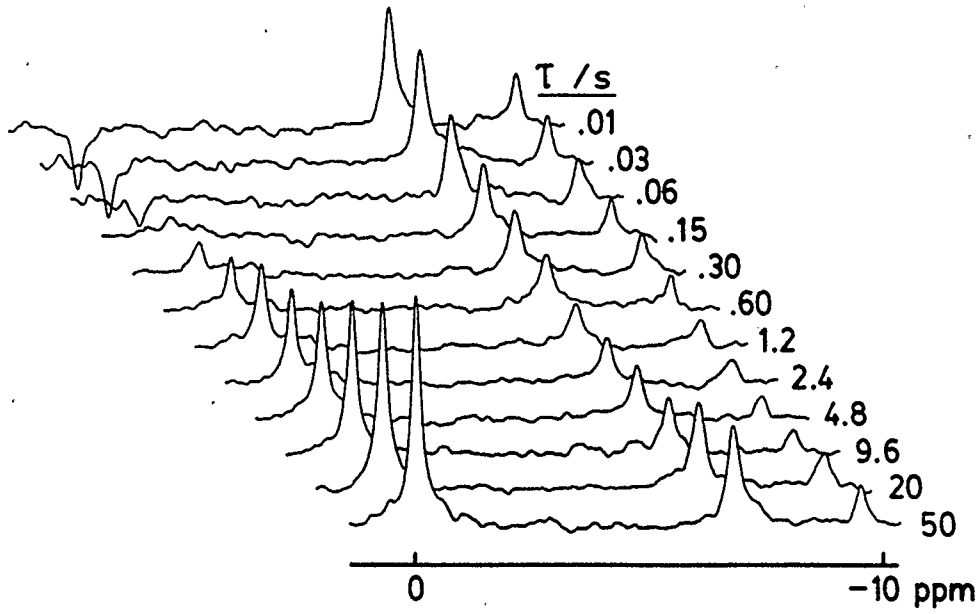

Figure 3-9. ^{29}Si spectra of a selective inversion-recovery experiment at 92°C for sample 24 with 2.80 mol kg^{-1} Si and $K^+:Si^{IV}$ = 4.5:1. The monomer signal is inverted 180° at τ = 0 s.

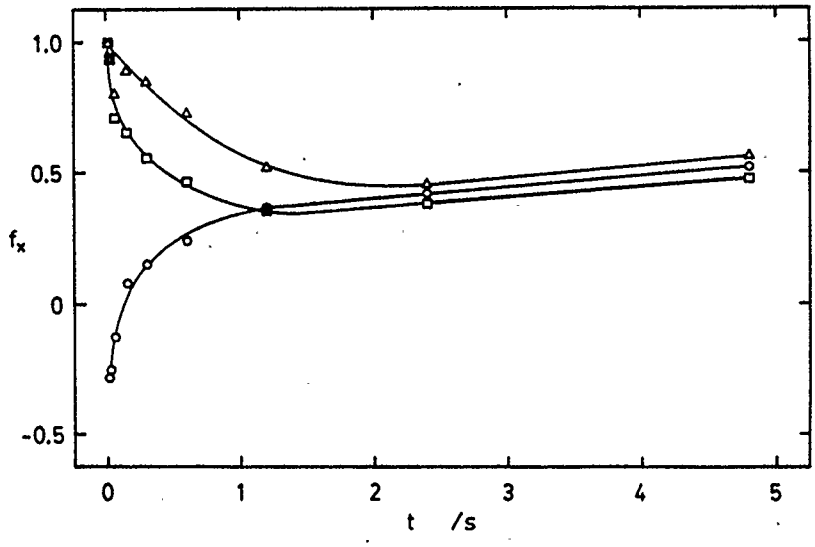

Figure 3-10. Inversion-recovery data for sample 24 (see Figure 3-9) The fractions (f_x) of equilibrium z-magnetization components for the monomer (○), dimer (□) and trimer (△) nuclei are represented as a function of time.

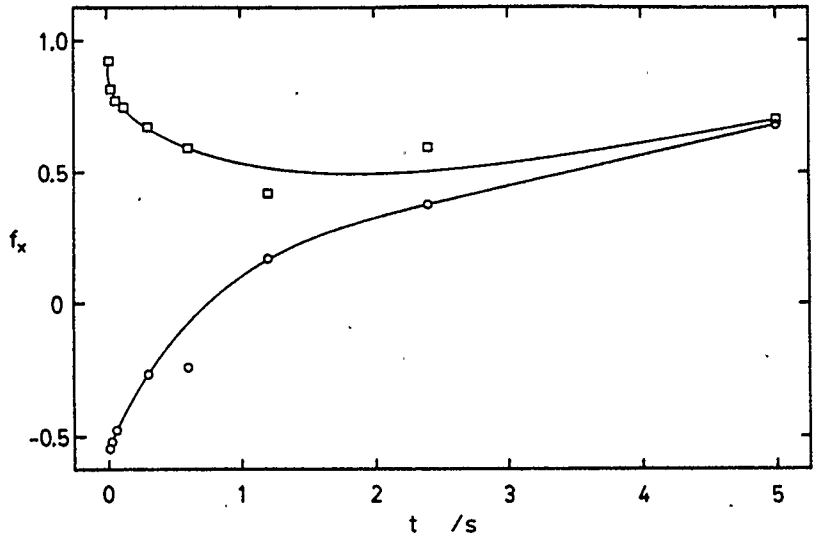

Figure 3-11. As Figure 3-10, for sample 25 with 2.80 mol kg^{-1} Si and $K^+:Si^{IV}$ = 1.0:1.

By assuming that dimer formation proceeds via straightforward monomer addition, Creswell et al.[58] calculated exchange rates from an SIR investigation of a 2.8 mol kg^{-1} solution with $K^+:Si^{IV}$ = 3.8:1. Arrhenius extrapolation of their published rate data yields a half-period in excess of 2 h at 0°C for monomer-dimer exchange. However, spectra which we acquired of samples (21 to 23) with nominal $M^+:Si^{IV}$ ratios from 1:1 to 6:1 all displayed an equilibrium distribution of peaks only 15 min after sample preparation at 0°C (e.g.: see Figure 3-12). Hence, although the present SIR experiments reveal that exchange becomes slower as alkalinity is raised, rates are certainly much faster than those calculated by Creswell et al.

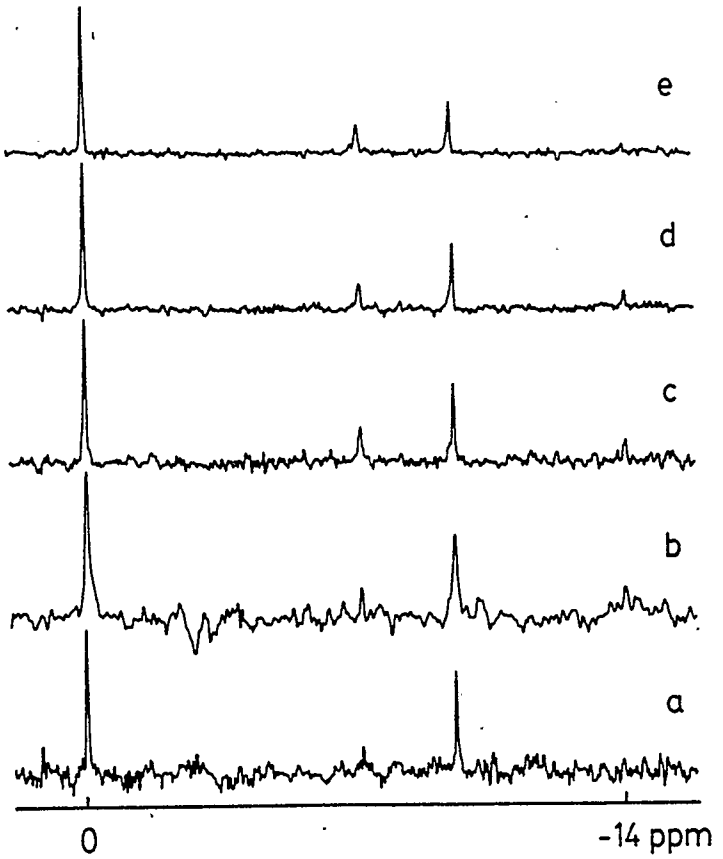

Figure 3-12. Spectra at 0°C of sample 22 (1.3 mol kg^{-1} Si and $Rb^+:Si^{IV}$ = 5.8:1) recorded 15 to 25 min (a), 25 to 35 min (b), 35 to 55 min (c), 55 to 85 min (d), and 85 to 115 min (e) from the start of sample preparation.

3.3.3. Ionization Equilibria

Sjöberg *et al.*[111] determined that pK_a = 9.473 for H_4SiO_4 and 12.65 for $H_3SiO_4^-$ at 298 K and ionic strength I = 0.6 M. Thus, variable degrees of deprotonation of aqueous silicate species can be expected over the pH range relevant to this study. They also found that the average charge per Si atom in alkaline solutions up to pH 12.2 (including those with $M^+:Si^{IV}$ = 1:1) is -0.98(4), and that ionization coefficients vary

between the different silicate oligomers (e.g.: pK_a = 10.25 for $Si_2O_2(OH)_5^-$)[14]. Thus, each Q-centre is singly deprotonated at $M^+:Si^{IV}$ = 1:1, while, at higher alkalinities, the extent of secondary or further deprotonation will depend on the species in which the Q-centre is located.

In the remaining discussion, local charge will be designated using the modified $^xQ^y$ symbol, which represents a SiO_4 centre with 4-y terminal hydroxy groups of which, on average, x are deprotonated.

So far, ^{29}Si nmr spectroscopy has revealed that, as the $M^+:Si^{IV}$ ratio is increased from 1:1, the degree of polymerization is reduced, resonances narrow, and the temperature dependence of broadening differs between resonances. These findings, plus the slow rate determinations of Creswell et al.[58], may be understood if the doubly deprotonated $^2Q^y$ centres, which must become increasingly important as pH rises, are much less reactive in the polymerization process than the singly deprotonated $^1Q^y$ centres. Figure 3-13 (cf. Figure 3-8) demonstrates that excellent spectral simulations can be achieved for a solution with $K^+:Si^{IV}$ = 3.80:1 (sample 26; cf. Creswell et al.[58]) if, and only if, the rate equation corresponding to ionization equilibrium 3.17 is included in exchange matrix K, and it is assumed that the rate of proton transfer is in excess of the fast exchange limit (e.g., if proton exchange is diffusion controlled,

$$^1Q^0 + OH^- \rightleftharpoons {}^2Q^0 + H_2O \qquad (3.17)$$

$k \sim 10^{10}$ to 10^{11} s^{-1} [112]). Hence two signals, a Si-exchange-broadened $^1Q^0$ resonance and a sharp non-broadened $^2Q^0$ peak have collapsed into a single monomer band. The site lifetimes determined by complete band-

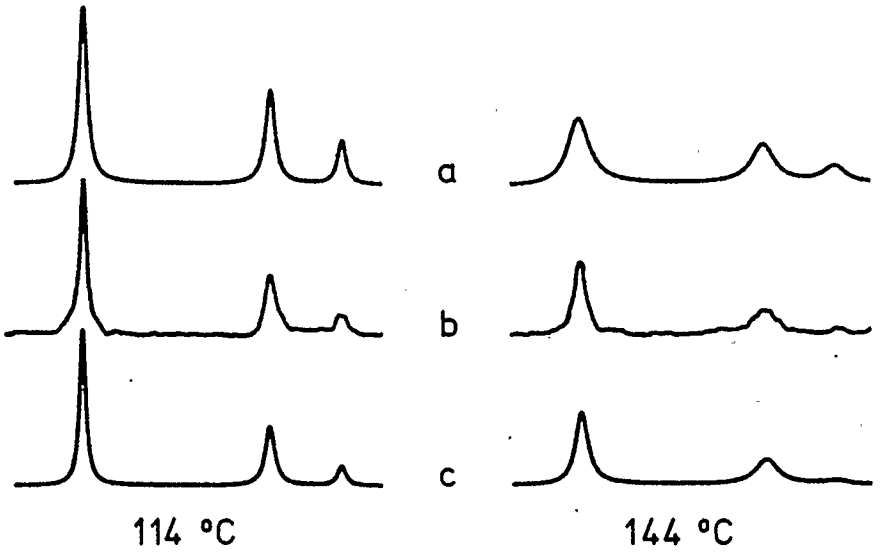

Figure 3-13. Simulations (a,c) and actual ^{29}Si spectra (b) for sample 26 which contains 2.79 mol kg^{-1} Si with $K^+:Si^{IV}$ = 3.80:1 (cf. Creswell et al.[58]). Spectral width = 14 ppm. Simulation (c) allows for deprotonation according to Eqn. 3.17, while (a) does not (see Figure 3-8).

shape analysis for sample 26 (listed in Table III-IV) are much longer than for $M^+:Si^{IV}$ = 1.0:1 (e.g., 0.10 s compared with 5.3×10^{-3} s, at 100°C), which is in accordance with the qualitative SIR observations. Arrhenius extrapolation would suggest that intermolecular Si-Si exchange has a half-period of 2 to 3 min at 0°C, which would account for the rapidly attained equilibrium conditions in freshly prepared samples 21 and 22.

Table III-IV. Inverse Spin-Site Lifetimes For Sample 26 (2.80 mol kg^{-1} Si and $K^+:Si^{IV}$ = 3.80:1.)[a]

T/°C	τ^{-1}/s^{-1}
83.2	4(1)
113.8	24(2)
131.5	47(2)
140.0	82(4)
144.2	98(4)

ΔH^* = 62.1(4.7) kJ mol^{-1}
ΔS^* = -61(11) J mol^{-1} K^{-1}

a. See footnote a in Table III-II.

The variation observed in the temperature dependence of $\Delta\nu_{1/2}$ at $M^+:Si^{IV}$ > 1:1 (Figures 3-5 and 3-6) would suggest that other Q-centres undergo secondary deprotonation at higher pH's than the monomeric centre, and that the relative ease of deprotonation is $Q^0 \sim Q^2{}_3 > Q^1{}_2 \sim Q^2{}_4$. Of course, Q^3 centres are completely deprotonated after losing just one proton.

3.3.4. Reaction Model

For solutions with $M^+:Si^{IV}$ = 1:1, the uniformity of temperature dependent line-broadening demonstrates that all silicate centres, except those in species which are rapidly cyclized, participate equally in Si-Si exchange. This independence from the nature of the reactive sites is typical of diffusion controlled processes, but aqueous diffusion rates are many orders of magnitude greater than the entire frequency range of ^{29}Si resonances.

Instead, Si-Si exchange-broadening is more likely to represent the comparatively slow (yet rapidly reversible) formation of "activated" silicate sites ($^{*}Q^{y}$) which go on to associate quickly, and indiscriminately, with other nearby Q-centres (See Scheme 1). If the activated $^{*}Q^{y}$ site is situated in an easily cyclizable anion, very rapid intramolecular $^{*}Q...^{1}Q$ encounter would be expected. This is consistent with the paucity of ring-precursors that have been detected by ^{29}Si-NMR, and also accounts for excessive broadening of the only resonances which have been "positively" assigned to such a species, i.e., lines 4 and 22 corresponding to the linear trimer[52,53]. Alternatively, if $^{*}Q^{y}$ is in a silicate anion which can not undergo intramolecular rearrangement, it may encounter and subsequently bond with a Q-centre of another anion before reverting to its non-activated $^{1}Q^{y}$ state. The different broadening observed, for example, between resonances of the dimer and linear trimer species is therefore indicative of the corresponding frequencies of intermolecular and intramolecular $^{*}Q...^{1}Q$ encounter. In contrast, the surprising uniformity of line-broadening observed for all non-cyclizable species would suggest that there may be a predominant vehicle of intermolecular Si-Si exchange. The small size (i.e., superior mobility) and high abundance of the monomer would make it the most likely candidate. If this assumption is correct, then monomer addition (Figure 3-14), which represents a significant part of the overall polymerization process in any event, would be the rate-controlling pathway for intermolecular Si-Si chemical exchange.

IONIZATION EQUILIBRIA

$$ {}^{0}Q^{y} + OH^{-} \rightleftharpoons {}^{1}Q^{y} + H_2O $$

$$ {}^{1}Q^{y} + OH^{-} \rightleftharpoons {}^{2}Q^{y} + H_2O \qquad y = 0 \text{ to } 3 $$

ACTIVATION ([H^+]-dependent)

$$ {}^{1}Q^{y} \rightleftharpoons {}^{*}Q^{y} \qquad y = 0 \text{ to } 3 $$

INTRAMOLECULAR POLYMERIZATION

$$ {}^{*}Q^{x} + {}^{1}Q^{y} \rightleftharpoons {}^{1}Q^{x+1}\text{—}{}^{1}Q^{y+1} \cdots\cdots\cdots\cdots \overset{\text{dissociation}}{\rightleftharpoons} \cdots\cdots $$

intramolecular rearrangement

(except dimer and cyclic trimer)

$$ {}^{*}Q^{x} + {}^{2}Q^{y} \rightarrow \text{(unimportant)} \qquad x = 1, 2 \text{ (or 3)}; \; y = 1, 2 \text{ (or 3)} $$

INTERMOLECULAR POLYMERIZATION

$$ {}^{*}Q^{x} + {}^{1}Q^{y} \rightleftharpoons {}^{1}Q^{x+1}\text{—}{}^{1}Q^{y+1} \cdots\cdots\cdots\cdots \overset{\text{dissociation}}{\rightleftharpoons} \cdots\cdots $$

intramolecular rearrangement

$$ {}^{*}Q^{x} + {}^{2}Q^{y} \rightarrow \text{(unimportant)} \qquad x = 0, 1, 2 \text{ or } 3; \; y = 0, 1, 2 \text{ or } 3 $$

Scheme 1. Summary of proposed silicate polymerization process. Side-products of the activation or polymerization steps (i.e., H_2O) depend on the mechanisms involved (see text).

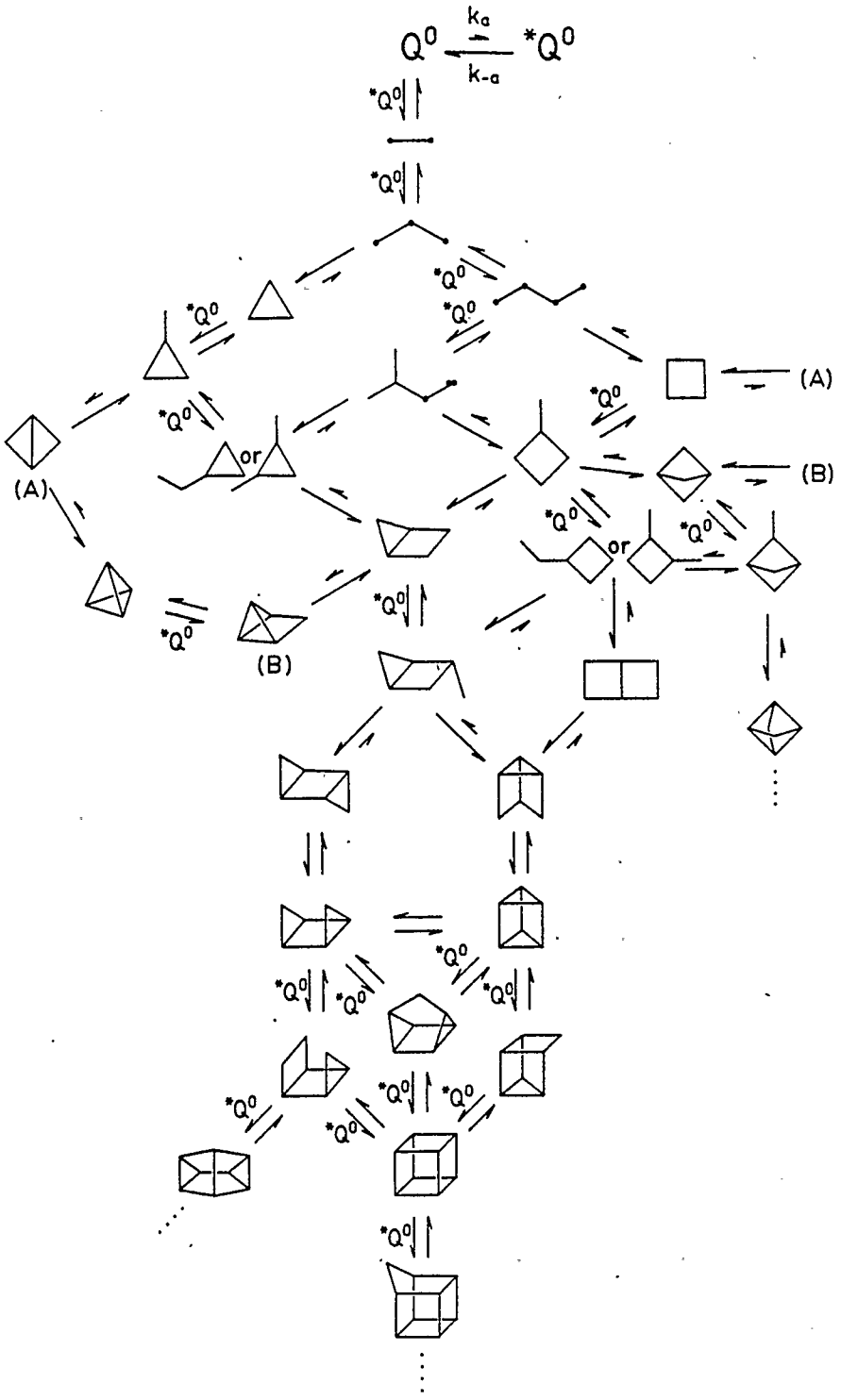

Figure 3-14. Stepwise monomer addition process. This is proposed as the rate-controlling pathway for intermolecular Si-Si chemical exchange. Monomer may be either in the activated $*Q^0$ form (as shown) which bonds with any singly deprotonated ^1Q-centre, or a singly deprotonated $^1Q^0$ anion which bonds with activated sites on other oligomers.

A single least-squares fit[109] of all τ^{-1} values in Table III-II to the Eyring equation[110] (3.18),

$$\tau^{-1} = \frac{k_B T}{h} \exp\left[(-\Delta H^* + T\Delta S^*)/RT\right] \qquad (3.18)$$

in which k_B is Boltzmann's constant and h is Planck's constant, yields activation parameters ΔH^* = 50.1 (1.4) kJ mol^{-1} and ΔS^* = -69.0 (3.8) J mol^{-1} K^{-1} for intermolecular $^*Q^X \ldots {}^1Q^Y$ encounter at $Na^+:Si^{IV}$ = 1.0:1 (Figure 3-15). The longer site lifetimes listed in Table III-IV for $K^+:Si^{IV}$ = 3.80:1 yield activation parameters ΔH^* = 62.1 (4.7) kJ mol^{-1} and ΔS^* = -61 (11) J mol^{-1} K^{-1} (Figure 3-16.)

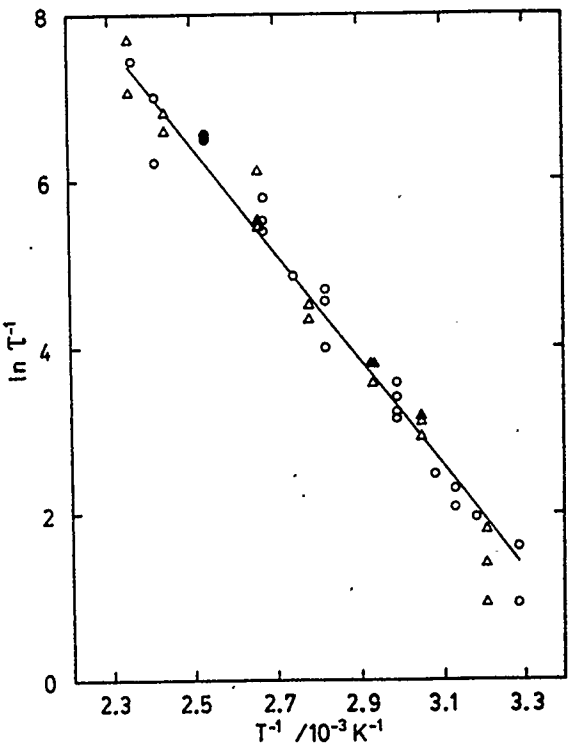

Figure 3-15. Least-squares fit[109] to the Eyring equation (3.18) of the weighted (by experimental uncertainty) τ^{-1} values in Table III-II (sample 37 excluded). The corresponding silicate solutions were prepared from ^{29}Si-enriched silica (batch A (○) and batch B (△) and contained $Na^+:Si^{IV}$ = 1:1.

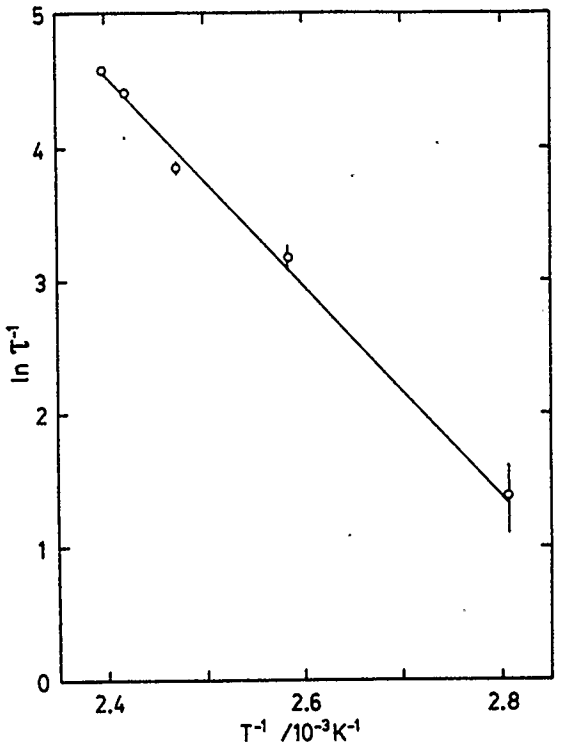

Figure 3-16 Least-squares fit to the Eyring equation (3.18) of the weighted τ^{-1} values in Table III-IV for sample 26 which contains 2.80 mol kg^{-1} Si with $K^+:Si^{IV}$ = 3.80:1.

Since the reactivity between activated and singly deprotonated silicate centres is unlikely to vary with the $M^+:Si^{IV}$ ratio, the $[H^+]$-dependence of τ^{-1} indicates that the activation mechanism is suppressed by high alkalinity. This would suggest that activation involves protonation of $^1Q^y$ to form a neutral $^0Q^y$ centre (e.g. for y=0, H_4SiO_4), followed at some stage by H_2O elimination. If loss of the water molecule occurs very soon after protonation, the activated *Q-site would be in effect a tricoordinated silicate centre (e.g. for y=0, H_2SiO_3) at which polymerization would occur via a S_N1 (dissociative) process[112]. Alternatively, S_N2-type association[112] might occur directly at the protonated ^0Q-site, such that H_2O is released during the polymerization step itself. Unfortunately, these two mechanisms are kinetically indistinguishable[113].

When an activated $^*Q$-site forms an encounter complex[112] with a singly deprotonated ^1Q-centre, repeated proton exchange back and forth will always result in the complementary pair of $^*Q$- and ^1Q-centres which eventually join together. Rapid proton transfer between $^*Q$- and doubly deprotonated ^2Q-centres, however, will result in two negatively charged centres that repel one another and are therefore less likely to join. This would account for the apparent unimportance of doubly deprotonated silicate centres in Si-Si exchange that is manifested by the inequality of temperature dependent line-broadening at high alkalinity.

Because the $^*Q$-condensation rate is the same at all major silicate centres, silicate dissociation rates must <u>differ</u> from one species to another. The ease with which a bridging Si-OSi bond is cleaved, therefore, will depend on the nature of the groups coordinated to each silicon. If monomer condensation was certain to be the rate-controlling step for polymerization, monomer elimination rates for all species could be determined from the τ^{-1} and integration measurements. In any case, the rate coefficient for cleavage of the dimer (k_-) may be estimated using Eqn. 3.19, in which $k_+[^*Q^0] = \tau^{-1}$ corresponds to the pseudo-first-order rate coefficient for dimerization, and P_1 and P_6 are the integrated areas of the monomer and dimer resonances (see Table II-I) at $M^+:Si^{IV} = 1:1$.

$$\begin{aligned} k_- &= k_+ \frac{[^*Q^0][^1Q^0]}{[^1Q^1{}_-{}^1Q^1]} \\ &= \tau_-{}^1 \frac{[^1Q^0]}{[^1Q^1{}_-{}^1Q^1]} \\ &= 2\tau^{-1} \frac{P_1}{P_6} \end{aligned} \qquad (3.19)$$

In the absence of extensive equilibrium data for the deprotonation reactions, a complete set of rate parameters spanning all concentrations and temperatures can not be derived exclusively from line-shape analysis. As discussed below, however, further work with the selective-inversion recovery technique could provide some additional information.

3.3.5. Reinterpretation of Selective Inversion-Recovery Data

A method of obtaining quantitative rate data from selective inversion recovery experiments can now be explored. In spectra of a 2.8 mol kg^{-1} silicate solution with $K^+:Si^{IV}$ = 3.8:1 (Figure 3-8), the three principal resonances correspond to monomer (A), dimer (B) and cyclic trimer (C). Lineshape analysis of these spectra (Figure 3-13c) indicates that the distribution of species can probably be approximated by the equilibria:

$$ {}^1Q^0 + OH^- \underset{}{\overset{K_{b2}}{\rightleftharpoons}} {}^2Q^0 + H_2O \qquad (3.20a) $$

$$ [{}^TQ^0] = [{}^1Q^0] + [{}^2Q^0] + [{}^*Q^0] \sim [{}^1Q^0] + [{}^2Q^0] $$

$$ [{}^1Q^0] = \phi[{}^TQ^0] $$

$$ \phi = (K_{b2}[OH^-]+1)^{-1} $$

$$ {}^1Q^0 + {}^*Q^0 \underset{k_{-1}}{\overset{k_1}{\rightleftharpoons}} {}^2Q^1{}_2 \qquad (3.20b) $$

$$ {}^2Q^1{}_2 + {}^*Q^0 \underset{k_{-2}}{\overset{k_2}{\rightleftharpoons}} ({}^1Q^2{}^2Q^1 \rightleftharpoons) \; {}^3Q^2{}_3 \qquad (3.20c) $$

At time t following the 180° inversion pulse train, the fraction (f_x) of the equilibrium z-magnetization for nucleus x is determined from the corresponding line intensities (Eqn. 3.21).

$$f_x = \frac{M_{zx(t)}}{M_{zx(\infty)}} \tag{3.21}$$

The proportionality between the z-magnetization components and species population is given in Eqn. 3.22.

$$M_{zA(\infty)} \propto [{}^{T}Q^{0}] \tag{3.22a}$$

$$M_{zB(\infty)} \propto 2[Q^{1}{}_{2}] \tag{3.22b}$$

$$M_{zC(\infty)} \propto 3[Q^{2}{}_{3}] \tag{3.22c}$$

The Bloch equation (3.1c) describing the time dependence of the M_{zA} component is modified to account for Si-exchange in Eqn. 3.23, from which the time dependence of the fractional magnetization (Eqn. 3.24a) can be obtained. Similar expressions for sites B and C are given in Eqns. 3.24b and c.

$$\frac{dM_{zA(t)}}{dt} = \frac{d(f_A M_{zA(\infty)})}{dt} = T_{1A}^{-1}(M_{zA(\infty)} - M_{zA(t)}) - v_A \gamma B_1$$

$$- k_1[{}^{*}Q^{0}]\phi M_{zA(t)} + k_{-1}\frac{M_{zB(t)}}{2}$$

$$= T_{1A}^{-1}(1-f_A)M_{zA(\infty)} - v_A\gamma B_1 - \phi k_1[{}^{*}Q^{0}]f_A M_{zA(\infty)} + k_{-1}\frac{f_B M_{zB(\infty)}}{2} \tag{3.23}$$

$$\frac{df_A}{dt} = T_{1A}^{-1}(1-f_A) - \frac{v_A\gamma B_1}{M_{zA(\infty)}} + \tau^{-1}(f_B - \phi f_A) \tag{3.24a}$$

$$\frac{df_B}{dt} = T_{1B}^{-1}(1-f_B) - \frac{v_A\gamma B_1}{M_{zB(\infty)}} + \phi f_A k_{-1} - f_B(k_{-1}+\tau^{-1}) + f_C\tau^{-1} \tag{3.24b}$$

$$\frac{df_C}{dt} = T_{1C}^{-1}(1-f_C) - \frac{v_A \gamma B_1}{M_{zC(\infty)}} + k_{-2}(f_B - f_C) \qquad (3.24c)$$

Iterative curve-fitting of Eqn. 3.24a to the experimental inversion recovery data (e.g., Figure 3-10) can provide a solution for τ^{-1}, but only if ϕ is known. Because Creswell et al.[58] did not account for ionization (which is equivalent to setting $\phi = 1$), their estimate for k_1 is averaged over all monomeric centres and yields inverted spin-site lifetime $\tau^{-1} = 0.31\ s^{-1}$ ($= k_1[^TQ^0] = 0.21\ mol\ kg^{-1}\ s^{-1} \times 1.47\ mol\ kg^{-1}$) at 83°C. Comparison with the value $\tau^{-1} = 3.7\ s^{-1}$ extrapolated from the CBA data in Table III-IV would suggest that only ca. 8% of all monomer is in the reactive $^1Q^0$ form at this temperature.

In principle, if a series of SIR and CBA experiments were conducted for the same sample, an estimate of ϕ could be obtained by substituting spin-site lifetimes derived from bandshape analysis into Eqn. 3.24a and, then, curve-fitting the SIR data. This was not attempted.

3.4. Conclusion

Our findings demonstrate that temperature dependent line-broadening in ^{29}Si spectra of aqueous silicate solutions is indeed the result of rapid Si-Si chemical exchange. Extreme broadening of the few resonances observed which correspond to easily cyclizable anions (e.g., acyclic trimer) indicates that intramolecular ring formation occurs more rapidly than intermolecular condensation. At $M^+:Si^{IV} = 1:1$, all other resonances broaden uniformly with temperature which signifies that the rate of intermolecular Si-Si exchange is the same at all singly deprotonated

silicate centres (ΔH^* = 50.1(1.4) kJ mol^{-1}, ΔS^* = -69.0(3.8) J mol^{-1} K^{-1}). Thus, the rate of intermolecular polymerization would appear to be controlled by the relatively rapid condensation of a common species which is most likely monomer.

As alkalinity is increased ($M^+:Si^{IV} > 1:1$), so is the level of secondary (and further) deprotonation depending on the pK_a's of the different centres. The nonuniformity of line-broadening and the equilibrium shift towards monomer and low-molecular-weight oligomers indicate that the doubly deprotonated centres are much less reactive in polymerization than singly deprotonated centres. In addition, the rate of Si-Si exchange is reduced overall due to a decrease in the number of activated (neutral) centres which mediate both intramolecular and intermolecular condensation.

Using unlined, glass NMR tubes, other workers have observed up to a 16-fold <u>increase</u> in broadening as alkalinity is raised.[57,60] There can be little doubt, therefore, that most of the controversy over ^{29}Si line-broadening and Si-Si exchange rates is due to leaching of unknown T_2-relaxation agents from the unprotected glass tubes. Indeed when deprotonation equilibria are taken into consideration, line-broadening analysis and selective-inversion recovery experiments do yield consistent results.

Finally, there is evidence to suggest that a small contribution to line-widths arises from ^{29}Si-M dipole-dipole relaxation, although the effect will be important only at very low temperature and/or high pH where Si-Si exchange-broadening is negligible.

CHAPTER IV. Longitudinal ^{29}Si Relaxation In Silicate Solutions.

4.1. Introduction

4.1.1. Previous Studies

An understanding of the dependence of the longitudinal nuclear magnetic relaxation time T_1 on sample composition and conditions is essential if quantitative NMR spectra are to be obtained, and can also provide useful information concerning molecular structure and dynamics. In the case of ^{29}Si NMR of $(HO)_3SiO^-$ and its polymers in aqueous alkaline solution, reported T_1 values are unusually short for silicon compounds[59,83] and range from about 0.5s in a solution containing 2 mol kg^{-1} of Si^{IV} with $Na^+:Si^{IV}$ = 3:1[44] to 26s in one containing <0.05 mol L^{-1} of Si^{IV} and 0.6 mol L^{-1} of Na^+ [15] for the dimer at 25°C.

Early on, it was suggested[44] that such efficient ^{29}Si relaxation could arise from rapid interchange between protonated and deprotonated silanol groups which, having different chemical shifts, should generate an appropriate fluctuating magnetic field. Harris and Newman[48], however, noted that this field would be parallel to the external field B_o and so could not cause longitudinal relaxation. Instead, they concluded from their observations of "aging" effects in silicate solutions contained in unlined, glass NMR tubes that unidentified paramagnetic contaminants were probably the dominant factors controlling transverse as well as longitudinal ^{29}Si relaxation[48,59]. However, we have shown in the preceding chapter that there is no evidence for transverse relaxation by paramagnetic impurities if reasonable care is taken to exclude them.

4.1.2. Theory of Longitudinal Relaxation

The longitudinal relaxation time characterizes the rate at which thermal equilibrium between spin states is restored following absorption of a radio-frequency signal (see Sect. 3.1.2). For spin 1/2 nuclei such as ^{29}Si, there is only one excited level besides the ground state and the total longitudinal relaxation rate T_1^{-1} can be expressed (Eqn. 4.1)

$$T_1^{-1} = T_{1DD}^{-1} + T_{1SC}^{-1} + T_{1UE}^{-1} + T_{1SA}^{-1} + T_{1SR}^{-1} \qquad (4.1)$$

in terms of contributions T_{1DD}^{-1} from nuclear magnetic dipole-dipole interactions, T_{1SC}^{-1} from scalar processes, T_{1UE}^{-1} from the presence of species with unpaired electrons, T_{1SA}^{-1} from shielding anisotropy, and T_{1SR}^{-1} from the spin-rotation mechanism[85,114,115]. Each of these relaxation pathways arises from intra- or intermolecular motions which modulate the effective magnetic field at the nucleus.

The general expression for T_1 relaxation is given by Eqn. 4.2,

$$T_1^{-1} = \frac{\mu_0 \gamma^2 \langle B^2 \rangle \tau_0}{6\pi(1+\omega^2\tau_0^2)} \qquad (4.2)$$

where $\langle B^2 \rangle$ is the mean-square average of the motionally induced, local fluctuating magnetic field[115]. The dependence of T_1 on the correlation time τ_0, which characterizes molecular motion, passes through a minimum at $\omega\tau_0 = 1$. When the correlation time is very small ($\omega^2\tau_0^2 \ll 1$), as for tumbling in a low viscosity medium, T_1 is inversely proportional to τ_0 and independent of ω. This is known as the <u>extreme narrowing condition</u>[114,115]. As molecular motion becomes slower and τ_0 approaches the magnitude of $\omega = \gamma B_0$, the longitudinal relaxation time becomes dependent on the external field B_0 and begins to rise with τ_0.

Dipole-dipole nuclear magnetic interactions between the nucleus of interest A and nucleus X can be modulated either by molecular tumbling, which will affect both intra- and intermolecular magnetic interactions, or by translational diffusion, which affects only intermolecular interactions. Equations 4.3 and 4.4 describe the contributions of intra- and

$$T_{1DD}^{-1}(\text{intra}) = \frac{1}{12\pi}\mu_o^2\gamma_A^2\gamma_X^2h^2I_X(I_X+1)\tau_C\Sigma r_{AX}^{-6} \qquad (4.3)$$

$$T_{1DD}^{-1}(\text{inter}) = \frac{1}{90\pi}\mu_o^2N_X\gamma_A^2\gamma_X^2h^2I_X(I_X+1)D^{-1}a^{-1} \qquad (4.4)$$

intermolecular dipole-dipole interactions to T_1 relaxation in the extreme narrowing condition, where nucleus A is spin 1/2, r_{AX} is the intramolecular nuclear separation, N_X is the concentration of X spins (per unit volume), D is the mutual translational self-diffusion coefficient of molecules containing A and X, and a is the distance of closest intermolecular approach between A and X[114,115].

The contribution of T_{1DD}^{-1} to the total longitudinal relaxation rate can be determined by the nuclear Overhauser effect (NOE). Complete saturation of the x nuclei increases the intensity (S) of the A signal by enhancement factor η (Eqn. 4.5), from which the fractional contribution of A-X dipole-dipole relaxation to the total T_1 relaxation rate can

$$\frac{S_A(\text{X irradiated})}{S_A} = 1 + \eta = 1 + \frac{\gamma_X}{2\gamma_A} \cdot \frac{T_{1DDX}^{-1}}{T_1^{-1}} \qquad (4.5)$$

be determined (Eqn. 4.6)[114,115]. Since most other nuclei have a positive gyromagnetic ratio, the negative value of γ_{Si} will usually lead to

$$\frac{T_{1DDX}^{-1}}{T_1^{-1}} = \eta\frac{2\gamma_A}{\gamma_X} \qquad (4.6)$$

a negative NOE enhancement.

Scalar contributions to longitudinal relaxation can occur when the spin-spin coupling constant J_{AX} becomes time dependent because of chemical exchange or internal rotation. They also arise if the relaxation rate of the X nucleus is fast compared with $2\pi J_{AX}$ (e.g.: if X is quadrupolar). Both processes are described by Eqn. 4.7 in which τ_X represents either the half period for exchange or T_{1X}[114,115].

$$T_{1SC}^{-1} = \frac{8}{3}\pi^2 J_{AX}^2 I_X(I_X-1)\tau_X[1+(\omega_A-\omega_S)^2(T_{1A})^2]^{-1} \qquad (4.7)$$

Unpaired electron interactions can contribute to relaxation either by transfer of electron density between molecules (more important to T_2 than T_1 relaxation), or by dipole-dipole interactions involving the very high magnetic moment of the electron. Very small concentrations of paramagnetic agents, including dissolved molecular oxygen, can significantly accelerate nuclear relaxation.

If the shielding tensor σ is anisotropic, molecular tumbling will modulate the local field B (see Eqn. 2.3). This relaxation contribution is recognizable by a quadratic dependency on the external field B_o[114,115].

The final contribution to T_1 relaxation of spin 1/2 nuclei is that of spin-rotation. Rotation of a molecule, and thus of the surrounding electron density, induces a magnetic field within the molecule which will fluctuate as the rotational frequency changes. This relaxation mechanism is most efficient for small, rapidly tumbling molecules in low viscosity media, and is unique among all the other contributions since T_{1SR}^{-1} <u>increases</u> with temperature[114,115].

4.1.3. Measurement of T_1 Relaxation Rates

Longitudinal relaxation rates are most commonly determined by the inversion-recovery experiment ($[180°-\tau(\text{varied})-90°(\text{FID})-T_d]_n$) or by some variation of it. The delay (T_d) after the 90° acquisition pulse must be at least 5 times longer than the maximum T_1 value to ensure that the entire spin system is returned to the equilibrium state. Values of T_1 are determined from the time (i.e., relaxation period τ) dependence of the natural logarithm of each peak height S (Eqn. 4.8; see Figure 4-1).

$$\ln[(S_\infty - S_t)(2S_\infty)^{-1}] = -\tau T_1^{-1} \qquad (4.8)$$

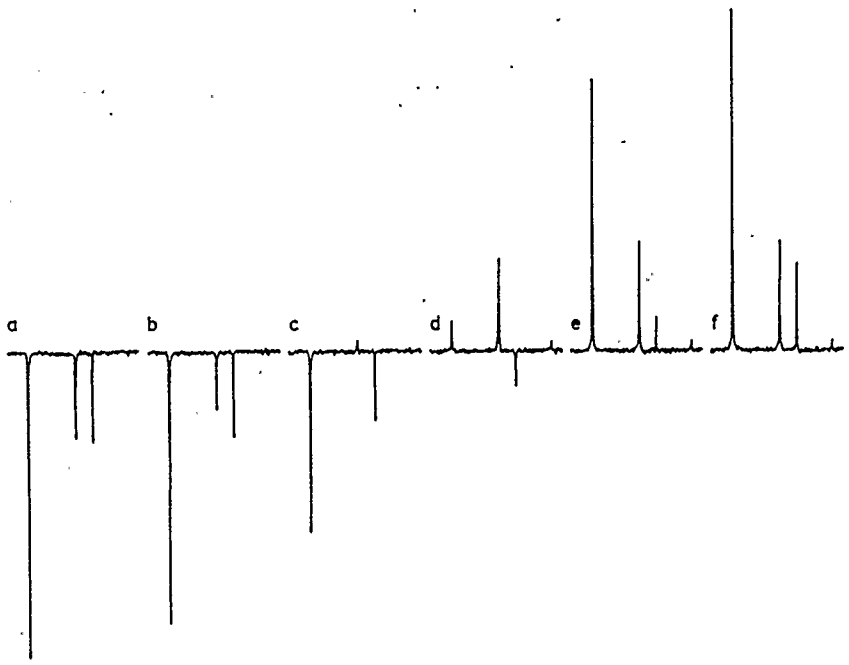

Figure 4-1. Inversion-recovery experiment at 22.9°C for sample 34 which contains 2.17 mol kg^{-1} Si with $Na^+:Si^{IV}$ = 4.0:1. Relaxation period τ = 0.04 (a), 0.11 (b), 0.33 (c), 1.00 (d), 3.00 (e) and 9.00 s (f). Spectral width = 18 ppm. Resultant T_1 values are: 1.31 s, Q^0; 0.41 s, $Q^1{}_2$; and 2.60 s, $Q^2{}_3$.

Errors due to magnetic field or temperature drift can be minimized by cycling τ values over the time-averaged inversion-recovery experiment, rather than employing them consecutively. The Freeman-Hill modification of the inversion-recovery sequence ($[180°-\tau-90°(FID1)-T_d-90°-(FID2)-T_d]_n$, in which FID1 is subtracted from FID2) compensates for spectrometer instability[114]; however, it is very time-consuming and relatively unnecessary when employing a superconducting magnet.

4.2. Experimental

Longitudinal relaxation times were measured for samples 4, 31 and 33 to 42 (as indicated in Table II-II) by the inversion recovery method (relaxation period τ cycled) at temperatures from ca. 0 to 100°C. Samples 33 to 42 were purged with nitrogen to minimize dissolved oxygen prior to T_1 measurements. For sample 33, relaxation times were also determined before dissolved oxygen was removed. Gated ^1H decoupling was employed in the nuclear Overhauser enhancement measurements of samples 33 to 35, 37 to 39, 41 and 42. Among the forest of signals that can appear for ^{29}Si-enriched solutions, singlets corresponding to the totally symmetric species are the easiest to follow over varying sample conditions (Figure 4-2).

4.3. Results and Discussion

All measured ^{29}Si longitudinal relaxation times (for 79 spectra) are listed in Table IV-I. Even at the lowest temperatures employed, Si-Si exchange was sufficiently rapid (see Ch. III) that T_2 was less

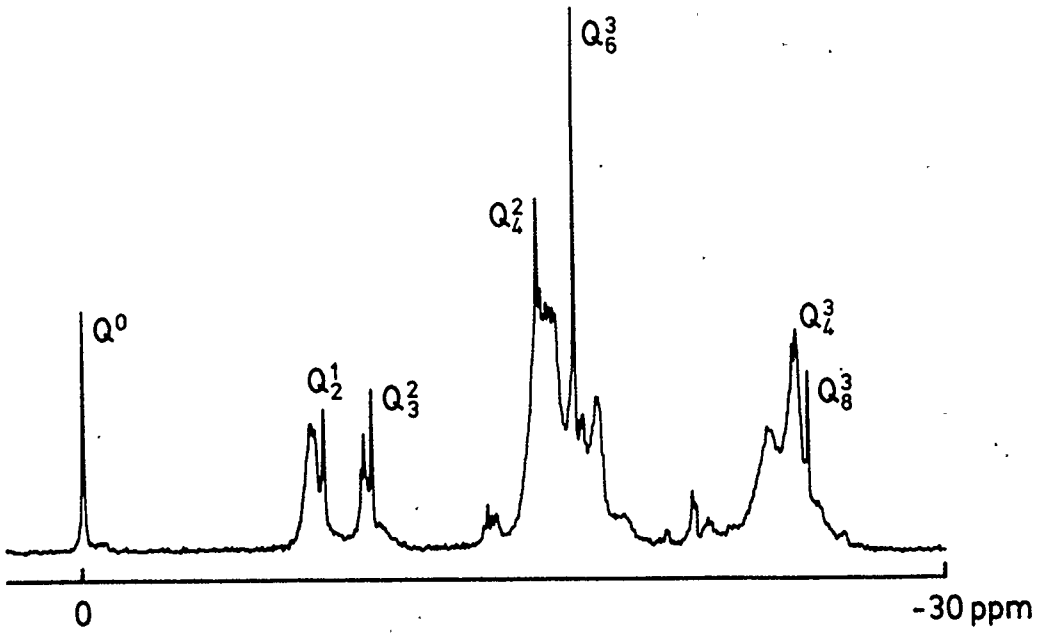

Figure 4-2. ^{29}Si NMR spectrum of sample 33 (2.17 mol kg^{-1} Si with $Na^+:Si^{IV}$ = 1.0:1) at 22.4°C showing singlets corresponding to the totally symmetric species for which T_1 relaxation rates were measured.

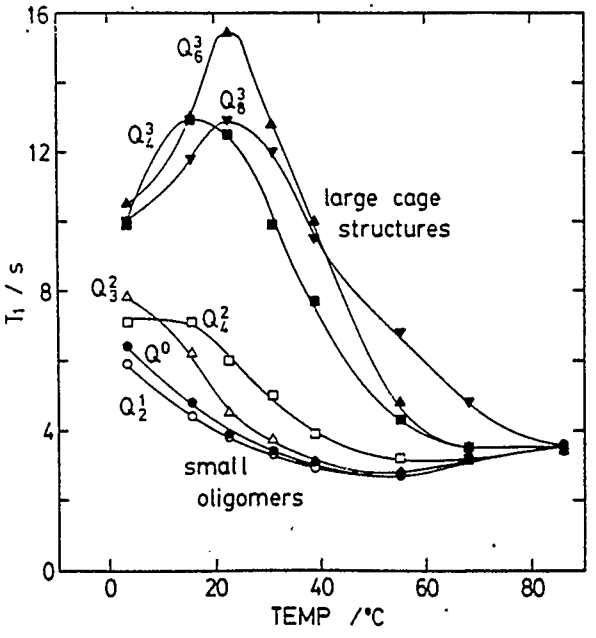

Figure 4-3. Temperature dependence of longitudinal relaxation time for sample 33 with 2.17 mol kg^{-1} Si (95% ^{29}Si-enriched) and $Na^+:Si^{IV}$ = 1.0:1.

Table IV-I. ^{29}Si Longitudinal Relaxation Times (T_1)[a].

Temp/°C	Q^0	$Q^1{}_2$	$Q^2{}_3$	$Q^2{}_4$	$Q^3{}_6$	$Q^3{}_4$	$Q^3{}_8$
a. Sample 4[b] (1.40 mol kg^{-1} Si; $Na^+:Si^{IV}$ = 1.0:1)							
1.2	9.0	8.4	9.9		11.8	10.7	25
11.2	9.0	9.0	9.6	9.8	16.0	12.3	25
21.2	7.7	7.5	7.7	9.0	14.1	14.2	19
31.0	7.3	7.5	7.4	8.1	12.4	11.5[c]	12[c]
41.5	5.7	5.0	5.0	8.3[c]	7.3		
51.6	4.4						
62.1	4.2						
b. Sample 31[b] (1.49 mol kg^{-1} Si; $K^+:Si^{IV}$ = 10.3:1)							
3.3	2.2	0.8	3.8				
29.6	3.0	0.5	7.1				
53.2	5.5	1.3					
59.3	6.0	1.2					
83.2	7.7	2.7					
100.8	14.4						
c. Sample 33[b] (2.17 mol kg^{-1} Si; $Na^+:Si^{IV}$ = 1.0:1)							
3.3	6.4	5.9	7.8	7.1	10.5	9.9	10.0
15.2	4.8	4.1	5.8	6.9	15	13.2	12.5
22.4	3.4	3.2	3.9	5.3	15.4	12.6	14
30.6	3.1	3.0	3.0	4.5	12.8	9.9	14.3
38.8	2.6	2.5	2.7	3.6[c]	7.9	7.2	8.8
55.0	2.7	2.8	2.8	3.2[c]	4.8	4.3[c]	6.8
68.0	3.2	3.2[c]	3.1[c]	3.2[c]	3.5	3.5[c]	4.8
86.7	3.6	3.4[c]	3.4[c]	3.5[c]	3.5	3.5[c]	
d. Sample 33 (2.17 mol kg^{-1} Si; $Na^+:Si^{IV}$ = 1.0:1)							
15.2	4.8	4.4	6.2	7.1	13	12.9	11.8
22.4	3.9	3.8	4.5	6.0	17[d]	12.5	12.9
30.6	3.4	3.3	3.7	5.0	15[d]	10.3[d]	12[d]
38.8	3.1	2.9	3.1	3.9[c]	10	7.7	9.5

Table IV-I. (Continued)

Temp/°C	Q^0	$Q^1{}_2$	$Q^2{}_3$	$Q^2{}_4$	$Q^3{}_6$	$Q^3{}_4$	$Q^3{}_8$
e. Sample 34 (2.17 mol kg^{-1} Si; $Na^+:Si^{IV}$ = 4.0:1)							
3.3	1.33	0.92	3.2				
23.1	1.20	0.37	2.7	0.12			
37.2	1.78	0.40	3.3				
65.4	3.3	1.2	2.0				
83.2	3.5	2.0	1.2				
100.8	3.6	2.9	2.5				
122.7	4.5	(3.9)					
131.5	5.7						
f. Sample 34 (using Nicolet 300)							
-3.0	2.17	1.68	4.4				
8.6	1.44	0.72	3.26	0.7			
22.9	1.31	0.41	2.60	(0.3)			
39.0	1.77	0.42	2.93				
48.3	2.33	0.57	2.8				
g. Sample 35 (1.55 mol kg^{-1} Si; $Na^+:Si^{IV}$ = 1.0:1)							
3.3	7.9	7.0	9.7	8.8	13.1	11.4	10.7
15.2	7.5	6.4	8.5	9.2	19	15.2	15.0
22.4	6.5	6.4	7.1	8.2	16.5	13.3	15
30.6	5.6	5.3	5.6	6.8	15	11.2	15
38.8	4.9	4.8	5.0	6.0	13	9.5	13
55.0	4.2	4.3	4.3[c]	4.6	5.5	5.5	6.4
68.0	4.0	4.5[c]	4.6[c]	4.6[c]	5.0	4.4	5.9
86.7	4.6	4.4[c]	4.5[c]	4.5[c]	4.4	4.4[c]	
102.5	4.0	4.6[c]	4.6[c]	4.5[c]	4.5[c]	4.5[c]	
h. Sample 36 (1.20 mol kg^{-1} Si; $Na^+:Si^{IV}$ = 1.0:1)							
22.4	8.2	7.7	7.5	9.2	15	12.9	12.8
38.8	6.5	6.6	6.3	6.8	9.0	8.2	10.3

Table IV-I. (Continued)

Temp/°C	Q^0	$Q^1{}_2$	$Q^2{}_3$	$Q^2{}_4$	$Q^3{}_6$	$Q^3{}_4$	$Q^3{}_8$
i. Sample 37 (0.80 mol kg^{-1} Si; $Na^+:Si^{IV}$ = 1.0:1)							
3.3	13.4	11.7	13.2	11.4	13.3	13.6	12.6
15.2	11.6	11.5	13.0	14	19	17	20
22.4	11.8	11.0	11.5	12.7	16.9	17.9	
38.8	9.7	10.0	10.3	10.6	13.3	12.0	
55.0	8.4	8.9	11.9	8.7[c]		9.2[c]	
68.0	7.2	7.5	15	8.8[c]		9.3[c]	
86.7	6.9	8.4[c]	8.4[c]	9.1[c]		7.4[c]	
j. Sample 38 (2.18 mol kg^{-1} Si; $Na^+:Si^{IV}$ = 1.0:1)							
3.3	3.7	3.5	8.9	7.8	14.8	11.4	
22.4	2.5	2.4	3.4	5.4	15.7	17.4	
38.8	3.2	2.5	3.9	4.4		15.4	
k. Sample 39 (2.17 mol kg^{-1} Si; $K^+:Si^{IV}$ = 4.0:1)							
3.3	4.05	1.38	7.4	1.0			
14.5	4.72	1.09	9.0	0.7			
23.1	6.2	1.49	8.9	0.9			
37.2	8.7	2.53	9.2				
53.2	10.0	4.4	8.0				
74.3	12	9.0	10				
100.8	15	12	10				
l. Sample 40 (2.17 mol kg^{-1} Si; $Na:Si^{IV}$ = 4.0:1)							
1.5	1.32	0.90	2.7				
23.1	1.31	0.38	2.80				
37.2	2.14	0.50	2.8				

Table IV-I. (Continued)

Temp/°C	Q^0	$Q^1{}_2$	$Q^2{}_3$	$Q^2{}_4$	$Q^3{}_6$	$Q^3{}_4$	$Q^3{}_8$
m. Sample 41 (2.17 mol kg^{-1} Si; $Rb^+:Si^{IV}$ = 4.0:1)							
1.5	1.97	0.83	4.7	0.8			
3.3	1.96	0.77	4.8	1.1			
14.5	2.32	0.58	4.7	0.41			
23.1	2.76	0.66	5.2	0.37			
37.2	4.08	0.90	5.0				
53.2	5.0	1.80	5.5				
74.3	4.9	4.0	3.5				
n. Sample 42 (0.30 mol kg^{-1} Si; $Na^+:Si^{IV}$ = 1.0:1)							
22.4	26.8	28		34	(28)	28	
38.8	24.1	22.8	(36)[c]	27[c]		33[c]	(36)[c]
86.7	10	16[c]	16[c]	27[c]	17[c]	(12)[c]	(12)[c]

[a] In seconds^{-1} with uncertainty typically ±5%. [b] Not purged of O_2. [c] Peak indistinct from nearest neighbours. [d] Unreliable due to short ($< 5T_1$) delay used in inversion recovery pulse sequence.

than T_1 in all solutions. Data for sample 33 with 2.17 mol kg^{-1} Si and $Na^+:Si^{IV}$ = 1.0:1 are presented in Figure 4-3. Gross averaging of T_1 values for the various Si centres is evident above 30°C and, as revealed by line-broadening (cf. Figure 3-3), this is attributable to rapid Si-Si exchange during the inversion-recovery pulse sequence. When exchange averaging can be disregarded, e.g., in these 1.0:1 solutions below 20°C, T_1 is seen to increase with temperature for the larger and less flexible anions, most notably for the Q^3-containing species.

When the averaging effect of Si-Si chemical exchange is allowed for, it should be possible to account for the observed values of T_1^{-1} in terms of the contributions summarized in Eqn. 4.1. Small increases in T_1 were observed when air-saturated sample 33 was purged of O_2 with bubbled nitrogen (see Table IV-I). The corresponding unpaired electron relaxation contribution, T_{1UE}^{-1}, was calculated from the T_1 differences and ranged from 0.04 s^{-1} for the monomer to $\leq 0.01 s^{-1}$ for the largest species, and is similar in magnitude to findings with organosilicon compounds saturated in O_2[116]. Thus, dissolved oxygen makes, at most, a trivial contribution to T_{1UE}^{-1}, and was in any case removed from most other solutions. Contributions to T_{1UE}^{-1} from other paramagnetic species were negligible; the solutions were prepared and handled in Teflon equipment to obviate leaching of contaminants, and consistent T_1 data were obtained from samples 33 and 38 having similar compositions but made with silica from different sources. The T_1 data reported here are also consistent with those listed by Harris[59], once the influence of solution composition and temperature, as analyzed below, are taken into

account.

Scalar coupling can be disregarded as a source of longitudinal relaxation, since no nuclei with resonant frequencies near that of ^{29}Si were present (see Eqn. 4.7). Any significant contribution to T_1^{-1} from shielding anisotropy would be detectable through its second-power dependence on B_0, but in no case was the ^{29}Si relaxation rate increased when B_0 was increased from 4.70 to 7.05 T (Figure 4-4). On the contrary, relaxation rates T_1^{-1} were slightly reduced below 20°C as a result of this

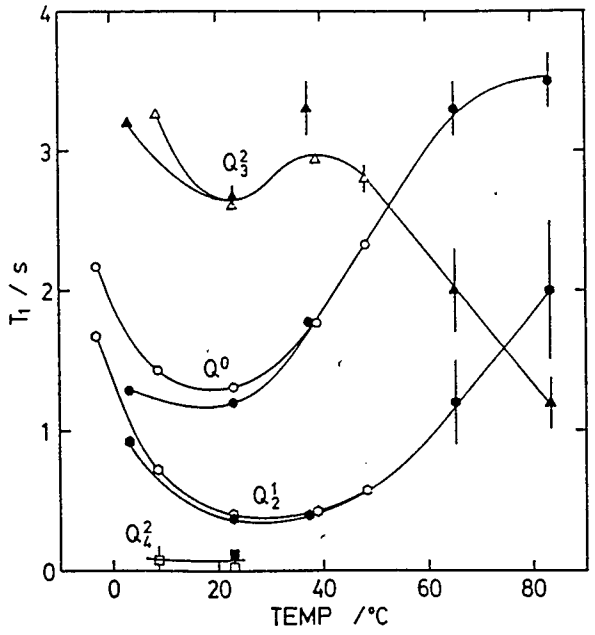

Figure 4-4. Temperature dependence of longitudinal relaxation for sample 34 with 2.17 mol kg^{-1} Si and $Na^+:Si^{IV}$ = 4.0:1; B_0 = 4.70 T (solid symbols) and 7.10 T (open symbols).

increase in B_0, which suggests that, whatever the principal relaxation mechanism, the extreme narrowing condition ceases to be strictly valid for these solutions at low temperatures.

For the less condensed species, the modest shortening of T_1 with rising temperature (cf. Figure 4-3, discounting T_1 averaging above 20°C) evidently reflects a contribution from the spin-rotation mechanism, since this is the only relaxation process that would of itself give this

kind of temperature dependence. For the larger silicate oligomers, this effect is greatly reduced, which is in accordance with expectations for the spin-rotation mechanism since whole-molecule rotation is limited and internal rotation is, in the case of Q^3 centres at least, impossible.

This leaves the dipole-dipole mechanism as the probable chief cause of ^{29}Si longitudinal relaxation in alkaline aqueous silicate solutions. The only nuclei present that could be responsible for these processes are ^1H and ^2H from the H_2O/D_2O solvent, and the M^+ nuclei. The fractional contribution T_{1DDH}^{-1}/T_1^{-1} of ^{29}Si-^1H dipole-dipole relaxation (DDH) to the total longitudinal relaxation rate (values in Table IV-III) was calculated (by Eqn. 4.6) from the NOE data listed in Table IV-II. The DDH contribution was significant only at low temperatures, decreasing eight-fold from 0 to 60°C (Figure 4-5). In absolute terms, T_{1DDH}^{-1} was smallest for the silicate oligomers of high molar mass and decreased

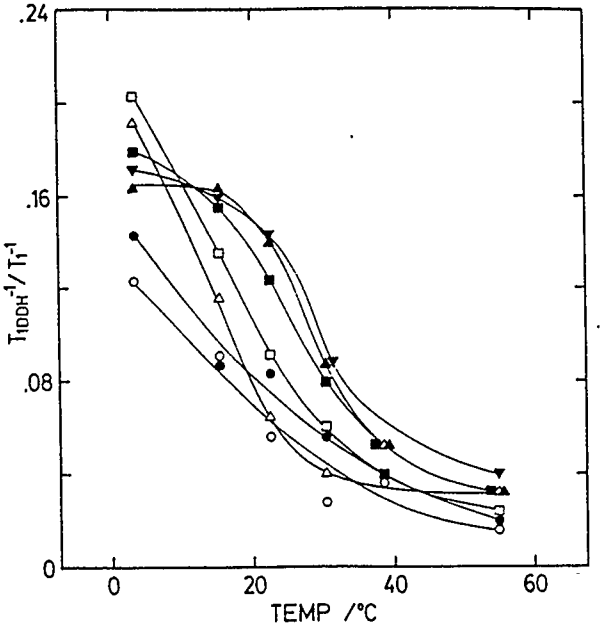

Figure 4-5. Temperature dependence of the proportional DDH contribution to T_1 relaxation. Solution composition and symbols are as in Figure 4-3.

Table IV-II. $^{29}Si\{^{1}H\}$ Nuclear Overhauser Enhancement Factor (η)[a].

Temp/°C	Q^0	$Q^1{}_2$	$Q^2{}_3$	$Q^2{}_4$	$Q^3{}_6$	$Q^3{}_4$	$Q^3{}_8$
a. Sample 33 (2.17 mol kg^{-1} Si; $Na^+:Si^{IV}$ = 1.0:1)							
3.3	-0.36	-0.31	-0.48	-0.51	-0.41	-0.45	-0.43
15.2	-0.22	-0.23	-0.29	-0.34	-0.41	-0.39	-0.40
22.4	-0.21	-0.14	-0.16	-0.23	-0.35	-0.31	-0.36
30.6	-0.14	-0.07	-0.10	-0.15	-0.22	-0.20	-0.22
38.8	-0.10	-0.09	-0.13	-0.10	-0.13	-0.13	-0.22
55.6	-0.05	-0.04	-0.08	-0.06	-0.08	-0.08	-0.10
b. Sample 34 (2.17 mol kg^{-1} Si; $Na^+:Si^{IV}$ = 4.0:1)							
3.3	-0.20	-0.16	-0.25	-0.28			
23.1	-0.08	-0.04	-0.16	0			
37.2	-0.02	-0.04	-0.10				
53.2	-0.03	-0.04	-0.03				
65.4	-0.02	0	0				
83.2	-0.02	-0.01	0				
100.8	-0.04						
c. Sample 35 (1.55 mol kg^{-1} Si; $Na^+:Si^{IV}$ = 1.0:1)							
3.3	-0.38	-0.32	-0.47	-0.50	-0.41	-0.45	-0.44
22.4	-0.22	-0.21	-0.21	-0.26	-0.32	-0.31	-0.35
38.8	-0.13	-0.13	-0.12	-0.10	-0.15	-0.16	-0.18
55.0	-0.05	-0.07	-0.06	-0.08	-0.09	-0.08	-0.17
86.7	-0.07	-0.04[b]	-0.08[b]	-0.04[b]	-0.04	-0.02[b]	
102.5	-0.08	-0.06[b]	-0.06[b]	-0.03[b]	-0.04[b]	-0.01[b]	
d. Sample 37 (0.80 mol kg^{-1} Si; $Na^+:Si^{IV}$ = 1.0:1)							
3.3	-0.62	-0.58	-0.61	-0.59	-0.49	-0.52	-0.52
15.2	-0.37	-0.37	-0.38	-0.42	-0.45	-0.44	-0.46
22.4	-0.31	-0.29	-0.31	-0.33	-0.39	-0.36	-0.39
38.8	-0.19	-0.19	-0.21	-0.19	-0.22	-0.25	-0.25
55.0	-0.10	-0.08	-0.11	-0.11[b]	-0.10	-0.10	
77.4	-0.06	-0.10	-0.08	-0.08[b]		-0.06	

Table IV-II. (Continued)

Temp/°C	Q^0	$Q^1{}_2$	$Q^2{}_3$	$Q^2{}_4$	$Q^3{}_6$	$Q^3{}_4$	$Q^3{}_8$
e. Sample 38 (2.18 mol kg^{-1} Si; $Na^+:Si^{IV}$ = 1.0:1)							
22.4	-0.12		-0.08	-0.26	-0.25	-0.31	
38.8	-0.08	-0.09	-0.12	-0.13	-0.17	-0.11	
f. Sample 39 (2.17 mol kg^{-1} Si; $K^+:Si^{IV}$ = 4.0:1)							
3.3	-0.30	-0.14	-0.49				
14.5	-0.28	-0.11	-0.41				
23.1	-0.26	-0.11	-0.37				
37.2	-0.24	-0.08	-0.21				
53.2	-0.18	-0.10	-0.14				
g. Sample 41 (2.17 mol kg^{-1} Si; $Rb^+:Si^{IV}$ = 4.0:1)							
1.5	-0.19	-0.09	-0.37	-0.13			
14.5	-0.14	-0.04	-0.24				
23.1	-0.10	-0.05	-0.20				
37.2	-0.12	-0.08	-0.13				
53.2	-0.10	-0.07	-0.12				
74.3	-0.07	-0.14	-0.09				
100.8	-0.11	-0.06	-0.13				
h. Sample 42 (0.30 mol kg^{-1} Si; $Na^+:Si^{IV}$ = 1.0:1)							
22.4	-0.60	-0.61	-0.57	-0.59	-0.63	-0.61	
38.8	-0.35	-0.36	-0.37	-0.31	-0.35	-0.36	

[a] Dimensionless with uncertainty ±0.01. [b] Peak indistinct from nearest neighbours.

Table IV-III. Proportional DDH Contribution to T_1 Relaxation (T_{1DDH}^{-1}/T_1^{-1}) [a].

Temp/°C	Q^0	$Q^1{}_2$	$Q^2{}_3$	$Q^2{}_4$	$Q^3{}_6$	$Q^3{}_4$	$Q^3{}_8$
a. Sample 33 (2.17 mol kg^{-1} Si; $Na^+:Si^{IV}$ = 1.0:1)							
3.3	0.143	0.123	0.191	0.203	0.163	0.179	0.171
15.2	0.087	0.091	0.115	0.135	0.163	0.155	0.159
22.4	0.083	0.056	0.064	0.091	0.139	0.123	0.143
30.6	0.056	0.028	0.040	0.060	0.087	0.079	0.087
38.8	0.040	0.036	0.052	0.040	0.052	0.052	0.087
55.0	0.020	0.016	0.032	0.024	0.032	0.032	0.040
b. Sample 34 (2.17 mol kg^{-1} Si; $Na^+:Si^{IV}$ = 4.0:1)							
3.3	0.079	0.064	0.099	0.111			
23.1	0.032	0.016	0.064	0			
37.2	0.008	0.016	0.040				
53.2	0.012	0.016	0.010				
65.4	0.008	0	0				
83.2	0.008	0.004	0				
100.8	0.016						
c. Sample 35 (1.55 mol kg^{-1} Si; $Na^+:Si^{IV}$ = 1.0:1)							
3.3	0.15	0.127	0.187	0.199	0.163	0.179	0.175
22.4	0.087	0.083	0.083	0.103	0.127	0.129	0.139
38.8	0.052	0.052	0.048	0.040	0.060	0.064	0.072
55.0	0.020	0.028	0.024	0.032	0.036	0.032	0.068
86.7	0.028	0.016[b]	0.032[b]	0.016[b]	0.016	0.008[b]	
102.5	0.032	0.024[b]	0.024[b]	0.012[b]	0.016[b]	0.004[b]	
d. Sample 37 (0.80 mol kg^{-1} Si; $Na^+:Si^{IV}$ = 1.0:1)							
3.3	0.246	0.230	0.242	0.234	0.195	0.207	0.207
15.2	0.147	0.147	0.151	0.167	0.179	0.175	0.183
22.4	0.123	0.115	0.123	0.131	0.155	0.143	0.151
38.8	0.076	0.076	0.083	0.076	0.087	0.099	0.099
55.0	0.040	0.032	0.044	0.044[b]	0.040	0.040	
77.4	0.024	0.039	0.032	0.032[b]		0.024	

Table IV-III. (Continued)

Temp/°C	Q^0	$Q^1{}_2$	$Q^2{}_3$	$Q^2{}_4$	$Q^3{}_6$	$Q^3{}_4$	$Q^3{}_8$
e. Sample 38 (2.18 mol kg^{-1} Si; $Na^+:Si^{IV}$ = 1.0:1)							
22.4	0.048		0.032	0.103	0.099	0.123	
30.6	0.032	0.036	0.048	0.052	0.068	0.044	
f. Sample 39 (2.17 mol kg^{-1} Si; $K^+:Si^{IV}$ = 4.0:1)							
3.3	0.119	0.056	0.195				
14.5	0.111	0.044	0.163				
23.1	0.103	0.044	0.147				
37.2	0.095	0.032	0.083				
53.2	0.072	0.040	0.056				
g. Sample 41 (2.17 mol kg^{-1} Si; $Rb^+:Si^{IV}$ = 4.0:1)							
1.5	0.075	0.036	0.147	0.052			
14.5	0.056	0.016	0.095				
23.5	0.040	0.020	0.079				
37.2	0.048	0.032	0.052				
53.2	0.040	0.028	0.048				
74.3	0.028	0.056	0.036				
100.8	0.044	0.024	0.052				
h. Sample 42 (0.30 mol kg^{-1} Si; $Na^+:Si^{IV}$ = 1.0:1)							
22.4	0.238	0.242	0.226	0.234	0.250	0.242	
38.8	0.139	0.143	0.147	0.123	0.139	0.143	

[a] Dimensionless with uncertainty ±0.004. [b] Peak indistinct from nearest neighbours.

with rising temperatures for all silicate species. It was not possible to determine whether the DDH process was intra- or intermolecular but, in any case, it was never a major contributor to T_1 relaxation of ^{29}Si, as the close simularity of T_1 values in 75 and 99% ^2H-enriched solutions (samples 34 and 40) proved. If the contribution of the DDH process was not important, that of the deuterium dipole-dipole (DDD) mechanism was necessarily even less so, since, whether the dipole-dipole interaction is inter- or intramolecular (Eqns. 4.3 and 4.4), the ratio of the DDD and DDH contributions at mole fractions f_D and f_H is determined largely by the squares of the respective magnetogyric ratios γ_D and γ_H:

$$T_{1DDH}^{-1}/T_{1DDD}^{-1} = 8\gamma_D^2 f_D/3\gamma_H^2 f_H = 0.189 \text{ for } 75\% \ D_2O \qquad (4.9)$$

When, however, the concentrations of Na^+ and Si^{IV} were increased with $M^+:Si^{IV} = 1.0:1$, longitudinal relaxation was clearly accelerated (Figure 4-6). Although some of this additional relaxation was demonstrably due to DDH interactions, especially in the smaller silicate anions, the <u>proportional</u> contribution of DDH relaxation to T_1^{-1} actually decreased at the higher Si^{IV} concentrations (Figure 4-7). When the $Na^+:Si^{IV}$ ratio was increased from 1.0:1 to 4.0:1 at constant [Si] = 2.2 mol kg^{-1} (samples 33 and 34), T_1 was shortened for all four species examined, especially the dimer $Q^1{}_2$ and the cyclic tetramer $Q^2{}_4$ (Figures 4-4 and 4-7; <u>cf.</u> Figure 4-3). Clearly, then, the sodium ion concentration exerted a major influence on T_1. It may also be noted that, since averaged Si-Si chemical exchange is slower at higher pH because of secondary deprotonation of the silicate anions (see Ch. III), the onset of exchange averaging of T_1 values occurs at higher temperatures in Figure

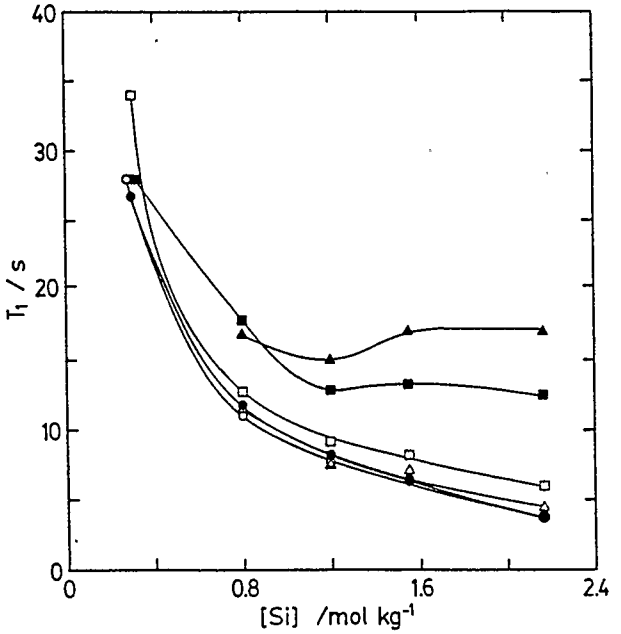

Figure 4-6. Si concentration dependence of longitudinal relaxation at 22.4°C for ^{29}Si-enriched solutions with $Na^+:Si^{IV}$ = 1.0:1 (Samples 33, 35 to 37, and 42). Symbols are as in Figure 4-3.

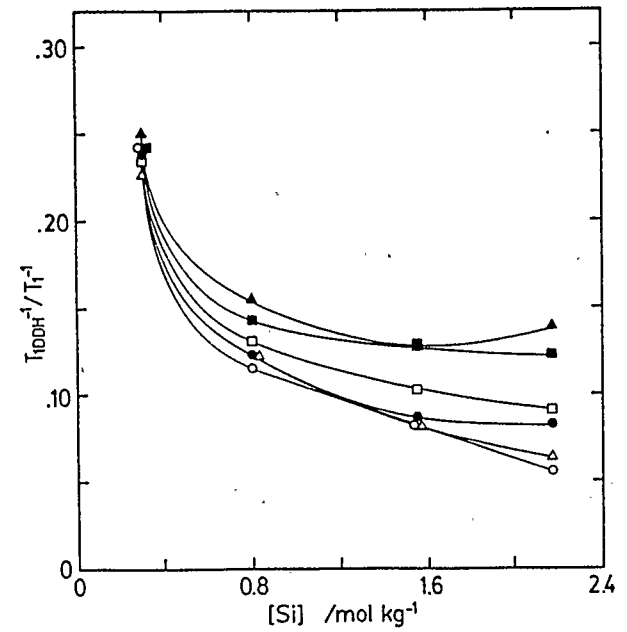

Figure 4-7. Si concentration dependence of the proportional DDH contribution to T_1 relaxation at 22.4°C. Solution composition and symbols are as in Figure 4-6.

4-4 than in Figure 4-3. It is significant that, of the four species under consideration here, those (Q^0 and $Q^2{}_3$) for which the least T_1 shortening was observed were also those which appear to be most susceptible to secondary deprotonation (see Sect. 3.3.3).

Thus, it becomes apparent that the primary cause of the relatively rapid longitudinal relaxation in aqueous, alkali-metal silicate solutions is dipole-dipole interaction between ^{29}Si and the nuclei of the counterion M^+ ("DDM" mechanism).

$$T_1^{-1} \sim T_{1DD}^{-1} = (T_{1DDH}^{-1} + T_{1DDD}^{-1} + T_{1DDM}^{-1}) \sim T_{1DDM}^{-1} \quad (4\text{-}10)$$

This was substantiated by the observation of very different values and temperature dependences of T_1 when Na^+ was replaced by $M^+ = K^+$ or Rb^+ (Figure 4-8). Incontrovertible proof of the predominance of the DDM mechanism could be obtained through appropriate NOE experiments, but a

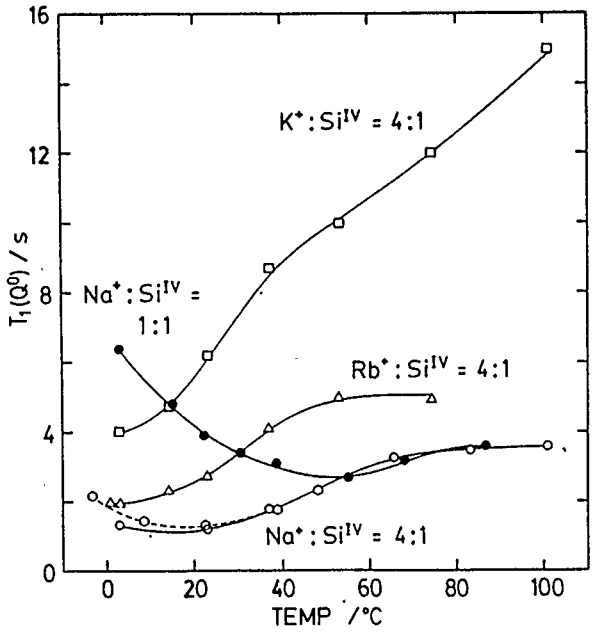

Figure 4-8. Temperature dependence of the monomer T_1 relaxation time for samples 33 ($Na^+:Si^{IV}$ = 1:1), 34 ($Na^+:Si^{IV}$ = 4:1), 39 ($K^+:Si^{IV}$ = 4:1), and 41 ($Rb^+:Si^{IV}$ = 4:1); all with 2.17 mol kg^{-1} Si. Broken line represents increase of B_0 to 7.05 from 4.70 T.

decoupler operable at the resonance frequency of the various M nuclei was not available to us and, in this respect, our conclusion remains tentative.

The relative efficacy Na > Rb >> K in producing longitudinal relaxation of ^{29}Si remains to be explained. Calculations based on an assumed intermolecular dipole-dipole relaxation mechanism (Eqn. 4.4) gave values of T_{1DD} that were some 10^5-fold too long, so an intramolecular process involving a silicate-M^+ ion pair that is long-lived on the T_1 time scale must be invoked. Several factors combine to make a realistic calculation of T_{1DDM}^{-1} on this basis impossible; M^+ ion-pair formation constants K_{IP} for the various anions are unknown, as are the structures of the ion pairs and the M^+-Si distances within them (upon which T_{1DDM} has a sixth-power dependence; Eqn. 4.3). There is evidence, however, that M^+-anion "contact" distances in water vary surprisingly little[117], and, furthermore, crude Fuoss-type calculations[92] (Sect. 2.3.2) suggest K_{IP} is nearly the same for the Na^+-, K^+-, and Rb^+-$H_3SiO_4^-$ pairs. We can therefore expect that the relative T_{1DDM}^{-1} values will be roughly proportional to $R = \Sigma[n\gamma_M^2 I(I+1)]$, where n is the fractional abundance of an isotope of spin I for a given M (from Eqn. 4.3). For M = ^{23}Na, (^{85}Rb + ^{87}Rb), and (^{39}K + ^{41}K), the respective values of $10^{-5}R$ are 19, 12 and 0.6, and these explain the qualitative trend in T_1^{-1} (Figure 4-8) satisfactorily.

4.4. Conclusion

The available evidence leaves little doubt that the major mechanism of longitudinal ^{29}Si relaxation in aqueous alkali-metal silicate solutions is a dipole-dipole interaction involving the counterion M^+, probably through an intramolecular process within a silicate-M^+ ion pair. Thus, measured T_1 values are influenced by both the nature and concentration of M^+, as well as by the temperature. Furthermore, at higher temperatures, chemical Si-Si exchange leads to apparent averaging of the T_1 values of the individual species and, since both the relative abundances of these species (Ch. II) and the rates of Si-Si exchange (Ch. III) are markedly temperature- and pH-dependent, the apparent T_1 values given by the inversion-recovery method can vary considerably with conditions when averaging is occurring.

In retrospect, then, it is not surprising that aqueous silicate ^{29}Si T_1 data in the literature are inconsistent, and the involvement of the cations in the DDM process explains why these T_1 values are shorter than for most other silicon compounds in the pure liquid state or in solutions not containing alkali-metal ions. The results of Harris and co-workers[48,59] can be seen to be consistent with ours on the basis of the foregoing conclusions, without the need to invoke the presence of paramagnetic contaminants in the silicate solutions. Indeed, experiments in which paramagnetic contaminants were deliberately introduced into silicate solutions revealed only a minor influence of these solutes on T_1[48].

CHAPTER V. Epilogue

The principal conclusions resulting from our ^{29}Si NMR investigation of alkali-metal silicate solutions are summarized below. In addition, we explore several avenues for further research.

5.1. Summary of Findings

(1) Causes of the shielding differences between ^{29}Si nuclei in aqueous, alkali-metal silicate solutions have been identified empirically. This understanding has led to the identification of a hitherto unknown silicate structure with adamantane-type geometry ($Si_4O_{10}^{4-}$).

(2) Precise knowledge of T_1 relaxation rates, combined with the elimination of background resonances, has made possible very accurate spectral integrations. These have verified that silicate condensation is favoured by low temperature, low $M^+:Si^{IV}$ ratio (i.e., low alkalinity) and high Si concentration. Heavy alkali-metal cations were observed to cause a slight increase in the extent of polymerization.

(3) Bandshape analysis indicates that temperature dependent ^{29}Si line-broadening is indeed due to Si-Si chemical exchange. Intramolecular condensation (i.e., ring formation) is revealed to be much faster than intermolecular condensation by the extreme broadening of resonances corresponding to easily cyclizable anions. Since all other resonances broaden uniformly at $M^+:Si^{IV} = 1:1$, the rate of intermolecular Si-Si exchange must be the same at all singly deprotonated silicate centres (these are the main constituents of silicate solutions at this alkalinity). This would suggest that the rate of intermolecular polymerization

is controlled by the condensation of one predominant species (i.e., monomer).

(4) The extent of polymerization is suppressed at high alkalinity by the formation of doubly deprotonated silicate centres which are much less reactive in condensation than the singly deprotonated sites. When ionization equilibria are taken into account, Si-Si exchange rates calculated from line-broadening analysis are consistent with the results of selective inversion-recovery experiments. The decrease in exchange-rates observed at high alkalinity indicates that the mechanism of polymerization is $[H^+]$ dependent.

(5) At sufficiently high temperatures, Si-Si chemical exchange causes gross averaging of the apparent T_1 values measured by the inversion-recovery method. This becomes evident at ~20°C for $M^+:Si^{IV}$ = 1:1 and at higher temperatures for higher $M^+:Si^{IV}$ ratios.

(6) Dipole-dipole interaction with the M^+ counterion is the major mechanism of longitudinal ^{29}Si relaxation. Minor contributions from ^{29}Si-^{1}H (and ^{29}Si-^{2}H) dipole-dipole interactions become increasingly important as temperature, $M^+:Si^{IV}$ ratio and/or overall concentration are reduced. Contributions to T_1^{-1} from the spin-rotation mechanism are apparent for the smaller silicate species but in general are of minor importance. These observations explain why previously reported T_1 values for ^{29}Si in aqueous alkali-metal silicates were much shorter than for other silicon compounds, such as organosilanes, and varied markedly from study to study because of differing experimental conditions.

(7) Paramagnetic contaminants have negligible influence on T_1 relaxation rates, and reasonable precautions (e.g., use of lined NMR

tubes) are sufficient to exclude them in any case.

(8) The usefulness of NMR spectroscopy for investigating hydrothermal chemistry in solutions containing relatively insensitive nuclei (up to at least 200°C) has been demonstrated.

5.2 Future Work

5.2.1 Identification of Silicate Anions

Evidence for assigning further ^{29}Si NMR resonances (see Figure 2-4) can be obtained by comparing chemical shifts, measured over a variety of sample conditions, with the patterns established in Ch. II. Such measurements should be conducted using the highest possible magnetic field in order to minimize signal overlap. Some of the currently unassigned ^{29}Si resonances may correspond to the following structures which are from Figure 3-14.

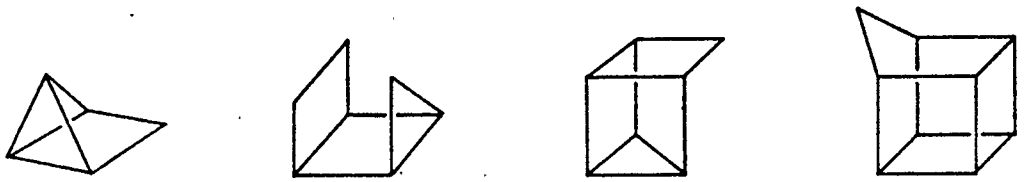

XX XXI XXII XXIII

(cis- and trans-)

5.2.2. Silicate-Cation Pairing

The extent to which dissolved silicates associate with cations to form stable complexes is important geochemically, especially in high-

temperature/pressure solutions[118]. For example, a $FeSi_3O_3(OH)_8^0$ complex has been cited recently to account for an anomalously high Fe concentration in the slightly reducing pore waters of deep sea sediments[119]. Similarily, silicate-sulphide (or bisulphide) complexing has been postulated to account for high sulphur solubilities measured in the presence of dissolved silica[120,121].

Solubility studies of Crerar and Anderson[121] indicate that Na-silicate complexing is of no importance at temperatures up to 325°C. In contrast, Seward[122] claimed that the formation of $NaSiO(OH)_3$ contributes to the solubility of quartz in borate-buffered solutions with pH > 8, and reported formation constants of 18 to 24 L mol^{-1} corresponding to temperatures 135 to 301°C. A weak Na^+ dependence was found in the potentiometric studies of Busey and Mesmer[26] and Sjöberg et al.[123], but in neither case was an unambiguous interpretation of the results possible.

The present ^{29}Si NMR investigation has shown that silicate-M^+ interactions influence nuclear shielding and the equilibrium distribution of silicate anions. In addition longitudinal relaxation measurements indicate that ion pairs are relatively long-lived within the T_1 time frame. Further information can be obtained by monitoring ^{29}Si (or M) nuclear relaxation rates in dilute silicate solution as various metal salts are added.

Raman[29] and trimethylsilylation[38] studies indicate that the addition of MCl salts to a silicate solution stimulates further condensation. However, there is disagreement about the effect of changing the cation. This question could be resolved unambiguously by ^{29}Si NMR.

5.2.3. Equilibria and Kinetics in Aqueous Organic-Base Silicate Solutions.

Organic cations (e.g., tetraalkylammonium ions) play a critical role in determining the structure of most synthetic zeolites[5]. They are also employed in the manufacture of glasses and ceramics by the sol-gel process[124].

The distribution of silicate anions in aqueous tetraalkylammonium silicate solutions has been characterized by ^{29}Si NMR and trimethylsilylation studies[125-128]. The double 4-ring ($Q^3{}_8$) is the dominant species below ca. 50°C in solutions containing the tetramethylammonium cation[125-127] (or any tetraalkylammonium cation with 3 methyl groups[128]), while at higher temperatures, the distribution of oligomers is similar to that found in alkali-metal silicate solutions. Tetraethylammonium and tetrapropylammonium silicate solutions contain high concentrations of the double 3-ring ($Q^3{}_6$) species, but only at near freezing temperatures[127]. Reportedly, when large quantities of methanol, ethanol or dimethylsulphoxide are added to a tetrapropylammonium silicate solution, the double 5-ring species predominates at ambient temperatures[65]. The double 3- and 4-ring cages have also been identified as the principal silicate anions in N-(2)hydroxyalkylpyridinium silicate solutions[129].

Very recently, Knight, Kirkpatrick and Oldfield[130] reported that a boiled tetramethylammonium silicate solution, which was rapidly frozen and returned to 20°C, required several weeks to reestablish the equilibrium $Q^3{}_8$-anion concentration. Hence, the dynamics of Si-Si exchange are very different from what we have observed in alkali-metal silicate solutions.

A comprehensive ^{29}Si NMR study of the aqueous organic-base silicate solutions may help in understanding the processes which stabilize the large cage structures.

5.2.4. Equilibria and Kinetics in Non-aqueous Silicate Solutions

Silica can be readily solvated by many organic hydroxy- and amine-compounds[10]. For example, Bibby and Dale[131] recently prepared aluminum-free zeolites from ethylene glycol and propanol solutions which contained only NaOH and SiO_2. To our knowledge, no ^{29}Si NMR studies have been conducted of non-aqueous silicate solutions.

5.2.5. Equilibria and Kinetics in Aqueous Aluminosilicate Solutions

Although both silicate and aluminate[132-134] solutions have been relatively well characterized by NMR techniques, very little work has been done with aluminosilicates. The first and (to our knowledge) only systematic identification of ^{27}Al shifts in aluminosilicate solutions was reported by Mueller, Hoebbel and Gessner in 1981[135]. Using a low field spectrometer operating at 15.8 MHz, they observed 4 overlapping resonances in spectra of solutions containing roughly 0.1 mol kg^{-1} Al, 0.06 mol kg^{-1} Si and 0.2 mol kg^{-1} OH^-. Assuming that Al-O-Al bonds are unlikely (in accordance with Loewenstein's rule for solid aluminosilicates[136]), they assigned the four ^{27}Al signals to AlO_4 centres coordinated to 0, 1, 2 or 3 silicons.

The only ^{29}Si studies conducted have been of solutions with Si:Al ratios ranging from 60:1 to 100:1[63-65]. Under these conditions, any resonances corresponding to aluminosilicate species are swamped by the normal silicate spectrum. Dibble, DeJong and Cary[63] noted, however,

that after small amounts of $AlCl_3 \cdot 6H_2O$ were added to a 3 mol kg^{-1} sodium silicate solution with $Na^+:Si^{IV}$ = 3:1, the linewidth of the Q^0 and Q^1 ^{29}Si resonances temporarily increased 100% and 37%, respectively. No other ^{29}Si signals were affected. In addition, the ^{27}Al resonance was found to be 70-fold broader than the corresponding signal in a Na-aluminate solution. These observations indicate that Al reacts primarily with Q^0 and Q^1 silicate centres.

There is clearly significant scope for further research of this system using NMR techniques. Since ^{27}Al has spin I = 5/2, the structural information that can be obtained from this nucleus will be limited because of quadrupolar line-broadening. Nevertheless, a high-field spectrometer should be able to separate the 4 overlapping resonances recorded by Mueller et al., and possibly resolve others. Silicon-29 investigations must be conducted using dilute solutions (< 0.1 mol kg^{-1} Si) as these permit a wide range in the Al:Si concentration ratio. Fortunately, the normal silicate spectrum is very simple under these conditions and changes can be monitored easily.

REFERENCES

1. Hurlburt, C.S.; Klein, C. Manual of Mineralogy, 19th ed.; John Wiley and Sons: New York, 1977; p. 336.
2. Wollast, R.; Mackenzie, F.T. in Silicon Geochemistry and Biogeochemistry; Aston, S.R. Ed.; Academic Press: London, 1983; pp. 39-76.
3. Aston, S.R. ibid; pp. 77-100.
4. Crerar, D.A.; Axtmann, E.V.; Axtmann, R.C. Geochim. Cosmochim. Acta **1981**, 45, 1259.
5. Barrer, R.M. Hydrothermal Chemistry of Zeolites; Academic Press: London, 1982.
6. Tremaine, P.R.; Isaacs, E.E.; Boon, J.A. Chemistry in Canada **1983**, April, 29.
7. Rothbaum, H.P.; Rohde, A.G. J. Colloid Interface Sci. **1979**, 71, 533.
8. Fleming, B.A.; Crerar, D.A. Geotherm. **1982**, 11, 15.
9. Hurd, D.C. in ref. 2; pp. 187-244.
10. Iler, R.K. The Chemistry of Silica; John Wiley and Sons: New York, 1979.
11. Bendz, G.; Lindqvist, I., Eds. Biochemistry of Silicon and Related Problems; Plenum Press: New York, 1978.
12. Chem. Eng. News **1986**, June 9, 32.
13. Barby, D.; Griffiths, J.; Jacques, A.R.; Pawson, D. in The Modern Inorganic Chemicals Industry; Thompson, R., Ed.; Chem. Soc. Special Publ. No. 31, 1977; p. 321.
14. Lagerstrom, G. Acta Chem. Scand. **1959**, 13, 722.

15. Sjöberg, S.; Öhman, L.-O.; Ingri, N. Acta Chem. Scand., Ser. A **1985**, 39, 93.

16. Stumm, W.; Morgan, J. J. Aquatic Chemistry; John Wiley and Sons: New York, 1981; p. 541.

17. Smith, R.M.; Martell, A.E. Critical Stability Constants, Vol. 4; Plenum Press: New York, 1976.

18. Engelhardt, G.; Jancke, H.; Hoebbel, D.; Wieker, W. Z. Chem. **1974**, 14, 109.

19. Main, V.R. J. Phys. Chem. **1926**, 30, 535.

20. Hägg, G. Z. Anorg. Allg. Chem. **1926**, 155, 21.

21. Harman, R.W. J. Phys. Chem. **1928**, 32, 44.

22. Jander, G.; Heukeshoven, W. Z. Anorg. Allg. Chem. **1931**, 201, 301.

23. Nauman, R.V.; Debye, P. J. Phys. Chem. **1951**, 55, 1.

24. Ingri, N. Acta Chem. Scand. **1959**, 13, 758.

25. Aveston, J. J. Am. Chem. Soc. **1965**, 4444.

26. Busey, R.H.; Mesmer, R.E. Inorg. Chem. **1977**, 16, 2444.

27. Fortnum, D.; Edwards, J.O. J. Inorg. Nucl. Chem. **1956**, 2, 264. Also: Earley, J.E.; Fortnum, D.; Wojcicki, A.; Edwards, J.O. J. Am. Chem. Soc. **1959**, 81, 1295.

28. Freund, E. Bull. Soc. Chim. Fr. **1973** (No. 7-8), 2238 and 2244.

29. Dutta, P.K.; Shieh, D.C. Zeolites **1985**, 5, 135; J. Raman Spectr. **1985**, 16, 312.

30. Beard, W.C. Adv. Chem. Ser. **1973**, 121, 162.

31. Marinangeli, A.; Morelli, M.A.; Simoni, R.; Bertoluzza, A. Can. J. Spectr. **1978**, 23, 174.

32. Alexander, G.B. J. Am. Chem. Soc. **1954**, 76, 2094.

33. Thilo, E.; Wieker, W.; Stade, H. Z. Anorg. Allg. Chem. **1965**, 340, 261.

34. Hoebbel, D.; Wieker, W. Z. Anorg. Allg. Chem. **1973**, 400, 148.

35. Lentz, C.W. Inorg. Chem. **1964**, 3, 574.

36. Dent Glasser, L.S.; Sharma, S.K. Br. Polym. J. **1974**, 6, 283.

37. Dent Glasser, L.S.; Lachowski, E.E.; Cameron, G.G. J. Appl. Chem. Biotechnol. **1977**, 27, 39. Dent Glasser, L.S.; Lachowski, E.E. J. Chem. Soc., Dalton Trans. **1980**, 393 and 399.

38. Ray, N.H.; Plaisted, R.J. J. Chem. Soc., Dalton Trans. **1983**, 475.

39. Holzman, G.R.; Lauterbur, P.C.; Anderson, J.H.; Koth, W. J. Chem. Phys. **1956**, 25, 172.

40. Marsmann, H.C. Chem.-Ztg. **1973**, 97, 128.

41. Gould, R.O.; Lowe, B.M.; MacGilp, N.A. J. Chem. Soc., Chem. Commun. **1974**, 720.

42. Marsmann, H.C. Z. Naturforsch. **1974**, 29b, 495.

43. Engelhardt, G.; Zeigan, D.; Jancke, H.; Hoebbel, D.; Wieker, W. Z. Anorg. Allg. Chem. **1975**, 418, 17.

44. Engelhardt, G. Z. Chem. **1975**, 15, 495.

45. Engelhardt, G.; Hoebbel, D. J. Chem. Soc., Chem. Commun. **1984**, 514.

46. Harris, R.K.; Kimber, B.J. J. Organomet. Chem. **1974**, 70, 43; **1976** 116, 391.

47. Harris, R.K.; Newman, R.H. Org. Magn. Reson. **1977**, 9, 426.

48. Harris, R.K.; Newman, R.H. J. Chem. Soc., Faraday Trans. 2 **1977**, 73, 1204.

49. Harris, R.K.; Jones, J.; Knight, C.T.G.; Pawson, D. J. Mol. Struct. **1980**, 69, 95.

50. Harris, R.K.; Knight, C.T.G. J. Am. Chem. Soc. **1981**, 103, 1577.

51. Harris, R.K.; Knight, C.T.G. J. Mol. Struct. **1982**, 78, 273.

52. Harris, R.K.; Knight, C.T.G. J. Chem. Soc., Faraday Trans. 2 **1983**, 79, 1525.

53. Harris, R.K.; Knight, C.T.G. J. Chem. Soc., Faraday Trans. 2 **1983**, 79, 1539.

54. Iler, R.K. in ref. 11; p. 58.

55. Harris, R.K.; O'Connor, M.J.; Curzon, E.H.; Howarth, O.W. J. Magn. Reson. **1984**, 56.

56. Knight, C.T.G.; Kirkpatrick, R.J.; Oldfield, E. J. Am. Chem. Soc. **1986**, 108, 30.

57. Harris, R.K.; Jones, J.; Knight, C.T.G.; Newman, R.H. J. Mol. Liquids **1984**, 29, 63.

58. Creswell, C.J.; Harris, R.K.; Jageland, P.T. J. Chem. Soc., Chem. Commun. **1984**, 1261.

59. Knight, C.T.G.; Harris, R.K. Magn. Reson. Chem. **1986**, 24, 872; cf. Harris, R.K. in The Multinuclear Approach to NMR Spectroscopy; Lambert, J.B.; Riddell, F.G., Eds.; D. Reidel Publishing Co.: Dordrecht, 1983; pp. 343-359.

60. Griffiths, L.; Cundy, C.S.; Plaisted, R.J. J. Chem. Soc., Dalton Trans. **1986**, 2265.

61. Farrer, T.C.; Becker, E.D. Pulse and Fourier Transform NMR; Academic Press: London, 1971, p. 104.

62. Cary, L.W.; DeJong, B.H.W.S.; Dibble, Jr., W. Geochim. Cosmochim. Acta **1982**, 46, 1317.

63. Dibble, W.E.; DeJong, B.H.W.S.; Cary, L.W. in Proceedings of 3rd International Symposium on Water-Rock Interaction; Edmonton, 1980; pp. 47-48.

64. Donahoe, R.J.; Liou, J.G. Geochim. Cosmochim. Acta **1985**, 49, 2349.

65. Boxhoorn, G.; Sudmeijer, O.; Van Kasteren, P.H.G. J. Chem. Soc., Chem. Commun. **1983**, 1416.

66. Cruickshank, D.W.J. J. Chem. Soc. **1961**, 5486.

67. Chakoumakos, B.C.; Hill, R.J.; Gibbs, G.V. Am. Miner. **1981**, 66, 1237.

68. Pauling, L. The Nature of the Chemical Bond; Cornell University Press: Ithaca, New York, 1960.

69. Glidewell, C. Inorg. Chim. Acta Rev. **1973**, 7, 69.

70. Pauling, L. Am. Miner. **1984**, 1261.

71. Stewart, R.F.; Whitehead, M.A.; Donnay, G. Am. Miner. **1980**, 65, 324.

72. Janes, N.; Oldfield, E. J. Am. Chem. Soc. **1986**, 108, 5743.

73. Janes, N.; Oldfield, E. J. Am. Chem. Soc. **1985**, 107, 6769.

74. Pitt, C.G. J. Organomet. Chem. **1973**, 61, 49.

75. O'Keeffe, M.; Hyde, B.G. Acta Cryst. **1978**, B34, 27.
1971, p. 104.

76. DeJong, B.H.W.S.; Brown, Jr., G.E. Geochim. Cosmochim. Acta **1980**, 44, 491.

77. Lasaga, A.C. Phys. Chem. Minerals **1982**, 8, 36.

78. See references sited in: Marsmann, H. NMR **1981**, 17, 65; and in ref. 73.

79. Wells, P.R. Progr. Phys. Org. Chem. **1968**, 6, 111.

80. Smith, J.V.; Blackwell, C.S. Nature **1983**, 303, 223. Lippman, E.; Mägi, M.; Samoson, A.; Engelhardt, G.; Grimmer, A.-R. J. Am. Chem. Soc. **1980**, 102, 4889.

81. Pople, J.A. Discuss. Faraday Soc. **1962**, 34, 7.

82. Ramsey, N.F. Phys. Rev. **1950**, 78, 699; **1952**, 86, 243. cf.: Ebraheem, K.A.K.; Webb, G.A. Prog. NMR Spectr. **1977**, 9; **1977**, 11, 149.

83. Ebraheem, K.A.K.; Webb, G.A.; Witanowski, M. Org. Magn. Reson. **1976**, 8, 317.

84. Mason, J. J. Chem. Soc.(A) **1971**, 1038.

85. Marsmann, H. NMR **1981**, 17, 65.

86. Rummens, F.H.A. NMR **1975**, 10, 1.

87. Onsager, L. J. Am. Chem. Soc. **1936**, 58, 1486.

88. Laszlo, P. Prog. NMR Spectrosc. **1967**, 3 231.

89. Vespel® Technical Bulletin A-52349; E.I. du Pont de Nemours & Co..

90. Weale, K.E. Chemical Reactions at High Pressures; E.& F.N. Spon Ltd.: London, 1967; p. 81.

91. Ammann, C.; Meier, P.; Merbach, A.E. J. Magn. Reson. **1982**, 46, 319.

92. Fuoss, R.M. J. Am. Chem. Soc. **1958**, 80, 5059.

93. Haas, A.; Hitze, R.; Krueger, C.; Angermund, K. Z. Naturforsch. **1984**, 39B, 890.

94. Schwarzenbach, G.; Geier, G. Helv. Chim. Acta **1963**, 46, 906.

95. Kaplan, J.I.; Fraenkel, G. NMR of Chemically Exchanging Systems; Academic Press: New York, 1980.

96. Binsch, G. in Dynamic Nuclear Magnetic Spectroscopy; Jackman, L.M.; Cotton, F.A., Eds.; Academic Press: New York, 1975.

97. Bloch, F. Phys. Rev. **1946**, 70, 460.

98. Abragam, A. The Principles of Nuclear Magnetism; Oxford University Press; London, 1961.

99. In practice, the applied field is kept within the "zero saturation" limit such that $M_z \sim M_o$ (ref. 112).

100 Steigel, A. NMR **1978**, 15, 1.

101. Rogers, M.T.; Woodbrey, J.C. J. Phys. Chem. **1962**, 66, 540.

102. Sandström, J. Dynamic NMR Spectroscopy; Academic Press: London, 1982.

103. Sack, R.A. Mol. Phys. **1958**, 1, 163.

104. Gordon, R.G.; McGinnes, R.P. J. Chem. Phys. **1969**, 49, 2455.

105. Reeves, L.W.; Shaw, K.N. Can. J. Chem. **1970**, 48, 3641.

106. Forsén, S.; Hoffman, R.A. J. Chem. Phys. **1963**, 39, 2892.

107. Morris, G.; Freeman, R.J. J. Magn. Reson. **1978**, 29, 433.

108. Program written by R. Haseltine and K. Wagstaff (this department), utilizing a matrix diagonalization routine by J. Rinzel and R. Funderlic of Union Carbide Corp., Oak Ridge.

109. Using the derivative-free, non-linear regression program BMDPAR from BMDP Statistical Software Inc., California.

110. Eyring, H. J. Chem. Phys. **1935**, 3, 107.

111. Sjöberg, S.; Nordin, A.; Ingri, N. Mar. Chem. **1981**, 10, 521.

112. Moore, J.W.; Pearson, R.G. Kinetics and Mechanism; John Wiley and Sons: New York, 1981; p. 262.

113. Wilkins, R.G. The Study of Kinetics and Mechanism of Reactions of Transition Metal Complexes; Allyn and Bacon, Inc.: Boston, 1974; p. 67.

114. Harris, R.K. Nuclear Magnetic Resonance Spectroscopy; Pitman: London, 1983; pp. 85-91.

115. Ando, I.; Webb, G.A. Theory of NMR Parameters; Academic Press: London, 1983.

116. Levy, G.C.; Cargioli, J.D.; Juliano, P.C.; Mitchell, T.D. J. Am. Chem. Soc. **1973**, 95, 3445.

117. Sφrensen, T.S.; Sloth, P.; Schrφder, M. Acta Chem. Scand., Ser. A **1984**, 38, 735.

118. Walther, J.V.; Helgeson, H.C. Am. J. Sci. **1977**, 277, 1315.

119. Winters, G.V.; Buckley, D.E. Geochim. Cosmochim. Acta **1986**, 50, 277.

120. Learned, R.L.; Dickson, F.W.; Tunnell, G. Trans. Am. Geophys. Union **1967**, 48, 249.

121. Crerar, D.M.; Anderson, G.M. Chem. Geol. **1971**, 8, 107.

122. Seward, T.M. Geochim. Cosmochim. Acta **1974**, 38, 1651.

123. Sjöberg, S.; Hagglund, Y.; Nordin, A.; Ingri, N. Mar. Chem. **1983**, 13, 35.

124. Kelts, L.W.; Effinger, N.J.; Melpolder, S.M. J. Non-Cryst. Solids **1986**, 83, 353.

125. Harris, R.K.; Knight, C.T.G. J. Mol. Struct. **1982**, 78, 273.

126. Hoebbel, D.; Garzo, G.; Engelhardt, G.; Vargha, A. Z. Anorg. Allg. Chem. **1982**, 494, 31.

127. Engelhardt, G.; Rademacher, O. J. Mol. Liquids **1984**, 27, 125.

128. Hasegawa, I.; Kuroda, K.; Kato, C. Bull. Chem. Soc. Jpn. **1986**, 59, 2279.

129. Rademacher, O.; Ziemens, O.; Scheler, H. Z. Anorg. Allg. Chem. **1984** 519, 165.

130. Knight, C.T.G.; Kirkpatrick, R.J.; Oldfield, E. J. Chem. Soc., Chem. Commun. **1986**, 66.

131. Bibby, D.M.; Dale, M.P. Nature **1985**, 317, 157.

132. Akitt, J.W.; Greenwood, N.N.; Khandelwal, B.L.; Lester, G.D. J. Chem. Soc., Dalton Trans. **1972**, 604.

133. Akitt, J.W.; Farthing, A. J. Chem. Soc., Dalton Trans. **1981**, 1617.

134. Bottero, J.Y.; Cases, J.M.; Fiessinger, F.; Poirier, J.E. J. Phys. Chem. **1980**, 84, 2933.

135. Mueller, D.; Hoebbel, D.; Gessner, W. Chem. Phys. Letters **1981**, 84, 25.

136. Loewenstein, W. Am. Mineral. **1954**, 39, 92.

137. Turner, C.J.; Smallcombe, S.H. Varian Instruments at Work, NMR-5, September 1979.

138. Method devised by S.L. Patt, Varian Instrument Group, Florham Park, New Jersey, U.S.A..

139. Dahlquist, F.W.; Longmuir, K.J.; Du Vernet, R.B. J. Magn. Reson. **1975**, 17, 406.

Appendix A. Program GNMR

The Fortran listing which follows is of program GNMR[108]. The program, based on Eqn. 3.15, is used to simulate exchange-broadened spectra and to determine the first-order rate constants for nuclear spin- transfer.

Also presented are:

(i) information files "gnmr.gi.info" and "gnmr.info" which describe program operation (pgs. 161 and 163);

(ii) input data file "d Figure3-2" which describes the 2-site equilibrium in Eqn. 3.7 (p. 165);

(iii) the "matrix.fortran" routine representing the corresponding transposed 2×2 exchange matrix (K) (p. 165); and

(iv) the output listing which accompanies the calculated spectra shown in Figure 3-2 (p. 166).

gnmr.fortran

```
%global card,static;
c
      subroutine gnmr
```

GNMR calculates and plots n.m.r. spectra (with or without first-order coupling) that are broadened by exchange of nuclei between two or more sites. The first-order coupling is taken into account by calculating an independent spectrum for each energy level (spin state), and then summing the spectra to obtain a composite spectrum.

GNMR performs classical multi-site exchange analysis based on matrix formulations of the exchange-modified Bloch equations. The band-shape is derrived from the complex xy magnetization G which can be expressed in either of the forms:

$$(1) \quad G = -iCPA^{-1}1$$

$$(2) \quad G = -iC1B^{-1}P$$

where C is a constant, P is the population vector, and 1 is a transition intensity (unit) vector. The nxn (n = no. of resonances) matrices, A and B, are transpose to one another with:

> $B = S(D+ixI)^{-1}S^{-1}P$

> $D = S^{-1}RS$ (diagonalized eigenvalue matrix corresponding to R, where S is the eigenvector matrix)

> $R = (T_2^{+K-iW})$

> $((T_2^{+K})+iw) = R + ixI$

> W is a diagonal matrix of spin-site Larmor freqencies (w)

> I is the nxn unit matrix

> T_2 is the diagonal nxn matrix with element T_{2j}^{-1}

and > K is the "kinetic matrix" with each row representing the general first-order rate equation for transfer at a nuclear site.

****

This program is written in the form of equation (1) such that the kinetic matrix entered as "matrix.fortran" is actually the TRANSPOSE of K !! (Note that, in equation (1), P is a 1xn row vector and 1 is a nx1 column vector, whereas in (2), 1 is a row vector and P is a column vector.)

```
c
c     ***********************************************************************
c
c
c
c           GNMR was written by R. Haseltine in 1975 employing diagonalization
c        routines found in DNMR3 (QCPE 165), and was later revised by K.
c        Wagstaff and then by S.D. Kinrade (last: 10/1986).
c
c
c           SUGGESTED READING:
c        1)  Reeves,L.W.; Shaw,K.N., Can. J. Chem.; 1970; <48>; 3641.
c        2)  Chan,S.O.; Reeves,L.W., J. Am. Chem. Soc.; 1973; <95>; 670 & 673.
c        3)  Sandstrom,J., "Dynamic NMR Spectroscopy", Academic Press; 1982.
c        4)  Steigel,A., in: "NMR Basic Principles and Progress 15"; 1978.
c
c
c
c
c
      external kdate (descriptors)                                          gnmr   3
      external ktime (descriptors)                                          gnmr   4
                                                                            gnmr   5
c
      character*8 date,time                                                 gnmr   6
      character*20 text3(10)                                                gnmr   7
      character*36 text2                                                    gnmr   8
      character*80 textl                                                    gnmr   9
                                                                            gnmr  10
c
      logical input,output,copy_input,copy_output,no_calc
      logical normalize,label                                               gnmr  12
                                                                            gnmr  13
c
      complex a(70,70),b(70,70),c(70),d(70),bl(70),pa(70),pabl(70)          gnmr  14
      complex g(20000)                                                      gnmr  15
                                                                            gnmr  16
c
      dimension w(8,70),t2(8,70),width(70),nn(8),greal(20000),rc(10)        gnmr  17
                                                                            gnmr  18
c
      common /text/ textl,text2,text3,length3                               gnmr  19
      common /pltpar/ scale,height,frl,fr2,jj,normalize,label               gnmr  20
      common /areal/ areal(70,70)                                           gnmr  21
      common /pop/ pop(8,70)                                                gnmr  22
                                                                            gnmr  23
c
      data pi/3.1415927/,twopi/6.2831853/                                   gnmr  24
                                                                            gnmr  25
c                                                                           gnmr  26
c
c         nn    = the no. of peaks
c         w     = relative shift of each resonance
c         pop   = the relative population of each nulceus
c         width= the half-height linewidth of each resonance
c         nsum = the no. of spectra to be added to give a total spectrum
c         ncal = the no. of composite spectra to be calculated
c         frl   = the left hand plot limit (hz)
c         fr2   = the right hand plot limit (hz)  ( frl<fr2 )
c         scale= mm/hz for the plot
c         r     = the resolution of the plot (hz) ( r > (fr2-frl)/20000 )
c         height = the height of the tallest peak in the spectrum (mm)
c         if nfactor=0, each plot will be 'height' high
c         if    " not=0, subsequent plots will be normalized to the peak areas
c            of the first.
c
c
 1001 format (//" PROGRAM GNMR",5x,2a8/)                                   gnmr  27
 1002 format (" Enter response following prompt (?).")                      gnmr  28
 1003 format (/" Plot title")                                               gnmr  29
 1004 format (a80)                                                          gnmr  30
 1005 format (/" Plotting Parameters:"/                                     gnmr  31
              6x."Left hand plot limit (hz)")                               gnmr  32
```

```
1006 format (v)                                                        gnmr  33
1007 format (6x,"Right hand plot limit (hz)")                          gnmr  34
1008 format (6x,"Plot scale (mm/hz)")                                  gnmr  35
1009 format (6x,"Plot resolution (hz)")                                gnmr  36
1010 format (6x,"Height of tallest peak (mm)")                         gnmr  37
1011 format (6x,"Do you want to have all plots normalized ",           gnmr  38
     .       "to the area of the first one")                           gnmr  39
                                                                       gnmr  40
1012 format (a4)                                                       gnmr  41
1013 format (6x,"Please answer 'yes' or 'no'")                         gnmr  42
1014 format (6x,"Do you want the plot to have a labelled x-axis")      gnmr  43
1015 format (//1x,a80//" Plotting parameters:"/                        gnmr  44
     .        6x,"Left hand plot limit =",f10.1," hz."/                gnmr  45
     .        6x,"Right hand plot limit =",f9.1," hz:"/                gnmr  46
     .        6x,"Plot scale =",f8.5," mm/hz."/                        gnmr  47
     .        6x,"Plot resolution =",f8.5," hz."/                      gnmr  48
     .        6x,"Plot height =",f6.1," mm.")                          gnmr  49
1016 format (6x,"Plots are not to be normalized.")                     gnmr  50
1017 format (6x,"Plots are to be normalized.")                         gnmr  51
1018 format (6x,"Plots are not to have labelled x-axis.")              gnmr  52
1019 format (6x,"Plots are to have labelled x-axis.")                  gnmr  53
1020 format (a80/e15.8,5x,"Left hand plot limit"/                      gnmr  54
     .        e15.8,5x,"Right hand plot limit"/                        gnmr  55
     .        e15.8,5x,"Plot scale"/e15.8,5x,"Plot resolution"/        gnmr  56
     .        e15.8,5x,"Plot height")                                  gnmr  57
1021 format ("yes",17x,"Normalize")                                    gnmr  58
1022 format ("no",18x,"Normalize")                                     gnmr  59
1023 format (//" How many spectra are to be summed to give each ",     gnmr  60
     .        "composite spectrum")                                    gnmr  61
1024 format (" How many composite spectra are to be plotted")          gnmr  62
1025 format (" How many rate constants are there for each ",           gnmr  63
     .        "composite spectrum")                                    gnmr  64
1026 format (i15,5x,"Number of spectra summed"/                        gnmr  65
     .        i15,5x,"Number of composite spectra plotted"/            gnmr  66
     .        i15,5x,"Number of rate constants")                       gnmr  67
1027 format (//" gnmr expects to calculate ",i3," composite ",        gnmr  68
     .        "spectra."/" Each will be the sum of",i3," spectra."/    gnmr  69
     .        " There will be",i3," different rate constants for ",    gnmr  70
     .        "each spectrum."/)                                       gnmr  71
1028 format (/" How many peaks are there in energy level",i3)          gnmr  72
1029 format (i15,5x,"Number of peaks in energy level",i3)              gnmr  73
1030 format (" Peak",i3)                                               gnmr  74
1031 format (3(e15.8,5x))                                              gnmr  75
1032 format (//1x,46("*")/" Energy Level",i3/1x,46("*")//" Peak",      gnmr  76
     .        3x,"Chemical",9x,"Line",9x,"Relative",/7x,"Shift (hz)",  gnmr  77
     .        5x,"Width (hz)",5x,"Population"/)                        gnmr  78
1033 format (1x,i3,2x,f10.3,6x,f9.3,7x,f7.3)                           gnmr  79
1034 format (//" What are the rate constants for plot number ",        gnmr  80
     .        i3,":")                                                  gnmr  81
1035 format (" rc(",i3,")")                                            gnmr  82
1036 format (e15.8,5x,"rc(",i3,")")                                    gnmr  83
1037 format ("Plot Number",i3,6x,2a8)                                  gnmr  84
1038 format ("rc(",i2,")=",1pe11.5,2x)                                 gnmr  85
1039 format (//" The plot will be labelled as follows:"/               gnmr  86
     .        6x,a80/6x,a36/6x,10a20)                                  gnmr  87
1040 format (/" Enter the following parameters for each peak (in ",    gnmr  88
     .        "this order):"/6x,"Chemical shift (hz)"/                 gnmr  89
     .        6x,"Line width (hz)"/6x,"Relative population"/)          gnmr  90
1041 format ("yes",17x,"Label")                                        gnmr  91
1042 format ("no",18x,"Label")                                         gnmr  92
1043 format (//" Do you want to run gnmr again using the same ",       gnmr  93
     .        "-matrix")                                               gnmr  94
1044 format ("yes",17x,"Another gnmr run")                             gnmr  95
1045 format ("no",18x,"Another gnmr run")                              gnmr  96
1046 format (/" Virtual CPU time =",f7.3," sec. to generate plot ",    gnmr  97
     .        "number",i3,".")                                         gnmr  98
1047 format (/" Total virtual CPU time for this gnmr run =",f7.3,
```

```
     .       " sec."/)                                                  gnmr  99
c                                                                       gnmr 100
c                                                                       gnmr 101
      tstart=cputim(i)                                                  gnmr 102
c                                                                       gnmr 103
      call open_files(input,output,copy_input,copy_output,no_calc)
      call kdate(date)                                                  gnmr 105
      call ktime(time)                                                  gnmr 106
      if (.not.no_calc) call plots
c                                                                       gnmr 108
c     INPUT SECTION                                                     gnmr 109
      write (6,1001) date,time                                          gnmr 110
      if (copy_output) write (8,1001) date,time                         gnmr 111
      if (.not.input) write (9,1002)                                    gnmr 112
    5 if (.not.input) write (9,1003)                                    gnmr 113
      read (5,1004) textl                                               gnmr 114
      if (.not.input) write (9,1005)                                    gnmr 115
      read (5,1006) frl                                                 gnmr 116
      if (.not.input) write (9,1007)                                    gnmr 117
      read (5,1006) fr2                                                 gnmr 118
      if (.not.input) write (9,1008)                                    gnmr 119
      read (5,1006) scale                                               gnmr 120
      if (.not.input) write (9,1009)                                    gnmr 121
      read (5,1006) r                                                   gnmr 122
      if (.not.input) write (9,1010)                                    gnmr 123
      read (5,1006) height                                              gnmr 124
      if (.not.input) write (9,1011)                                    gnmr 125
   10 read (5,1012) answer                                              gnmr 126
      if (answer.eq."yes") normalize=.true.                             gnmr 127
      if (answer.eq."no") normalize=.false.                             gnmr 128
      if (answer.eq."yes".or.answer.eq."no") go to 15                   gnmr 129
c     Invalid answer:                                                   gnmr 130
      if (input) go to 2001                                             gnmr 131
      write (9,1013)                                                    gnmr 132
      go to 10                                                          gnmr 133
   15 if (.not.input) write (9,1014)                                    gnmr 134
   20 read (5,1012) answer                                              gnmr 135
       if (answer.eq."yes") label=.true.                                gnmr 136
      if (answer.eq."no") label=.false.                                 gnmr 137
      if (answer.eq."yes".or.answer.eq."no") go to 25                   gnmr 138
c     Invalid answer:                                                   gnmr 139
      if (input) go to 2001                                             gnmr 140
      write (9,1013)                                                    gnmr 141
      go to 20                                                          gnmr 142
   25 write (6,1015) textl,frl,fr2,scale,r,height                       gnmr 143
      if (copy_output) write (8,1015) textl,frl,fr2,scale,r,height      gnmr 144
      if (normalize) go to 30                                           gnmr 145
      write (6,1016)                                                    gnmr 146
      if (copy_output) write (8,1016)                                   gnmr 147
      go to 35                                                          gnmr 148
   30 write (6,1017)                                                    gnmr 149
      if (copy_output) write (8,1017)                                   gnmr 150
   35 if (label) go to 40                                               gnmr 151
      write (6,1018)                                                    gnmr 152
      if (copy_output) write (8,1018)                                   gnmr 153
      go to 45                                                          gnmr 154
   40 write (6,1019)                                                    gnmr 155
      if (copy_output) write (8,1019)                                   gnmr 156
   45 if (.not.copy_input) go to 50                                     gnmr 157
      write (7,1020) textl,frl,fr2,scale,r,height                       gnmr 158
      if (normalize) write (7,1021)                                     gnmr 159
      if (.not.normalize) write (7,1022)                                gnmr 160
      if (label) write (7,1041)                                         gnmr 161
      if (.not.label) write (7,1042)                                    gnmr 162
   50 if (.not.input) write (9,1023)                                    gnmr 163
      read (5,1006) nsum                                                gnmr 164
```

```
      if (.not.input) write (9,1024)                                    gnmr 165
      read (5,1006) ncal                                                gnmr 166
      if (.not.input) write (9,1025)                                    gnmr 167
      read (5,1006) nrc                                                 gnmr 168
      if (copy_input) write (7,1026) nsum,ncal,nrc                      gnmr 169
      write (6,1027) ncal,nsum,nrc                                      gnmr 170
      if (copy_output) write (8,1027) ncal,nsum,nrc                     gnmr 171
c                                                                       gnmr 172
c                                                                       gnmr 173
      do 60 j=1,nsum                                                    gnmr 174
         if (.not.input) write (9,1028) j                               gnmr 175
         read (5,1006) nn(j)                                            gnmr 176
         n=nn(j)                                                        gnmr 177
         if (copy_input) write (7,1029) n,j                             gnmr 178
         if (.not.input) write (9,1040)                                 gnmr 179
         do 55 i=1,n                                                    gnmr 180
            if (.not.input) write (9,1030) i                            gnmr 181
            read (5,1006) w(j,i),width(i),pop(j,i)                      gnmr 182
            if (copy_input) write (7,1031) w(j,i),width(i),pop(j,i)     gnmr 183
            t2(j,i)=1.0/(width(i)*pi)                                   gnmr 184
   55    continue                                                       gnmr 185
         write (6,1032) j                                               gnmr 186
         write (6,1033) (i,w(j,i),width(i),pop(j,i),i=1,n)              gnmr 187
         if (copy_output) write (8,1032) j                              gnmr 188
         if (copy_output)                                               gnmr 189
     .      write (8,1033) (i,w(j,i),width(i),pop(j,i),i=1,n)           gnmr 190
   60 continue                                                          gnmr 191
c                                                                       gnmr 192
      length3=nrc*20                                                    gnmr 193
      kk=0                                                              gnmr 194
      npoint=abs(fr1-fr2)/r                                             gnmr 195
      do 150 jx=1,ncal                                                  gnmr 196
         pstart=cputim(i)                                               gnmr 197
         jj=jx                                                          gnmr 198
         kk=kk+1                                                        gnmr 199
         if (.not.input) write (9,1034) kk                              gnmr 200
         do 65 i=1,nrc                                                  gnmr 201
            if (.not.input) write (9,1035) i                            gnmr 202
            read (5,1006) rc(i)                                         gnmr 203
            if (copy_input) write (7,1036) rc(i),i                      gnmr 204
   65    continue                                                       gnmr 205
         encode (text2,1037) kk,date,time                               gnmr 206
         encode (text3,1038) (i,rc(i),i=1,10)                           gnmr 208
         write (6,1039) text1,text2,(text3(i),i=1,nrc)                  gnmr 209
         if (copy_output) write (8,1039) text1,text2,                   gnmr 210
     .                                   (text3(i),i=1,nrc)
         if (no_calc) go to 147                                         gnmr 211
         do 140 j=1,nsum                                                gnmr 212
            n=nn(j)
c     write(6,1006) (pop(1,k),k=1,n)
            call matrix(rc,n,pop)
c
c            Subroutine matrix generates 'areal', the real part of the kinetic
c           matrix. Matrix 'a' is the complex, frequency-independent kinetic
c           matrix. Below, the off-diagonal elements of 'areal' are converted to
c           complex numbers and stored in array 'a'.
c
c     write(6,1006) (pop(1,k),k=1,n)
c                                                                       gnmr 213
            do 75 i=1,n                                                 gnmr 214
               do 70 k=1,n                                              gnmr 215
                  if (i.eq.k) go to 70                                  gnmr 216
                  a(k,i)=cmplx(areal(k,i),0.0)                          gnmr 217
   70          continue                                                 gnmr 218
   75       continue                                                    gnmr 219
c                                                                       gnmr 220
```

```
            do 80 i=1,n                                                    gnmr 221
   80       a(i,i)=cmplx(1.0/t2(j,i),-twopi*w(j,i))+areal(i,i)             gnmr 222
                                                                           gnmr 223
c
            call allmat(a,n,b,c)                                           gnmr 224
c
c            Allmat diagonalizes the frequency-independent complex kinetic
c          matrix. The eigenvector and inverted eigenvector matrices returned
c          by allmat are the same as those for the total frequency-dependent
c          kinetic matrix. The eigenvector matrix is overwritten on the original
c          'a' matrix so that 'a' is now the eigenvector matrix. Matrix 'b' is
c          the inverted eigenvector matrix, and 'c' is the one-dimensional
c          frequency-independent eigenvalue matrix.  Below, matrix 'b' is
c          multiplied from the right by the unit column vector, and the result-
c          ing column vector is stored as 'b1'.
c
c                                                                          gnmr 225
            do 90 i=1,n                                                    gnmr 226
               b1(i)=cmplx(0.0,0.0)                                        gnmr 227
               do 85 k=1,n                                                 gnmr 228
                  b1(i)=b1(i)+b(i,k)                                       gnmr 229
   85          continue                                                    gnmr 230
   90       continue                                                       gnmr 231
                                                                           gnmr 232
c
            do 100 i=1,n                                                   gnmr 233
               pa(i)=cmplx(0.0,0.0)                                        gnmr 234
               do 95 k=1,n                                                 gnmr 235
                  pa(i)=pa(i)+pop(j,k)*a(k,i)                              gnmr 236
   95          continue                                                    gnmr 237
  100       continue                                                       gnmr 238
                                                                           gnmr 239
c
c            'pa' is multiplied from the right by b1 to give column vector
c          'pabl'.
c
            do 105 i=1,n                                                   gnmr 240
  105       pabl(i)=pa(i)*b1(i)                                            gnmr 241
                                                                           gnmr 242
c
            freq=fr1+sign(r,fr1-fr2)
            do 120 m=1,npoint                                              gnmr 244
               freq=freq-sign(r,fr1-fr2)
c
c          The frequency-dependent inverted eigenvalue matrix 'd' is defined:
c
               do 110 i=1,n                                                gnmr 246
  110           d(i)=1.0/(c(i)+cmplx(0.0,twopi*freq))                       gnmr 247
c
c             The row vector 'd' is multiplied from the right by 'pabl' to give
c          the net complex xy-magnetization component 'g'.
c
               g(m)=cmplx(0.0,0.0)                                         gnmr 248
               do 115 i=1,n                                                gnmr 249
  115          g(m)=g(m)+d(i)*pabl(i)                                      gnmr 250
  120       continue                                                       gnmr 251
                                                                           gnmr 252
c
c
            if (j.ne.1) go to 130                                          gnmr 253
            do 125 i=1,npoint                                              gnmr 254
  125       greal(i)=0.0                                                   gnmr 255
  130       do 135 i=1,npoint                                              gnmr 256
  135       greal(i)=greal(i)+abs(real(g(i)))                              gnmr 257
  140    continue                                                          gnmr 258
  145    call spect(greal,npoint)                                          gnmr 259
  147    pstop=cputim(i)                                                   gnmr 260
         ptotal=pstop-pstart                                               gnmr 261
         write (6,1046) ptotal,kk                                          gnmr 262
         if (copy_output) write (8,1046) ptotal,kk                         gnmr 263
  150 continue                                                             gnmr 264
```

```
c                                                                       gnmr 265
      if (.not.input) write (9,1043)                                    gnmr 266
  155 read (5,1012,end=160) answer                                      gnmr 267
      if (answer.eq."yes") go to 160                                    gnmr 268
      if (answer.eq."no") go to 165                                     gnmr 269
c     Invalid input:                                                    gnmr 270
      if (input) go to 2001                                             gnmr 271
      write (9,1013)                                                    gnmr 272
      go to 155                                                         gnmr 273
  160 if (copy_input) write (7,1044)                                    gnmr 274
      call kdate(date)                                                  gnmr 275
      call ktime(time)                                                  gnmr 276
      go to 5                                                           gnmr 277
  165 if (copy_input) write (7,1045)                                    gnmr 278
      if (.not.no_calc) call plot(0.0,0.0,999)
      tstop=cputim(i)                                                   gnmr 280
      ttotal=tstop-tstart                                               gnmr 281
      write (6,1047) ttotal                                             gnmr 282
      if (copy_output) write (8,1047) ttotal                            gnmr 283
c                                                                       gnmr 284
c     CLOSE FILES                                                       gnmr 285
  170 close (5)                                                         gnmr 286
      close (6)                                                         gnmr 287
      if (copy_input) close (7)                                         gnmr 288
      if (copy_output) close (8)                                        gnmr 289
      if (.not.input) close (9)                                         gnmr 290
      stop                                                              gnmr 291
c                                                                       gnmr 292
c     ERROR SECTION                                                     gnmr 293
 2001 write (0,3001)                                                    gnmr 294
 3001 format ("gnmr:  Error:  Expecting 'yes' or 'no' answer ",         gnmr 295
     .        "in input read from file.")                               gnmr 296
      go to 170                                                         gnmr 297
      end                                                               gnmr 298
      subroutine open_files(input,output,copy_input,copy_output,no_calc)
c                                                                       open   2
      external utility_$get_arg (descriptors)                           open   3
c                                                                       open   4
      logical input,output,copy_input,copy_output,no_calc
c                                                                       open   6
      character*256 arg,input_file,output_file                          open   7
c                                                                       open   8
c                                                                       open   9
      input=.false.                                                     open  10
      output=.false.                                                    open  11
      copy_input=.false.                                                open  12
      copy_output=.false.                                               open  13
      no_calc=.false.
c                                                                       open  14
      i=0                                                               open  15
c                                                                       open  16
    5 i=i+1                                                             open  17
      call utility_$get_arg(i,arg,len)                                  open  18
      if (len.lt.0) go to 35                                            open  19
      if (arg.eq."-no_calc") go to 10
      if (arg.eq."-input") go to 15                                     open  21
      if (arg.eq."-output") go to 20                                    open  22
      if (arg.eq."-copy_input") go to 25                                open  23
      if (arg.eq."-copy_output") go to 30                               open  24
      go to 2001                                                        open  25
c                                                                       open  26
c     -no_calc
   10 if (no_calc) go to 2002
      no_calc=.true.
      go to 5
c                                                                       open  32
```

```
c     -input                                                                open  33
   15 if (input) go to 2002                                                 open  34
      if (copy_input) go to 2006                                            open  35
      i=i+1                                                                 open  36
      call utility_$get_arg(i,input_file,len)                               open  37
      if (len.lt.0) go to 2003                                              open  38
      if (input_file.eq.output_file) go to 2004                             open  39
      input=.true.                                                          open  40
      open (5,file=input_file,form="formatted",mode="in")                   open  41
      go to 5                                                               open  42
c                                                                           open  43
c     -output                                                               open  44
   20 if (output) go to 2002                                                open  45
      if (copy_output) go to 2005                                           open  46
      i=i+1                                                                 open  47
      call utility_$get_arg(i,output_file,len)                              open  48
      if (len.lt.0) go to 2003                                              open  49
      if (output_file.eq.input_file) go to 2004                             open  50
      output=.true.                                                         open  51
      open (6,file=output_file,form="formatted",mode="out")                 open  52
      go to 5                                                               open  53
c                                                                           open  54
c     -copy_input                                                           open  55
   25 if (copy_input) go to 2002                                            open  56
      if (input) go to 2006                                                 open  57
      i=i+1                                                                 open  58
      call utility_$get_arg(i,input_file,len)                               open  59
      if (len.lt.0) go to 2003                                              open  60
      if (input_file.eq.output_file) go to 2004                             open  61
      copy_input=.true.                                                     open  62
      open (7,file=input_file,form="formatted",mode="out")                  open  63
      go to 5                                                               open  64
c                                                                           open  65
c     -copy_output                                                          open  66
   30 if (copy_output) go to 2002                                           open  67
      if (output) go to 2005                                                open  68
      i=i+1                                                                 open  69
      call utility_$get_arg(i,output_file,len)                              open  70
      if (len.lt.0) go to 2003                                              open  71
      if (output_file.eq.input_file) go to 2004                             open  72
      copy_output=.true.                                                    open  73
      open (8,file=output_file,form="formatted",mode="out")                 open  74
      go to 5                                                               open  75
c                                                                           open  76
c     Open default files to user_input/output switches, if necessary,       open  77
c     before returning:                                                     open  78
   35 if (.not.input) open (5,form="formatted",mode="in",prompt=.true.)     open  79
      if (.not.input) open (9,form="formatted",mode="out",defer=.true.,     open  80
     .                      attach="syn_ user_output -inhibit get_line      open  81
     .                      get_chars",carriage=.true.)                     open  82
      if (.not.output) open (6,form="formatted",mode="out")                 open  83
      return                                                                open  84
c                                                                           open  85
c     ERROR SECTION                                                         open  86
c     Print out first error detected, close any open files and stop:        open  87
c                                                                           open  88
 2001 write (0,3001) arg                                                    open  89
 3001 format ("gnmr:  Error in subroutine open_files:  ",                   open  90
     .        "Illegal argument in call to gnmr:  ",a256)                   open  91
      go to 40                                                              open  92
c                                                                           open  93
c                                                                           open  94
 2002 write (0,3002) arg                                                    open  95
 3002 format ("gnmr:  Error in subroutine open_files:  ",                   open  96
     .        "Duplicate argument in call to gnmr:  ",a256)                 open  97
      go to 40                                                              open  98
```

```
c                                                                       open  99
 2003 write (0,3003) arg                                                open 100
 3003 format ("gnmr:  Error in subroutine open_files:  ",               open 101
     .        "Missing file name in call to gnmr:  ",a256)              open 102
      go to 40                                                          open 103
c                                                                       open 104
 2004 write (0,3004) input_file                                         open 105
 3004 format ("gnmr:  Error in subroutine open_files:  ",               open 106
     .        "Duplicate file names given in call to gnmr:  ",a256)     open 107
      go to 40                                                          open 108
c                                                                       open 109
 2005 write (0,3005)                                                    open 110
 3005 format ("gnmr:  Error in subroutine open_files:  ",               open 111
     .        "Use of -output and -copy_output arguments in the ",      open 112
     .        "same call to gnmr is illegal. ")                         open 113
      go to 40                                                          open 114
c                                                                       open 115
 2006 write (0,3006)                                                    open 116
 3006 format ("gnmr:  Error in subroutine open_files:  ",               open 117
     .        "Use of -input and -copy_input arguments in the ",        open 118
     .        "same call to gnmr is illegal. ")                         open 119
c                                                                       open 120
c                                                                       open 121
   40 if (input) close (5)                                              open 122
      if (output) close (6)                                             open 123
      if (copy_input) close (7)                                         open 124
      if (copy_output) close (8)                                        open 125
      stop                                                              open 126
      end                                                               open 127
      subroutine spect(y,n)                                             spec   1
c                                                                       spec   2
      character*20 text3(10)                                            spec   3
c
c         'text3' is a plot counter and label.
c
      character*36 text2                                                spec   4
      character*80 text1                                                spec   5
c                                                                       spec   6
      external symbol(descriptors)                                      spec   7
      external axis(descriptors)                                        spec   8
c                                                                       spec   9
      logical normalize,label                                           spec  10
c                                                                       spec  11
      dimension y(20000)                                                spec  12
      common /text/ text1,text2,text3,length3                           spec  13
     . common /pltpar/ scale,height,fr1,fr2,j,normalize,label           spec  14
                                                                        spec  15
                                                                        spec  16
                                                                        spec  17
c     the width of the plot in cm (xmax) is found, and the
c     x increment (xstep,inches) for each point is calculated.          spec  19
                                                                        spec  20
      xmax=scale*abs(fr1-fr2)/10.0
      xstep=xmax/n                                                      spec  22
                                                                        spec  23
c     the minimum and maximum values of y are found.                    spec  24
                                                                        spec  25
      ymin=y(1)                                                         spec  26
      ymax=y(1)                                                         spec  27
      do 20  i=1,n                                                      spec  28
      ymin=aminl(ymin,y(i))                                             spec  29
 20   ymax=amaxl(ymax,y(i))                                             spec  30
                                                                        spec  31
c     the y values are scaled to match the observed spectrum and        spec  32
c     converted to inch displacements.                                  spec  33
                                                                        spec  34
```

```
c     if nfactor is zero, each plot will be height mm high.  if nfactor spec  35
c     is not zero, the first plot will be height mm high, and all       spec  36
c     subsequent plots will be normalized to the peak area of the first.spec  37
                                                                        spec  38
      if (.not.normalize) go to 30                                     spec  39
      if(j.ne.1)  go to 35                                             spec  40
 30   yck=ymax-ymin                                                    spec  41
      if(yck.eq.0)  go to 81                                           spec  42
      factor=height/(10.0*yck)                                         spec  43
 35   do 40  i=1,n                                                     spec  44
 40   y(i)=(y(i)-ymin)*factor+5.0                                      spec  45
                                                                        spec  46
c     the pen is moved to the start of the plot.                       spec  47
                                                                        spec  48
      x=0.0                                                            spec  49
      call plot(x,y(1),3)                                              spec  50
                                                                        spec  51
c     the spectrum is plotted.                                         spec  52
                                                                        spec  53
      do 60  i=2,n                                                     spec  54
      x=x+xstep                                                        spec  55
 60   call plot(x,y(i),2)                                              spec  56
                                                                        spec  57
c     the following call axis and call symbol cards can be omitted     spec  58
c     to save on plotting costs and time.                              spec  59
c     if these cards are omitted and a subroutine library is being     spec  60
c     utilized, include this subroutine with the input deck even if it spec  61
c     is in the library.                                               spec  62
                                                                        spec  63
c     the x axis is drawn.                                             spec  64
                                                                        spec  65
      if (.not.label) go to 70                                         spec  66
      xmax=xmax+1.0                                                    spec  67
      nmax=xmax                                                        spec  68
      xmax=nmax                                                        spec  69
      dx=sign(10.0/scale,fr2-fr1)
      call axis(0.0,4.5,19hChemical Shift (hz),-19,xmax,0.0,fr1,dx)    spec  71
                                                                        spec  72
c     the plot is labeled.                                             spec  73
   70 call symbol(0.0,2.50,0.40,text1,0.0,80)                          spec  74
      call symbol(0.0,1.75,0.40,text2,0.0,36)                          spec  75
      call symbol(0.0,1.00,0.40,text3,0.0,length3)                     spec  76
c     a new orgin is established.                                      spec  77
                                                                        spec  78
      x=xmax+2.5                                                       spec  79
      call plot(x,0.0,-3)
      return                                                           spec  81
   81 write(6,82)                                                      spec  82
82    format (34h plot deleted,gives straight line.)                   spec  83
      return                                                           spec  84
      end                                                              spec  85
      subroutine nvrt(q,qnv,n)                                         nvrt   1
                                                                       nvrt   2
                                                                       nvrt   3
c     this subroutine inverts the a matrix transferred from gnmr.      nvrt   4
c     the arrays below must be dimensioned greater than  or equal to   nvrt   5
c     (n) or (n,n), where n is the size of the matrix to be inverted.  nvrt   6
                                                                       nvrt   7
      complex q(70,70),qqnv(70,70),temp(70,70),qnv(70,70),p(70)        nvrt   8
      common  /save/temp,qqnv,p                                        nvrt   9
      complex tfr                                                      nvrt  10
      if (n.ne.1) go to 1                                              nvrt  11
      qnv(1,1) = 1./q(1,1)                                             nvrt  12
      go to 120                                                        nvrt  13
    1 do 410 i = 1,n                                                   nvrt  14
      do 410 j=1,n                                                     nvrt  15
```

```
      temp(i,j)=q(i,j)                                                  nvrt  16
  410 qqnv(i,j)=cmplx(0.,0.)                                            nvrt  17
      do 11 i=1,n                                                       nvrt  18
   11 qqnv(i,i)=cmplx(1.,0.)                                            nvrt  19
      k=1                                                               nvrt  20
   92 i=k                                                               nvrt  21
      l=k                                                               nvrt  22
    9 s=cabs(temp(i,k))                                                 nvrt  23
      t=cabs(temp(l,k))                                                 nvrt  24
      if (s-t) 10,10,20                                                 nvrt  25
   20 l=i                                                               nvrt  26
   10 if (i-n) 30,40,30                                                 nvrt  27
   30 i=i+1                                                             nvrt  28
      go to 9                                                           nvrt  29
   40 if (l-k) 50,60,50                                                 nvrt  30
   50 j=k                                                               nvrt  31
    6 tfr=temp(k,j)                                                     nvrt  32
      temp(k,j)=temp(l,j)                                               nvrt  33
      temp(l,j)=tfr                                                     nvrt  34
      if (j-n) 8,7,8                                                    nvrt  35
    8 j=j+1                                                             nvrt  36
      go to 6                                                           nvrt  37
    7 do 69 in=1,n                                                      nvrt  38
      tfr=qqnv(k,in)                                                    nvrt  39
      qqnv(k,in)=qqnv(l,in)                                             nvrt  40
   69 qqnv(l,in)=tfr                                                    nvrt  41
   60 i=k+1                                                             nvrt  42
   71 tfr=temp(i,k)/temp(k,k)                                           nvrt  43
      temp(i,k)=cmplx(0.,0.)                                            nvrt  44
      j=k+1                                                             nvrt  45
    3 temp(i,j)=temp(i,j)-tfr*temp(k,j)                                 nvrt  46
      if (j-n) 5,4,5                                                    nvrt  47
    5 j=j+1                                                             nvrt  48
      go to 3                                                           nvrt  49
    4 do 39 in=1,n                                                      nvrt  50
   39 qqnv(i,in)=qqnv(i,in)-tfr*qqnv(k,in)                              nvrt  51
      if (i-n) 70,80,70                                                 nvrt  52
   70 i=i+1                                                             nvrt  53
      go to 71                                                          nvrt  54
   80 if (k-n+1) 90,91,90                                               nvrt  55
   90 k=k+1                                                             nvrt  56
      go to 92                                                          nvrt  57
   91 do 750 in=1,n                                                     nvrt  58
  750 qnv(n,in)=qqnv(n,in)/temp(n,n)                                    nvrt  59
      i=n-1                                                             nvrt  60
   99 j=i+1                                                             nvrt  61
      do 751 in=1,n                                                     nvrt  62
  751 p(in)=cmplx(0.,0.)                                                nvrt  63
  102 do 752 in=1,n                                                     nvrt  64
  752 p(in)=p(in)+temp(i,j)*qnv(j,in)                                   nvrt  65
      if (j-n) 100,101,100                                              nvrt  66
  100 j=j+1                                                             nvrt  67
      go to 102                                                         nvrt  68
  101 do 753 in=1,n                                                     nvrt  69
  753 qnv(i,in)=(qqnv(i,in)-p(in))/temp(i,i)                            nvrt  70
      if (i-1) 110,120,110                                              nvrt  71
  110 i=i-1                                                             nvrt  72
      go to 99                                                          nvrt  73
  120 return                                                            nvrt  74
      end                                                               nvrt  75
      subroutine allmat (a,m,cl,lambda)                                 allm   1
c allmat diagonalizes the nt by nt dimensional a matrix.  the           allm   2
c eigenvectors are overwritten on the original a matrix. the inverse of allm   3
c the eigenvector matrix is calculated as the cl matrix. the eigen-     allm   4
c values are contained in the one dimensional lambda array.             allm   5
      dimension int(70)                                                 allm   6
```

```
      complex a(70,70),c1(70,70),h1(70,70),lambda(70),vect(70),mult(70),allm   7
     1  shift(3),temp,sin,cos,temp1,temp2,trace,sumeig,csqrt              allm   8
      complex cr(70,70),h(70,70),eig(70)                                 allm   9
      common /save/cr,h,eig                                              allm  10
      integer r,rp1,rp2                                                  allm  11
      logical inth(70),twice                                             allm  12
c                                                                        allm  13
c prog. authors john rinzel,r.e.funderlic,union carbide corp.            allm  14
c nuclear division,central data processing facility,                     allm  15
c oak ridge tennessee                                                    allm  16
      n=m                                                                allm  17
      trace=cmplx(0.0,0.0)                                               allm  18
      do 61 i = 1,n                                                      allm  19
   61 trace = trace + a(i,i)                                             allm  20
      ncal=n                                                             allm  21
      if(n.ne.1)go to 1                                                  allm  22
      lambda(1)=a(1,1)                                                   allm  23
      a(1,1)=cmplx(1.0,0.0)                                              allm  24
      c1(1,1)=cmplx(1.0,0.0)                                             allm  25
      return                                                             allm  26
    1 icount=0                                                           allm  27
      shift(1)=cmplx(0.0,0.0)                                            allm  28
      if(n.ne.2)go to 4                                                  allm  29
    2 temp=(a(1,1)+a(2,2)+csqrt((a(1,1)+a(2,2))**2-                      allm  30
     14.*(a(2,2)*a(1,1)-a(2,1)*a(1,2))))/2.                             allm  31
      if(real(temp).ne.0..or.aimag(temp).ne.0.)go to 3                   allm  32
      lambda(m)=shift(1)                                                 allm  33
      lambda(m-1)=a(1,1)+a(2,2)+shift(1)                                 allm  34
      go to 37                                                           allm  35
    3 lambda(m)=temp+shift(1)                                            allm  36
      lambda(m-1)=(a(2,2)*a(1,1)-a(2,1)*a(1,2))/(lambda(m)-shift(1))+    allm  37
     1   shift(1)                                                        allm  38
      go to 37                                                           allm  39
c                                                                        allm  40
c     reduce matrix a to hessenberg form                                 allm  41
    4 nm2=n-2                                                            allm  42
      do 15 r=1,nm2                                                      allm  43
      rp1=r+1                                                            allm  44
      rp2=r+2                                                            allm  45
      abig=0.                                                            allm  46
      int(r)=rp1                                                         allm  47
      do 5 i=rp1,n                                                       allm  48
      abssq=real(a(i,r))**2+aimag(a(i,r))**2                             allm  49
      if(abssq.le.abig)go to 5                                           allm  50
      int(r)=i                                                           allm  51
      abig=abssq                                                         allm  52
    5 continue                                                           allm  53
      inter=int(r)                                                       allm  54
      if(abig.eq.0.)go to 15                                             allm  55
      if(inter.eq.rp1)go to 8                                            allm  56
      do 6 i=r,n                                                         allm  57
      temp=a(rp1,i)                                                      allm  58
      a(rp1,i)=a(inter,i)                                                allm  59
    6 a(inter,i)=temp                                                    allm  60
      do 7 i=1,n                                                         allm  61
      temp=a(i,rp1)                                                      allm  62
      a(i,rp1)=a(i,inter)                                                allm  63
    7 a(i,inter)=temp                                                    allm  64
    8 do 9 i=rp2,n                                                       allm  65
      mult(i)=a(i,r)/a(rp1,r)                                            allm  66
    9 a(i,r)=mult(i)                                                     allm  67
      do 11 i=1,rp1                                                      allm  68
      temp=cmplx(0.0,0.0)                                                allm  69
      do 10 j=rp2,n                                                      allm  70
   10 temp=temp+a(i,j)*mult(j)                                           allm  71
   11 a(i,rp1)=a(i,rp1)+temp                                             allm  72
```

```
      do 13 i=rp2,n                                                    allm  73
      temp=cmplx(0.0,0.0)                                              allm  74
      do 12 j=rp2,n                                                    allm  75
   12 temp=temp+a(i,j)*mult(j)                                         allm  76
   13 a(i,rpl)=a(i,rpl)+temp-mult(i)*a(rpl,rpl)                        allm  77
      do 14 i=rp2,n                                                    allm  78
      do 14 j=rp2,n                                                    allm  79
   14 a(i,j)=a(i,j)-mult(i)*a(rpl,j)                                   allm  80
   15 continue                                                         allm  81
c                                                                      allm  82
c     calculate epsilon                                                allm  83
c                                                                      allm  84
      eps=0.                                                           allm  85
      do 16 i=1,n                                                      allm  86
   16 eps=eps+cabs(a(1,i))                                             allm  87
      do 18 i=2,n                                                      allm  88
      sum=0.                                                           allm  89
      iml=i-1                                                          allm  90
      do 17 j=iml,n                                                    allm  91
   17 sum=sum+cabs(a(i,j))                                             allm  92
   18 if(sum.gt.eps)eps=sum                                            allm  93
      eps=sqrt(float(n))*eps*1.e-12                                    allm  94
      if(eps.eq.0.)eps=1.e-12                                          allm  95
      do 19 i=1,n                                                      allm  96
      do 19 j=1,n                                                      allm  97
   19 h(i,j)=a(i,j)                                                    allm  98
   20 if(n.ne.1)go to 21                                               allm  99
      lambda(m)=a(1,1)+shift(1)                                        allm 100
      go to 37                                                         allm 101
   21 if(n.eq.2)go to 2                                                allm 102
   22 mnl=m-n+1                                                        allm 103
      if(real(a(n,n)).ne.0..or.aimag(a(n,n)).ne.0.) go to 530          allm 104
      go to 540                                                        allm 105
  530 if(abs(real(a(n,n-1)/a(n,n)))+abs(aimag(a(n,n-1)/a(n,n)))-1.e-9) allm 106
     224,24,23                                                         allm 107
  540 continue                                                         allm 108
   23 if(abs(real(a(n,n-1)))+abs(aimag(a(n,n-1))).ge.eps)go to 25      allm 109
   24 lambda(mnl)=a(n,n)+shift(1)                                      allm 110
      icount=0                                                         allm 111
      n=n-1                                                            allm 112
      go to 21                                                         allm 113
c                                                                      allm 114
c     determine shift                                                  allm 115
c                                                                      allm 116
   25 shift(2)=(a(n-1,n-1)+a(n,n)+csqrt((a(n-1,n-1)+a(n,n))**2         allm 117
     1 -4.*(a(n,n)*a(n-1,n-1)-a(n,n-1)*a(n-1,n))))/2.                  allm 118
      if(real(shift(2)).ne.0..or.aimag(shift(2)).ne.0.)go to 26        allm 119
      shift(3)=a(n-1,n-1)+a(n,n)                                       allm 120
      go to 27                                                         allm 121
   26 shift(3)=(a(n,n)*a(n-1,n-1)-a(n,n-1)*a(n-1,n))/shift(2)          allm 122
   27 if(cabs(shift(2)-a(n,n)).lt.cabs(shift(3)-a(n,n)))go to 28       allm 123
      index=3                                                          allm 124
      go to 29                                                         allm 125
   28 index=2                                                          allm 126
   29 if (cabs(a(n-1,n-2)).ge.eps) go to 30                            allm 127
      lambda(mnl)=shift(2)+shift(1)                                    allm 128
      lambda(mnl+1)=shift(3)+shift(1)                                  allm 129
      icount=0                                                         allm 130
      n=n-2                                                            allm 131
      go to 20                                                         allm 132
   30 shift(1)=shift(1)+shift(index)                                   allm 133
      do 31 i=1,n                                                      allm 134
   31 a(i,i)=a(i,i)-shift(index)                                       allm 135
c                                                                      allm 136
c     perform givens rotations, qr iterates                            allm 137
c                                                                      allm 138
```

```
      if (icount.le.10) go to 32                                        allm 139
      ncal=m-n                                                          allm 140
      go to 37                                                          allm 141
   32 nml=n-1                                                           allm 142
      temp1=a(1,1)                                                      allm 143
      temp2=a(2,1)                                                      allm 144
      do 36 r=1,nml                                                     allm 145
      rp1=r+1                                                           allm 146
      rho=sqrt(real(temp1)**2+aimag(temp1)**2+                          allm 147
     1real(temp2)**2+aimag(temp2)**2)                                   allm 148
      if(rho.eq.0.0)  go to 201                                         allm 149
      cos=temp1/rho                                                     allm 150
      sin=temp2/rho                                                     allm 151
      index=max0(r-1,1)                                                 allm 152
      do 33 i=index,n                                                   allm 153
      temp=conjg(cos)*a(r,i)+conjg(sin)*a(rp1,i)                        allm 154
      a(rp1,i)=-sin*a(r,i)+cos*a(rp1,i)                                 allm 155
   33 a(r,i)=temp                                                       allm 156
  201 temp1 = a(rp1,rp1)                                                allm 157
      temp2=a(r+2,r+1)                                                  allm 158
      if(rho.eq.0.0)  go to 36                                          allm 159
      do 34 i=1,r                                                       allm 160
      temp=cos*a(i,r)+sin*a(i,rp1)                                      allm 161
      a(i,rp1)=-conjg(sin)*a(i,r)+conjg(cos)*a(i,rp1)                   allm 162
   34 a(i,r)=temp                                                       allm 163
      index=min0(r+2,n)                                                 allm 164
      do 35 i=rp1,index                                                 allm 165
      a(i,r)=sin*a(i,rp1)                                               allm 166
   35 a(i,rp1)=conjg(cos)*a(i,rp1)                                      allm 167
   36 continue                                                          allm 168
      icount=icount+1                                                   allm 169
      go to 22                                                          allm 170
c                                                                       allm 171
c     calculate vectors                                                 allm 172
c                                                                       allm 173
   37 if(ncal.eq.0)go to 57                                             allm 174
      ncalm = ncal - 1                                                  allm 175
      do 68 i = 1,ncalm                                                 allm 176
      ip1 = i + 1                                                       allm 177
      do 68  j=ip1,ncal                                                 allm 178
      if (cabs(lambda(i)) - cabs(lambda(j))) 68,68,69                   allm 179
   69 temp = lambda(i)                                                  allm 180
      lambda(i) = lambda(j)                                             allm 181
      lambda(j) = temp                                                  allm 182
   68 continue                                                          allm 183
      do 70 i = 1,ncalm                                                 allm 184
      ip1= i+1                                                          allm 185
      do 71 j = ip1,ncal                                                allm 186
      if (cabs(lambda(i) - lambda(j)) - (3.0e-07)*(cabs(lambda(i)))) 72,allm 187
     172,71                                                             allm 188
   72 lambda(i) = lambda(i) - (3.0e-07)*lambda(i)                       allm 189
      im = i-1                                                          allm 190
      do 73 k = 1,im                                                    allm 191
      if (cabs(lambda(i) - lambda(i-k)) -(3.0e-07)*(cabs(lambda(i)))) 74allm 192
     1,74,71                                                            allm 193
   74 lambda(i-k) = lambda(i-k) - (3.0e-07)*lambda(i)                   allm 194
   73 continue                                                          allm 195
   71 continue                                                          allm 196
   70 continue                                                          allm 197
      n=m                                                               allm 198
      nml=n-1                                                           allm 199
      if(n.ne.2)go to 38                                                allm 200
      eps=amax1(cabs(lambda(1)),cabs(lambda(2)))*1.e-8                  allm 201
      if(eps.eq.0.)eps=1.e-12                                           allm 202
      h(1,1)=a(1,1)                                                     allm 203
      h(1,2)=a(1,2)                                                     allm 204
```

```
      h(2,1)=a(2,1)                                                    allm 205
      h(2,2)=a(2,2)                                                    allm 206
   38 do 56 l=1,ncal                                                   allm 207
      do 40 i=1,n                                                      allm 208
      do 39 j=1,n                                                      allm 209
   39 hl(i,j)=h(i,j)                                                   allm 210
   40 hl(i,i)=hl(i,i)-lambda(l)                                        allm 211
      do 44 i=1,nml                                                    allm 212
      mult(i)=cmplx(0.0,0.0)                                           allm 213
      inth(i)=.false.                                                  allm 214
      ipl=i+1                                                          allm 215
      if(cabs(hl(i+1,i)).le.cabs(hl(i,i)))go to 42                     allm 216
      inth(i)=.true.                                                   allm 217
      do 41 j=i,n                                                      allm 218
      temp=hl(i+1,j)                                                   allm 219
      hl(i+1,j)=hl(i,j)                                                allm 220
   41 hl(i,j)=temp                                                     allm 221
   42 if(real(hl(i,i)).eq.0..and.aimag(hl(i,i)).eq.0.)go to 44         allm 222
      mult(i)=-hl(i+1,i)/hl(i,i)                                       allm 223
      do 43 j=ipl,n                                                    allm 224
   43 hl(i+1,j)=hl(i+1,j)+mult(i)*hl(i,j)                              allm 225
   44 continue                                                         allm 226
      do 45 i=1,n                                                      allm 227
45    vect(i)=cmplx(1.0,0.0)                                           allm 228
      twice=.false.                                                    allm 229
   46 if(real(hl(n,n)).eq.0..and.aimag(hl(n,n)).eq.0.)hl(n,n)=         allm 230
     1  cmplx(eps,0.0)                                                allm 231
      vect(n)=vect(n)/hl(n,n)                                          allm 232
      do 48 i=1,nml                                                    allm 233
      k=n-i                                                            allm 234
      do 47 j=k,nml                                                    allm 235
   47 vect(k)=vect(k)-hl(k,j+1)*vect(j+1)                              allm 236
      if(real(hl(k,k)).eq.0..and.aimag(hl(k,k)).eq.0.)hl(k,k)=         allm 237
     1  cmplx(eps,0.0)                                                allm 238
   48 vect(k)=vect(k)/hl(k,k)                                          allm 239
      sss = 0.                                                         allm 240
      do 1001 i = 1,n                                                  allm 241
1001  sss = sss + (real(vect(i)))**2 + (aimag(vect(i)))**2             allm 242
      sss = sqrt(sss)                                                  allm 243
      do 50 i = 1,n                                                    allm 244
   50 vect(i) = vect(i)/sss                                            allm 245
      if(twice)go to 52                                                allm 246
      do 51 i=1,nml                                                    allm 247
      if(.not.inth(i))go to 51                                         allm 248
      temp=vect(i)                                                     allm 249
      vect(i)=vect(i+1)                                                allm 250
      vect(i+1)=temp                                                   allm 251
   51 vect(i+1)=vect(i+1)+mult(i)*vect(i)                              allm 252
      twice=.true.                                                     allm 253
      go to 46                                                         allm 254
   52 if(n.eq.2)go to 55                                               allm 255
      nm2=n-2                                                          allm 256
      do 54 i=1,nm2                                                    allm 257
      nli=n-1-i                                                        allm 258
      nil=n-i+1                                                        allm 259
      do 53 j=nil,n                                                    allm 260
   53 vect(j)=h(j,nli)*vect(nli+1)+vect(j)                             allm 261
      index=int(nli)                                                   allm 262
      temp=vect(nli+1)                                                 allm 263
      vect(nli+1)=vect(index)                                          allm 264
   54 vect(index)=temp                                                 allm 265
   55 do 56 i = 1,n                                                    allm 266
   56  a(i,l) =vect(i)                                                 allm 267
      if (ncal.ne.n) go to 64                                          allm 268
      call nvrt(a,cl,n)                                                allm 269
c     sumeig=cmplx(0.0,0.0)                                            allm 270
```

```
c     do 59 i=1,ncal                                                    allm 271
c  59 sumeig = sumeig + lambda(i)                                       allm 272
c     write (6,60) trace, sumeig                                        allm 273
c  60 format (9h trace = e14.7,3h + e14.7,1hi10h sumeig = e14.7,3h + e14allm 274
c    1.7,1hi)                                                          allm 275
      go to 57                                                          allm 276
   64 ncalp = ncal + 1                                                  allm 277
      write (6,65) ncalp                                                allm 278
   65 format (43h convergence failure in calculation of no. i2,28h eigenallm 279
     1value - run terminated)                                           allm 280
      stop                                                              allm 281
   57 return                                                            allm 282
      end                                                               allm 283
      subroutine kdate (dt)                                             kdat   1
c                                                                       kdat   2
c     Returns the current date in the form mm/dd/yy as two 4 character  kdat   3
c     strings in dt.                                                    kdat   4
c                                                                       kdat   5
      dimension dt(2),halfdt(2)                                         kdat   6
      character*8 fulldt                                                kdat   7
      equivalence (halfdt(1),fulldt)                                    kdat   8
      double precision time                                             kdat   9
c                                                                       kdat  10
      external date_time_ (descriptors)                                 kdat  11
c                                                                       kdat  12
      call clock_ (time)                                                kdat  13
      call date_time_ (time,fulldt)                                     kdat  14
      dt(1)=halfdt(1)                                                   kdat  15
      dt(2)=halfdt(2)                                                   kdat  16
      return                                                            kdat  17
      end                                                               kdat  18
      subroutine ktime (tm)                                             ktim   1
c                                                                       ktim   2
c     Returns the current time in the form hhmm.m as two 4              ktim   3
c     character strings in tm.                                          ktim   4
c                                                                       ktim   5
      dimension tm(2),parttm(4)                                         ktim   6
      character*16 fulltm                                               ktim   7
      equivalence (parttm(1),fulltm)                                    ktim   8
      double precision time                                             ktim   9
c                                                                       ktim  10
      external date_time_ (descriptors)                                 ktim  11
c                                                                       ktim  12
      call clock_ (time)                                                ktim  13
      call date_time_ (time,fulltm)                                     ktim  14
      tm(1)=parttm(3)                                                   ktim  15
      tm(2)=parttm(4)                                                   ktim  16
      return                                                            ktim  17
      end                                                               ktim  18
      function cputim (i)                                               cput   1
c                                                                       cput   2
c     Returns the cpu usage time since login in seconds.                cput   3
c                                                                       cput   4
      double precision time                                             cput   5
      dimension itime(2)                                                cput   6
      equivalence (itime(1),time)                                       cput   7
      call virtual_cpu_time_ (time)                                     cput   8
      cputim=float(itime(2))/1000000.0                                  cput   9
      return                                                            cput  10
      end                                                               cput  11
```

gnmr.gi.info

12/19/79 gnmr.gi

Introduction:

The following is a description of the various programs and controlling routines required for execution of 'gnmr' and subsequent plotting. After describing the individual segments (or files) required for execution, the procedure for restoring these files from a tape_archive is given.

Object segments:
1) gnmr
2) matrix
3) display

gnmr: This is the object segment which contains the coding necessary for the actual calculations. It is obtained by compiling the fortran source segment 'gnmr.fortran'.

matrix: This is the object segment of subroutine 'matrix.fortran'. It is created by the user prior to execution of gnmr. 'matrix.fortran' must be edited by the user so that it contains a suitable kinetic matrix. Type 'help qedx' for instructions on using the editor. After editing, 'matrix.fortran' must be compiled to generate 'matrix'. This is done by typing 'ft matrix'.

To facilitate simultaneous work on different systems the user can create a different source segment, say 'matrix2.fortran', with the second kinetic matrix, then compile using 'ft matrix2'. When executing gnmr it is then necessary to use the control argument '-matrix matrix2'.

display: This is the object segment of the program 'display.pl1'. It may be used for displaying pre-calculated plots interactively at graphic terminals. Type 'help -pn display' for more information.

Exec_com segment:

There is a control segment which contains Multics command lines used to interpret the 'gnmr' command, and to call appropriate system routines. It is an exec_com segment named 'gnmr.ec'. For information on exec_coms type 'help exec_com'. This is the program which the user normally interacts with.

'gnmr.ec' is called by typing the following command line (either interactively or absentee):

```
     exec_com gnmr {-control_args}
```

Or if the following abbreviation has been defined:

```
     .ab gnmr exec_com gnmr
```

then one simply types:

```
     gnmr {-control_args}
```

For information on control arguments and syntax type 'help -pn gnmr'.

Info segments:

There are also three info segments concerning gnmr.

These are:
1) gnmr.gi.info
2) gnmr.info
3) display.info

An info segment is a specially formatted segment which may be interpreted using the 'help' command. For information on the use of the 'help' command type 'help help'. Since these are not system info segments they must be accessed using the -pathname control argument.
eg. help -pn display

gnmr.gi.info: is the segment containing general information (gi) on 'gnmr'. It is the one you are currently reading.

gnmr.info: contains the formal description of the syntax and control arguments of the gnmr exec_com.

display.info: describes the PL/I procedure 'display'.

Restoring files from a tape_archive:

The entire 'gnmr' system has been archived on the magnetic tape with volume id 000430. The system may be restored by using the 'tape_archive' command. Type 'help tape_archive' for more information.

Suggested restore procedure:
```
ta x 000430 (gnmr.fortran matrix.fortran display.pll gnmr.ec)
ta x 000430 (gnmr.gi.info gnmr.info display.info)
ta go 000430
```
If the tape_archive table '000430.ta' does not exist, the user must include the command 'ta load_table 000430.ta 000430' before the above commands.

After restoring the files from magnetic tape it is necessary to compile the source programs using:
```
ft gnmr
pll display
```
It is also necessary to edit 'matrix.fortran' and compile it as described above.

One should also define the abbreviation for 'gnmr' by typing
'.ab gnmr exec_com gnmr'.

gnmr.info

84-05-31 gnmr

Syntax: ec gnmr {-control_args}

Function: executes fortran program 'gnmr', which calculates and plots nmr spectra broadened by exchange of nuclei.

Control Arguments:

-copy_input PATH
specifies the path of the segment which is to receive an anotated copy of all input read by gnmr. This file is suitable for subsequent input to gnmr (see the -input control argument). If omitted no copy is made. Use of both -copy_input and -input is illegal.

-input PATH
specifies the path of the segment containing input for gnmr. This segment is normally generated by use of the -copy_input control argument during a previous run of gnmr. If omitted input is read from the user's terminal. Use of both -input and -copy_input is illegal.

-copy_output PATH
specifies the path of the segment which is to receive a duplicate copy of the output sent to the user's terminal. This file is suitable for sending to a printer. Type 'help eor' for information on the eor command. If the -copy_output control argument is omitted, no copy is made. Use of both -copy_output and -output is illegal.

-output PATH
specifies the path of the segment to which the output from gnmr is to be placed. If omitted output is sent to the user's terminal. Use of both -output and -copy_output is illegal.

-matrix PATH
specifies the path of the object segment generated from the compilation of the subroutine 'matrix.fortran'. If omitted, '-matrix matrix' is assumed.

-on DEVICE
specifies the name of the device on which the plots are to be displayed. DEVICE may be one of the following: cc_1051, cc_1051w, tk_4010, tk_1013, tk_4014 or tk_4662. Type 'help twigs_devices' for information on all graphic devices currently supported. If omitted, '-on cc_1051' is assummed.

-file_plot PATH
specifies that graphic output is to be placed in the segment whose path name is PATH. This argument must be given if '-on cc_1051' or '-on cc_1051w' are present, or the -on control argument has been omitted. If this control argument is omitted and a Calcomp plot is not being generated the output is sent to the user's terminal, in a form suited for display on the device given with the -on control argument.

-no_calc
specifies that data is to be read in, without performing any calculations or generating a plot. Only the -matrix, -input or -copy_input, and -output or -copy_output control arguments may be gven with the -no_calc control argument. If omitted calculations are performed.

Notes:
Due to restrictions of the 'value' active function PATH cannot exceed 32 characters.

Examples:

gnmr -copy_input my.input -no_calc
This will prompt the user for input and generate an input file without performing any calculations.

gnmr -file_plot test
This will prompt for input, write the program output on the terminal and generate a Calcomp plot (in file test.cc_1051).

dFigure3-2

```
Figure 3-2.
 0.00000000E+00    Left hand plot limit (Hz)
 1.00000000E+02    Right hand plot limit (Hz)
 0.20000000E+01    Plot scale (mm/Hz)
 0.02000000E+00    Plot resolution (Hz)
 0.60000000E+02    Plot height (mm)
yes        Normalize
no         Label
              1     Number of spectra summed
             14     Number of composite spectra plotted
              1     Number of rate constants
              2     Number of peaks in energy level  1
 2.50000000E+01     0.16000000E+01      0.33000000E+00
 0.75000000E+02     0.16000000E+01      0.66000000E+00
 0.10000000E+00    rc(  1)
 0.10000000E+01    rc(  1)
 0.20000000E+01    rc(  1)
 0.50000000E+01    rc(  1)
 0.10000000E+02    rc(  1)
 0.30000000E+02    rc(  1)
 0.50000000E+02    rc(  1)
 0.75000000E+02    rc(  1)
 0.10000000E+03    rc(  1)
 0.20000000E+03    rc(  1)
 0.50000000E+03    rc(  1)
 0.10000000E+04    rc(  1)
 0.10000000E+05    rc(  1)
 0.10000000E+06    rc(  1)
no         Another gnmr run
```

matrix.fortran

```
      %global card;
      subroutine matrix(rc,n,pop)
      dimension rc(10)
      common /areal/ areal(70,70)
      real pop(8,75)

      do 5  i=1,n
      do 5  j=1,n
    5 areal(j,i)=0.0

      areal(1,1) = rc(1)
      areal(2,1) = -(pop(1,1)/pop(1,2)) * rc(1)
      areal(1,2) = -(pop(1,2)/pop(1,1)) * rc(1)
      areal(2,2) = rc(1)

      return
      end
```

dFigure3-2.absout

```
PROGRAM GNMR      10/23/86  1559.6


Figure 3-2.

Plotting parameters:
     Left hand plot limit =      0.0 hz.
     Right hand plot limit =   100.0 hz.
     Plot scale = 2.00000 mm/hz.
     Plot resolution = 0.02000 hz.
     Plot height = 60.0 mm.
     Plots are to be normalized.
     Plots are not to have labelled x-axis.


gnmr expects to calculate  14 composite spectra.
Each will be the sum of  1 spectra.
There will be  1 different rate constants for each spectrum.


**********************************************
Energy Level  1
**********************************************

Peak   Chemical        Line          Relative
      Shift (hz)    Width (hz)     Population

  1      25.000         1.600          0.330
  2      75.000         1.600          0.660


The plot will be labelled as follows:
     Figure 3-2.
     Plot Number  1      10/23/86  1559.6
     rc( 1)=1.00000E-01

Virtual CPU time = 5.330 sec. to generate plot number  1.


The plot will be labelled as follows:
     Figure 3-2.
     Plot Number  2      10/23/86  1559.6
     rc( 1)=1.00000E+00

Virtual CPU time = 5.188 sec. to generate plot number  2.


The plot will be labelled as follows:
     Figure 3-2.
     Plot Number  3      10/23/86  1559.6
     rc( 1)=2.00000E+00

Virtual CPU time = 5.244 sec. to generate plot number  3.


The plot will be labelled as follows:
     Figure 3-2.
     Plot Number  4      10/23/86  1559.6
     rc( 1)=5.00000E+00                                    etc. ...
```

Appendix B. Pulse Sequence SINCERE

When a DANTE sequence of mini-pulses[107] is applied to a spin system, sidebands to the transmitter signal are created at frequency intervals equal to the inverse of the delay between pulses. This provides a method by which individual resonances can be detected selectively. In the Varian program QSEX[137], the selectivity of the basic DANTE sequence is improved by phase-cycling the mini-pulses. For instance, if the phase is cycled in a positive direction (i.e., 0°, 90°, 180°, and 270°), all sidebands are suppressed except the first sideband upfrequency of the transmitter signal[138]. Cycling the phase in the opposite direction (0°, 270°, 180°, 90°) leaves only the first downfrequency sideband.

In the pulse sequence program SINCERE (selective inversion in a chemical exchange rate experiment) which is based on QSEX, a non-selective 90° acquisition pulse (PW), preceded by a variable delay R2 (= 10^{-3} to 10^{2} s), is inverted after a phase-cycled DANTE pulse train. The number (NO) and width (P1) of the mini-pulses are set to provide a 180° selective-inversion signal. Pulse P2 and delay R3 can be tailored to minimize any imperfection in the inversion signal. The frequency separation (FE) between the transmitter signal and the resonance to be inverted is calculated from the spectral position of the resonance (EXFREQ). The program then calculates the delay between mini-pulses (R1) which is required to position the first transmitter signal sideband at EXFREQ.

The flag GETP permits a normal spectrum to be run prior to the selective inversion-recovery (SIR) experiment so that the EXFREQ value can be determined using all the same acquisition parameters.

The flag TSEQ provides the option of obtaining the difference between normal and SIR spectra. In this procedure, which is similar to a technique reported by Dahlquist et al.[139], chemical exchange can be observed directly since only spectral changes will be observed. Because line intensities are reduced, however, the method is not as accurate for obtaining quantitative rate measurements as the SIR experiment.

SINCERE Pulse Diagram

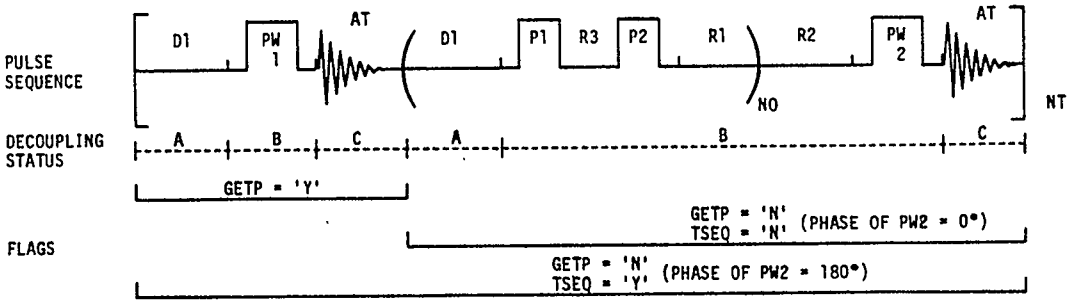

The program for SINCERE, listed on the next page, was written in the modified Pascal language used by the processing system of the Varian XL200 spectrometer.

```
"**** SINCERE ****
SELECTIVE INVERSION IN A
CHEMICAL EXCHANGE RATE
     EXPERIMENT

S.D. KINRADE (REVISED:  85.06.20)"

PROCEDURE PULSESEQUENCE;
     VAR EXFREQ,REFP,REFL,EF,SW,NO,P1,P2,NULL,R1,R2,R3:  REAL;
     TSEQ,GETP:  TEXT4;

BEGIN
     GETVAL(SW,'SW    ');
     GETVAL(NO,'NO    ');
     GETVAL(EXFREQ,'EXFREQ    ');
     GETVAL(R2,'R2    ');
     GETVAL(R3,'R3    ');
     GETVAL(P2,'P2    ');
     GETVAL(TSEQ,'TSEQ    ');
     GETVAL(GETP,'GETP    ');
     GETVAL(REFL,'REFL    ');
     GETVAL(REFP,'REFP    ');
     PUTVAL(REFP,'REFP    ');
     PUTVAL(REFL,'REFL    ');
     INITVAL(0.0,V3);

     P1:=2.0*PW/NO+P2;
     PUTVAL(P1,'P1    ');
     EF:=EXFREQ+(SW/2.0)-REFL+REFP;
     PUTVAL(EF,'EF    ');
     PUTVAL(EXFREQ,'EXFREQ    ');
     PUTVAL(SW,'SW    ');

     IF EF<>0.0
          THEN R1:=1.0/ABS(EF)-ROF1-ROF2-P1-P2
          ELSE R1:=1E-6;
     IF R1<1E-6
          THEN R1:=1E-6;
     PUTVAL(R1,'R1    ');

     NULL:=2.0*ABS(EF)/NO;
     PUTVAL(NULL,'NULL    ');
     ASSIGN(CT,V1);

     IF TSEQ[1]='Y'
          THEN ASSIGN(TWO,V2)
          ELSE ASSIGN(ZERO,V2);
          STATUS(A);
          HSDELAY(D1);
          STATUS(B);
          IF GETP[1]='Y'
               THEN OBSPULSE
               ELSE BEGIN
                    IF TSEQ[1]='Y'
                         THEN BEGIN
                              INCR(V1);
                              MOD2(V1,V3);
                         END;
                    IFZERO(1,V3);
                         LOOP(1,NO,V4);
                              RGPULSE(P1,V2,ROF1,0.0);
                              DELAY(R3);
                              RGPULSE(P2,V3,0.0,ROF2);
                              DELAY(R1);
                         ENDLOOP(1);
                         DELAY(R2);
                    ENDIF(1);
                    OBSPULSE;
               END;
          STATUS(C);
     END;
```